

INVESTIGATING CONTROLS ON TEMPORAL AND SPATIAL VARIATION OF
DISSOLVED URANIUM AT SPRINGS IN HORN CREEK DRAINAGE,
GRAND CANYON NATIONAL PARK, ARIZONA, USA

By

Collin Davidson

Bachelor of Arts – Environmental Geoscience
DePauw University
2021

A thesis submitted in partial fulfillment
of the requirements for the

Master of Science – Geoscience

Department of Geoscience
College of Sciences
The Graduate College

University of Nevada, Las Vegas
May 2024



Thesis Approval

The Graduate College
The University of Nevada, Las Vegas

March 25, 2024

This thesis prepared by

Collin Davidson

entitled

Investigating Controls on Temporal and Spatial Variation of Dissolved Uranium at Springs in Horn Creek Drainage, Grand Canyon National Park, Arizona, USA

is approved in partial fulfillment of the requirements for the degree of

Master of Science – Geoscience
Department of Geoscience

David Kreamer, Ph.D.
Examination Committee Chair

Gabriel Judkins, Ph.D.
Examination Committee Member

Jeremy Koonce, Ph.D.
Examination Committee Member

Sajjad Ahmad, Ph.D.
Graduate College Faculty Representative

Alyssa Crittenden, Ph.D.
*Vice Provost for Graduate Education &
Dean of the Graduate College*

Abstract

Groundwater is a critical resource in the Grand Canyon, providing water to local communities, millions of annual visitors, and ecosystems. One major concern for this critical resource is the potential for uranium contamination in conjunction with uranium mining efforts. Upper Horn Bedrock Spring (UHB) in the Horn Creek drainage of the Grand Canyon sits below the oldest uranium mine in the region, Orphan Lode mine. UHB spring contains the highest concentration of dissolved uranium in the region, eclipsing the Maximum Contaminant Level (MCL) set by the USEPA by an order of magnitude on average. This research and recent collaboration with the U. S. Geological Survey (USGS) provide further insight into the hydrogeochemical evolution of the groundwater within the drainage, with an emphasis on trying to understand the temporal and spatial variation of dissolved uranium within groundwater sampled in Horn Creek drainage. This thesis specifically investigates two environmental phenomena surrounding dissolved uranium in the drainage using stable isotopes, multivariate statistical analysis, inverse modeling in PHREEQC, and bivariate analysis. The first phenomenon is the relatively rapid change in dissolved uranium concentration as flow moves downgradient from Upper Horn Bedrock spring to Upper Horn Alluvium spring. Approximately 200 m apart, there is roughly an order of magnitude decrease in dissolved uranium between the two springs. Inverse modeling suggests that water-rock interactions could explain the observed change in uranium concentration if the mineral pyrite is present in trace concentrations along the flow path. Inverse modeling and multivariate analysis also suggest that mixing between UHB and a second spring, East Horn Creek – Battleship, could explain the observed change in chemistry. However, stable isotopes collected in 2013 do not support EHC-BS as a mixing partner. The second phenomenon investigated is the variable concentration of dissolved uranium at UHB over time.

Twenty-two samples have measured the concentration of dissolved uranium at Upper Horn Bedrock spring across nearly two decades, with concentrations ranging from 151 ppb to 509 ppb. Results indicate that although there is no trend in dissolved uranium over time, there is a relationship between recent precipitation and dissolved uranium. Bivariate analysis comparing recent precipitation (up to 120 days prior to sample collection) and dissolved uranium indicates that wetter periods 9 to 10 weeks prior to sampling correspond to the lowest concentrations of dissolved uranium recorded since 2003. Drier conditions 9 to 10 weeks prior to sampling correspond to higher concentrations of dissolved uranium, however significant variation is present among these higher concentrations.

Acknowledgements

Few things in life are a one-man show, and even though I may be the sole author of this thesis, I could have never finished this research without the help of so many people in my life. A special thank you to my advisor, Dave Kreamer, for his collaboration throughout this project, his unrelenting jovial attitude, and his infectious passion for groundwater. A special thank you to Luke Stevens for his mentorship, support, and expertise throughout our time together in the trenches of graduate school. Thanks to Venus Cruz and Austin Rodell-Davis for their help with data collection in the backcountry of Grand Canyon National Park. Thanks to my committee for taking the time out of their busy schedules to help guide my research. And of course, thanks to all of the geo friends I picked up along the way in our different classes and field trips.

I am beyond grateful to my parents for all of their love and support throughout this journey. Their belief, patience, and optimism helped me stay the course and keep progressing towards my degree on the days when I didn't believe I would ever finish. A huge thank you to the folks who helped fill my two years in Las Vegas with adventure and helped make LV feel like home (shout out Mountain Club). And of course, a huge thanks to the friends and family from across the country who supported me from afar. I am so grateful to have such an amazing community of people to lean on and learn from.

And last, but certainly not least, a huge thank you to the folks who lured me into geoscience in the first place and helped me find my path into a field I have found such a passion for. I would not be sitting where I am today, chasing a career in hydrogeology, without the guidance and mentorship from my professors at DePauw University. I feel so lucky to have had such great people to look up to from the very beginning.

Table of Contents

| | |
|--|------|
| Abstract | iii |
| Acknowledgements | v |
| List of Tables | viii |
| List of Figures | ix |
| Chapter 1: Introduction | 1 |
| Chapter 2: Background | 5 |
| 2.1 Study Area and Sampling Locations..... | 5 |
| 2.1.1 Geologic Setting | 7 |
| 2.1.2 Hydrogeologic Setting | 13 |
| 2.1.3 Uranium Hydrogeochemistry | 15 |
| 2.1.4 Stable Isotope Chemistry | 16 |
| 2.1.5 Principles of Applied Multivariate Statistics | 18 |
| 2.1.6 Principles of PHREEQC | 20 |
| 2.2 Hypotheses | 21 |
| Chapter 3: Materials and Methods | 22 |
| 3.1 Field Collection Methods | 22 |
| 3.2 Precipitation and Uranium Comparison Methods..... | 25 |
| 3.3 PHREEQC Inverse Modeling Methods | 27 |
| 3.4 Multivariate Statistical Methods | 31 |
| 3.5 Stable Isotopes and Water Chemistry Interpretation Methods | 35 |
| Chapter 4: Results | 36 |
| 4.1 General Results of Field Sampling | 36 |

| | |
|---|-----|
| 4.2 Stable Isotopes | 37 |
| 4.3 Multivariate Statistics | 39 |
| 4.4 PHREEQC Inverse Modeling | 42 |
| 4.5 Precipitation and Dissolved Uranium Comparison | 49 |
| Chapter 5: Discussion | 52 |
| 5.1 Multivariate Statistical Analyses | 52 |
| 5.2 PHREEQC Analyses | 59 |
| 5.3 Stable Isotopes Analysis | 64 |
| 5.4 Precipitation and Dissolved Uranium at UHB Analysis | 69 |
| Chapter 6: Conclusions | 73 |
| Appendix A: Figures Referenced in Text | 76 |
| Appendix B: Sampling Locations and Data Tables | 103 |
| Appendix C: PHREEQC Modeling Summaries | 113 |
| Appendix D: Precipitation Analysis Data..... | 120 |
| Appendix E: Additional Multivariate Analyses Plots | 121 |
| References Cited | 128 |
| Curriculum Vitae | 136 |

List of Tables

| | |
|--|-----|
| Table 1: Sampling Locations | 103 |
| Table 2: Groundwater chemistry collected in November 2022 | 104 |
| Table 3: Groundwater chemistry collected March 30 th -April 1 st , 2023, | 105 |
| Table 4: Dissolved Uranium Data at UHB | 106 |
| Table 5: Groundwater chemistry collected October 2013 by URS Inc. | 107 |
| Table 6: S1.R1 Summary | 110 |
| Table 7: S1.R2 Summary | 111 |
| Table 8: S1.R3 Summary | 112 |
| Table 9: S1.R4 Summary | 113 |
| Table 10: S1.R5 Summary | 114 |
| Table 11: S1.R6 Summary | 115 |
| Table 12: S2.R1 Summary | 116 |
| Table 13: S2.R2 Summary | 117 |
| Table 14: S2.R4 Summary | 118 |
| Table 15: S2.R5 Summary | 119 |
| Table 16: Precipitation vs. Dissolved Uranium Spearman's Rho Coefficients | 120 |

List of Figures

| | |
|--|----|
| Fig. 1: Study Area..... | 76 |
| Fig. 2: Sampling Sites..... | 77 |
| Fig. 3a Distribution of Total Dissolved Uranium in October 2013 | 78 |
| Fig. 3b Distribution of Total Dissolved Uranium in November 2022..... | 79 |
| Fig. 3c Distribution of Total Dissolved Uranium in March 2023..... | 80 |
| Fig. 4 Stratigraphic Column of Grand Canyon Lithology | 81 |
| Fig. 5 Horn Creek cross-section..... | 82 |
| Fig. 6 Locations of Weather Stations Relative to UHB Spring | 83 |
| Fig. 7 Correlation Matrix | 84 |
| Fig. 8 Piper Diagram of 2013 and 2023 Data..... | 85 |
| Fig. 9 Horn and Salt Creek Stable Isotopes | 86 |
| Fig. 10 3-D PCA of All Analytes Collected in 2013 | 87 |
| Fig. 11 All Analytes PCA: PC1-PC2 Biplot..... | 88 |
| Fig. 12 H-Kmeans for Multivariate Analysis of All Analytes Collected in 2013 | 89 |
| Fig. 13 Time PCA 3-D Plot | 90 |
| Fig. 14 Time PCA: PC1-PC-2 Biplot | 91 |
| Fig. 15 Time PCA: PC2-PC3 Biplot..... | 92 |
| Fig. 16 Time PCA: Cluster Plot..... | 93 |
| Fig. 17 Uranium Analytes PCA: 3-D Plot | 94 |
| Fig. 18 Uranium Analytes PCA: PC1-PC2 Biplot..... | 95 |
| Fig. 19 Uranium Analytes PCA: PC2-PC3 Biplot..... | 96 |
| Fig. 20 Uranium Analytes H-Kmeans Chart..... | 97 |

| | |
|--|-----|
| Fig. 21 Uranium Analytes K-means Plot..... | 98 |
| Fig. 22 Total Dissolved U Over Time at Upper Horn Bedrock Spring | 99 |
| Fig. 23 Precipitation vs. Total Dissolved Uranium at UHB Spring from 2002 to 2023..... | 100 |
| Fig. 24 Stable Isotope and Bedrock Lithology of Springs..... | 101 |
| Fig. 25 Stable Isotopes vs. Dissolved Uranium Plot..... | 102 |
| Fig. 26 All analytes PCA: PC2-PC3 Biplot..... | 121 |
| Fig. 27 All analytes PCA: Eigenvalues of Principal Components 1-10..... | 122 |
| Fig. 28 All analytes Kmeans: Optimal number of clusters | 123 |
| Fig. 29 Time PCA: Eigenvalues of Principal Components 1-9 | 124 |
| Fig. 30 Time Kmeans: Optimal number of clusters | 125 |
| Fig. 31 Uranium PCA: Eigenvalues of Principal Components 1-9 | 126 |
| Fig. 32 Uranium H-Kmeans: Optimal number of clusters | 127 |

Chapter 1: Introduction

Grand Canyon National Park is situated in Northern Arizona on the Colorado Plateau and is known around the world for its stunning views, unique geology, and spectacular wildlife. The lifeblood of the canyon is the water that flows above and below, sometimes traveling hundreds of miles before it emerges from the walls of the Grand Canyon or surges through the Colorado River. Over 1,400 springs have been documented within the walls of the Grand Canyon, one of the highest densities of springs in the United States (Tobin et al., 2018). These springs control the distribution of wildlife and are commonly hotspots for biodiversity: approximately 10 percent of the roughly 1,800 plant species identified within the canyon are found at springs (National Park Service, 2021(b)). In addition to its profound ecological significance, springs in the Grand Canyon hold strong cultural significance for Native American people who live within the canyon (Stevens and Meretsky, 2008). Groundwater is a critical resource for many that live in or nearby the Grand Canyon, with indigenous peoples of the canyon, such as the Havasupai and Hualapai, relying heavily on groundwater to support their way of life. Towns near the Grand Canyon such as Jacobs Lake, Tusayan, and Williams as well as the nearly 5 million visitors to the National Park also rely on groundwater resources (Tilman et al., 2021; National Park Service, 2021(a)).

Groundwater is not the only valuable resource situated in the region; some of the highest-grade uranium ores in the United States are found in the Grand Canyon (Alpine and Brown, 2010). In 1951, the first discovery of uranium ore was made in the Grand Canyon, at Orphan Mine (see Fig. 1 for location). In 1956, the first lode of uranium was extracted. Over the course of the mine's 13-year operation, 4.26 million pounds (1.93 million kg) of uranium oxide were

extracted (Chenoweth, 1986). New uranium mining operations have since followed in the region, but remain controversial (Tillman et al., 2021). At the heart of the controversy is the potential for uranium contamination of groundwater, with documented health impacts in humans with long term exposure (Zamora et al., 1998; Kurttio et al., 2002). In 2009, the U.S. Secretary of the Interior, Ken Salazar, put into place a 20-year moratorium on new uranium mining within the Grand Canyon, for the purpose of allowing time for further research on the impacts of uranium mining on groundwater resources (U.S. Department of the Interior, 2012). More recently in 2023, a new national monument, Baaj Nwaavjo I'tah Kukveni – Ancestral Footprints of the Grand Canyon National Monument, was created furthering conservation interests in the region (The White House, 2023). The creation of the new national monument recognizes existing mining claims that predate the 20-year moratorium but will spell an end to future claims in the newly protected region (The White House, 2023; Kanno-Youngs and Friedman, 2023). One site of interest in conjunction with recent policy decisions is the oldest uranium mine in the region (now defunct), Orphan Mine, and the springs below it, in the Horn Creek drainage.

Currently, the highest observed concentrations of uranium in groundwater in the Grand Canyon are found in the Horn Creek drainage at Upper Horn Bedrock (UHB) Spring (Tillman et al., 2021) (see Fig. 2 for spring locations or Appendix A for the latitude and longitude of all sampling locations evaluated in this study). Although significant sampling has been conducted at Horn Creek, no conclusion has been made connecting Orphan Mine and the anomalously high concentrations of total dissolved uranium. The highest concentration of total dissolved uranium sampled at UHB is 509 $\mu\text{g/L}$ (Scharr unpublished, 2011). However, concentrations at UHB spring fluctuate over time, with the lowest concentration of total dissolved uranium recorded at 151 $\mu\text{g/L}$ (Liebe, 2003; Monroe et al., 2005; Scharr, 2011; Tillman et al., 2021; U.S. Geological

Survey, 2022). Concentrations of total dissolved uranium also vary significantly across springs in Horn Creek drainage, with concentrations ranging from 5 µg/L to 310 µg/L across the eight sampled springs in October of 2013 (URS Group Inc., 2014). (Note: URS Inc., who sampled in the Grand Canyon in 2013, was acquired in October 2014 by AECOM). At present, there is no definitive explanation as to why the concentrations fluctuate over time or why concentrations vary significantly within the drainage. Controls could include variance in meteorological events, varying flow paths, water rock interactions, and proximity to the ore-bearing breccia pipe.

The objective of this graduate thesis is to investigate controls on the variation of dissolved uranium concentrations both spatially and temporally at Horn Creek drainage. Although the springs at Horn Creek have been sampled frequently over the past decades relative to other springs in the Grand Canyon region, measurements collected have varied significantly between studies, with only one study producing a robust set of data across the drainage in a short time window (URS Group Inc., 2014). The sampling record at Upper Horn Bedrock spring dates as far back as 1995, when dissolved uranium concentrations in spring water were first measured above the Environmental Protection Agency's (EPAs) Maximum Contaminant Levels (MCL) of 30 µg/L by Jim Fitzgerald (1996). Significant sampling followed, however precise locations of sampling sites remain unclear across studies and parameters collected vary significantly (Fitzgerald, 1996; Liebe, 2003; Monroe et al., 2005; Scharr, 2011; Tillman et al., 2021; Beisner et al., 2023). As such, the collection of modern groundwater data across springs in the Horn and Salt Creek drainage are warranted to allow for comparisons in spatial distribution of uranium in groundwater from October 2013 to present. A modern groundwater survey presented here was collected in November of 2022 over two weekends, and then again in March of 2023. The aim of the modern survey was to collect more data while minimizing temporal variation across water

quality sampling, allowing for the application of modeling approaches and chemistry analysis representing a more modern state of the groundwater in the study area. This thesis applies inverse modeling in PHREEQC, multivariate statistical analysis, bivariate regression analysis, stable isotope analysis, temporal climatic analysis, and major ion analysis to determine the likely controls on the rapid attenuation of uranium at Horn Creek and the temporal variation of uranium at Upper Horn Bedrock spring.

Chapter 2: Background

2.1 Study Area & Sampling Locations

The Horn Creek drainage is situated within Grand Canyon National Park, below the South Rim, roughly two miles in a direct line from the South Rim Visitor Center (Fig. 1). The Salt Creek drainage is situated to the west of Horn Creek drainage. The maximum elevation within the Horn Creek watershed is 2,150 m (7,053 ft) above mean sea level (AMSL) and the lowest elevation is 730 m (2,395 ft) AMSL (its confluence with the Colorado River). Within Horn Creek, there are three major subdrainages, West Horn Creek, East Horn Creek, and Lower Horn Creek. Within East Horn Creek, there are three sub-drainages. Upper Horn Bedrock Spring is located within the western most minor subdrainage of East Horn Creek. (Fig. 2). The East fork of East Horn Creek drainage hosts EHC-BS, which had the lowest observed dissolved uranium concentrations (5.4 µg/L) of any of the groundwater samples collected in a 2013 survey (URS Inc. 2014) (Fig. 3a). Groundwater has been sampled from springs discharging out of bedrock and alluvial deposits in the Salt Creek and Horn Creek drainages (Fig. 2). In Horn Creek drainage, 8 springs (Upper Horn Bedrock (UHB), Upper Horn Alluvium (UHA), Lower Horn Alluvium (LHA), Lower Horn Alluvium-Tonto (LHA-Tonto), Battleship Seep (EHC-BS), Lower Horn Bedrock (LHB), North East Horn Creek (NEHC-Top), and West Horn Bedrock (WHC)) were sampled in 2013, and three of these springs were sampled again in November of 2022 (UHB, UHA, LHA) and four in April of 2023 (UHB, UHA, LHB, WHC) (Fig. 3b, Fig 3c). Havasupai Gardens (previously named Indian Gardens) in the Bright Angel drainage, east of the Salt and Horn Creek drainages, was sampled for comparison purposes.

Groundwater in the Salt Creek drainage has also been found to have elevated dissolved uranium concentrations (Tillman et al., 2021). The maximum elevation within the Salt Creek watershed is 2,095 m (6,873 ft) AMSL, and the lowest elevation is 725 m (2,378 ft) AMSL (confluence of the Colorado River). Salt Creek does not bifurcate into two sub-drainages like Horn Creek, and consequently has a lower density of springs. Three springs were sampled in 2013, and the same three springs were sampled again in November of 2022 (Upper Salt Creek (SC-Top), Salt Creek – Tonto (SC-Tonto), and Lower Salt Creek (LSC-Vishnu)) (Fig. 2). No samples were collected in the Salt Creek drainage in the 2023 Spring survey. Uranium concentrations in groundwater ranged from 27 $\mu\text{g/L}$ to 13 $\mu\text{g/L}$ in 2013 and 25.7 $\mu\text{g/L}$ to 12.2 $\mu\text{g/L}$ in 2022, with concentrations decreasing in groundwater moving down drainage towards the confluence of the Colorado River in both data sets. These two drainages comprise the study area for this graduate thesis.

Precipitation and temperature varies within the study area due to the drastic change in elevation. Precipitation is bimodal, with the two wettest months on average being August and January (3.43 cm (1.35 in) and 2.59 cm (1.02 in) respectively) over the period of record at the Phantom Ranch weather station according to the Western Regional Climate Center (<https://wrcc.dri.edu/cgi-bin/cliMAIN.pl?az6471ary>). The driest months are on average April, May, and June, with June receiving the least amount of rainfall on average over the period of record at the Phantom Ranch weather station (0.51 cm or 0.2 in). Precipitation events are often intense and localized, and intense afternoon thunderstorms are common in late summer where flash-flooding can occur. In addition to seasonal variation, precipitation varies across elevations, with the South Rim receiving less than 40.64 cm (16 in) of rainfall and around 1.52 m (60 in) of snowfall on average annually (URS Inc., 2014) while Phantom Ranch (located approximately 4

km (2.5 mi) upriver of Horn Creek rapids on the Colorado River) typically receives between 20 to 25 cm (8 to 10 in) of rain and minimal snowpack on average annually. Temperatures also range drastically across seasons and elevations in the study area. The hottest month of the year on average is July, with an average temperature of 19.86°C (67.75°F) at the South Rim (2070 m amsl or 6800 ft AMSL) according to the Western Regional Climate Center (<https://wrcc.dri.edu/cgi-bin/cliMAIN.pl?az3596>). The coldest month of the year on average is January, with an average temperature of -0.5°C (31°F) at the South Rim. For comparison, the average temperature at the Phantom Ranch weather station (783 m AMSL or 2569 ft AMSL) in the month of July is 32.94°C (91.3°F), while the average temperature at Phantom Ranch in the month of January is 8.25°C (46.85°F). This variability in mean temperature demonstrates the relatively dramatic variation in climate between the rim and inner-canyon climates.

2.1.1 Geologic Setting

The Colorado River incises the Colorado Plateau, exposing at its deepest point over 2 km (1.24 mi) of Paleozoic and Proterozoic stratigraphy (Fig. 4). Moving up the stratigraphic column from the bottom, the basement consists of metamorphic rocks as well as some igneous intrusions (such as the Zoroaster Granite). Above the basement is the Grand Canyon Supergroup, consisting mostly of sedimentary rocks with some smaller areas of igneous rock units that are Proterozoic in age. Above the Grand Canyon Super Group is the Great Unconformity. Above this is the Tonto Group, consisting of the Tapeats Sandstone, Bright Angel Shale, Muav Limestone, and Frenchman Mountain Dolostone, all of which are Cambrian in age. Directly above these units lie the Temple Butte Limestone (Devonian in age) and Redwall Limestone (Mississippian in age). Above these units exists the Supai Group, followed by the Hermit Shale,

Coconino Sandstone, Toroweap Formation, and Kaibab Formation, which are Pennsylvanian to Permian in age. Moenkopi and Chinle Formations reside at the top, both Triassic in age. Key structural features in the canyon include faults (such as the Bright Angel Fault), monoclines, synclines, and collapse features, such as breccia pipes. The geologic units found within the study area are described in more detail below.

Proterozoic Crystalline Rocks

Formed in the early to middle Proterozoic, sediments and volcanics were deposited in the range of 2.0 to 1.8 Ga. And then in the range of 1.5 to 1.4 Ga, voluminous granites were emplaced as part of an incipient transcontinental rift. Two major episodes of metamorphism in addition to magmatic intrusive events make this a complex unit that forms the crystalline basement of the Grand Canyon stratigraphy (Beus and Morales, 1990). Proterozoic crystalline rocks can be found in the lower Horn Creek drainage, with two metamorphic rock units (Vishnu schist and Brahma Schist) and two intrusive rock units (young granite and pegmatite), as well as older granite, granitic pegmatite, and aplite (URS Inc., 2014).

Tapeats Sandstone

The Tapeats Sandstone is Middle to Lower Cambrian in age and was originally characterized by Noble (1914). The unit is generally classified as “medium- to course-grained feldspar and quartz-rich sandstone with granule and pebble-size conglomerate present locally near the base” and is tan to medium-brown in color (Middleton and Elliot, 1990). The first unit can be separated into two packages, with the first package outcropping as a cliff with bedding less than 3 feet (1 m) thick. Planar and cross stratification are present along with “crudely

developed” horizontal stratification. As one moves up the stratigraphic column, both the scale and cross stratification decrease. Overlying the first unit is the second unit, which is described as a zone of “interbedded fine- to medium-grained sandstone and mudstone,” marking a major facies transition to the Bright Angel Shale, a conformable contact (Middleton and Elliot, 1990). The unit can range in thickness from 100 to 325 feet (30.5-100.7m). The contact between the Tapeats Sandstone and either the Grand Canyon Super Group or the Proterozoic basement is unconformable and is prominently known as the Great Unconformity.

Bright Angel Shale

The Bright Angel Shale is Middle Cambrian in age. The unit is generally composed of shale, siltstone, and fine-grained sandstone (Middleton and Elliott, 1990), and its period of deposition has been further defined to occur between 507 to 502 Ma in the region (Karlstrom et al., 2020). The contact between the Bright Angel Shale and Muav Limestone is gradational, and thickness of the unit varies across the Grand Canyon, with a thickness described as 348 ft (106 m) by Noble (1914). The mineral glauconite gives the rock unit its green hue. A reddish-brown hue also observed within the rock unit is due to the presence of hematitic ooids and iron oxide cement within some sandstone and siltstone beds (Middleton and Elliot, 2003).

Muav Limestone

The Muav Limestone is Middle Cambrian in age and the unit’s composition consists of limestone, dolomite, mudstone, siltstone and conglomerate (Middleton and Elliot, 1990). The thickness of the unit is also variable across the region, ranging from 45 m (148 ft) to 245 m (804 ft) thick (Spamer, 1984). Mckee and Resser (1945) characterized the unit into 7 members:

Havasu, Gateway Canyon, Kanab Canyon, Peach Springs, Spencer Canyon, Sanup Platform, Rampart Cave (from top to bottom). As mentioned previously, the lower contact with the Bright Angel Shale is gradational, and the upper contact is an unconformity with what was once characterized as ‘undifferentiated dolostone’ and has been recently characterized as Frenchman Mountain Dolostone by Karlstrom and others (2020) and Rowland and others (2023).

Frenchman Mountain Dolostone

The Frenchman Mountain is the youngest member of the Tonto Group, with an age that has been constrained to a range of approximately 7.3 Ma, ranging from 502.8 Ma to 495.5 Ma (Rowland et al., 2023). The thickness of the unit ranges significantly across the Grand Canyon and its outcropping at Frenchman Mountain, near Las Vegas, NV. The unit thickness ranges from 8 -30 m in eastern Grand Canyon, with thickness increasing moving westward in the region. Eight lithofacies have been identified, however the Frenchman Mountain Dolostone has been pervasively dolomitized, resulting in the original textures being obliterated beyond recognition. The eight lithofacies represent a peritidal and shallow subtidal depositional environment (Brathovde, 1986; Rowland et al., 2023).

Temple Butte Formation

The Temple Butte Formation is Middle-Upper Devonian in age, is a carbonate unit, and can be characterized as a dolomite or sandy dolomite. The unit is laterally discontinuous as it was deposited as the Muav Limestone was incised. The Temple Butte Formation is not present continuously within the field area and, where present, is described as stained red similar to the Redwall Limestone that sits above it stratigraphically (URS Group Inc., 2014). Spamer (1984)

describes the lower contact with the Muav Limestone and the upper contact with the Redwall Limestone as unconformable. Fitzgerald (1996) describes the unit thickness in the field area as ranging from 0-140 ft (0-43 m).

Redwall Limestone

The Redwall Limestone is Lower to Middle Mississippian in age, and broadly can be understood as a limestone and dolomite unit. Within the geologic unit, McKee and Gutschick (1969) characterized four members: Whitmore Wash, Thunder Springs, Mooney Falls, and Horseshoe Mesa, listed from oldest to youngest. All four members are characterized as cliff-forming (Billingsley, 2000), and although the geologic unit and its members are not actually red, they often appear red within canyon due to the leaching of iron-oxides from the overlying Supai Group. The Whitmore Wash member is mostly limestone and dolomite with thickness ranging from 15 m (49 ft) to 36 m (118 ft) in the canyon (Beus and Billingsley, 1989). Billingsley (2000) characterizes the member as a fine-grained, yellowish and brownish-gray dolomite. The Thunder Springs unit is often recognized for its unique banding, a function of alternating, interbedded chert and carbonate beds. The member ranges in thickness from 30-43 m (98-141 ft) (Beus & Billingsley, 1989). Billingsley (2000) characterizes the member as either a brownish-gray, thin-bedded, crystalline dolomite and limestone interbedded with white beds of chert lenses or gray, thin-bedded, fossiliferous limestone. The Mooney Falls member is the thickest of the four members 76-104 m (249-341 ft), and Billingsley (2000) characterizes the member as a fine to coarse grained, fossiliferous limestone, light gray in color. The Horseshoe Mesa member is the youngest of the four members and has a thickness ranging from 0-30 m (0-98 ft) and is

composed of limestone ledges (Beus and Billingsley, 1989). Billingsley (2000) characterizes the unit as a thin-bedded, fine-grained limestone, light-olive-gray in color.

Other important characteristics of the geologic setting include structural features found within the region and locally at Horn Creek. Breccia Pipes are common throughout the Grand Canyon region (Otten and Van Gosen, 2010), and can be understood as localized vertical collapse features. Dissolution of CaCO_3 in the Redwall Limestone results in karst formation. Occasionally, when these karst features collapse, the column of rock directly above these karst features collapses over time. The result is a pipe-like structure of brecciated rock that has propagated upwards. A small subset of breccia pipes has been mineralized in the region, and subsequently host a variety of ore-grade minerals unique to their local surroundings (Chenoweth, 1986). One of these mineralized breccia pipes is found on the South Rim of the Grand Canyon, directly above Horn Creek drainage.

The breccia pipe hosts the ore body of Orphan Lode Mine, and was mined from 1953 to 1969 (Amundson, 2001). The breccia pipe is contained to part of the Redwall Limestone, Supai Group, Hermit Shale, and Coconino Sandstone (Fig. 5). Its diameter is variable and dependent upon the lithology of the surrounding geologic unit (Chenoweth, 1986). Uraninite is the primary uranium mineral of the ore body, while copper-bearing minerals are also commonly associated with uraninite in the ore body. Pyrite and Calcite were frequently documented in the Orphan Lode Mine, while ores found in the breccia pipe also contained silver, nickel, cobalt, lead, zinc, and vanadium (Chenoweth, 1986). Gornitz and Kerr (1970) characterized the minimum age of uranium mineralization at 141 Ma using U-Pb dating. The depth of the breccia pipe was determined to be approximately 400 m (1,311 feet) below the Orphan Lode adit, however active mining operations only commenced 166 m (545 feet) below the adit. An exploratory drill hole,

P-13, was drilled from the 550-level (550 feet below the mine's adit) to an extra depth of 583 m (1,914 feet) (Fig. 5). This hole drilled through the entire extent of the Redwall Limestone, Muav Limestone, Bright Angel Shale, and infiltrated the top 18 m (60 feet) of the Tapeats Sandstone (Chenoweth, 1986).

2.1.2 Hydrogeologic Setting

As this study examines the environmental controls on temporal and spatial variation of dissolved uranium in springs situated in Horn and Salt Creek drainage, it is critical to understand the larger hydrogeologic framework of the Grand Canyon region. Two major aquifers supply groundwater to the region. The first aquifer, known as the C-aquifer, is an overlying aquifer with an aquitard underneath, underlain by a second aquifer. The C-aquifer is comprised of the Kaibab Formation, the Toroweap Formation, and the Coconino Sandstone (Fig. 4). It is important to note that although the C-aquifer is commonly referred to as “perched,” due to vertical fracturing, some areas of the C-aquifer are vertically connected with the R-aquifer. Directly beneath the Coconino Sandstone lies the Hermit Shale, an aquitard. Below the Hermit shale and the Supai group lies the second aquifer, known as the R-aquifer. The R-aquifer is a confined aquifer composed of the Redwall Formation, the Temple Butte Formation, the Frenchman Mountain Dolostone, and the Muav Formation. Directly beneath the Muav Formation lies the Bright Angel Shale, an aquitard. The R-aquifer is the regional aquifer, and supplies groundwater to many ephemeral springs in the Grand Canyon region (Tobin et al., 2018).

The hydrogeology of the Grand Canyon has been the interest of research for decades (Metzger, 1961, Tobin et al., 2018), and can most simply be characterized as complex and highly variable. Response times and average residence times of groundwater within the region have

been shown to vary immensely, ranging from days to centuries (Goings, 1985; Monroe et al., 2005; Schindel, 2015; Jones et al., 2017). This complexity and heterogeneity can be in part attributed to the complex structural features and karst formation common in the R-aquifer that result in vertical connectivity between the C and R aquifers (Metzger, 1961; Huntoon, 1974; Zukosky, 1995). Further variation occurs between the South and North Rims, with most high flow springs occurring along the North Rim beneath the Kaibab Plateau (Tobin et al., 2018). The South Rim hosts ephemeral springs which often have lower discharge than their North Rim counter parts, in large part due to the higher elevation of the North Rim, subsequent prevalence of larger snowpacks, and orientation of the geologic strata. A further layer of complexity is the role of inner-basin alluvial material acting as small drainage-confined aquifers. It is likely that groundwater discharging from the R-aquifer mixes with small alluvial aquifers contained within drainages (e.g. Horn Creek and Salt Creek). These small, localized aquifers may act as a sink for recent rainfall, potentially introducing a more modern component to groundwater from the R-aquifer as flow moves toward the Colorado River.

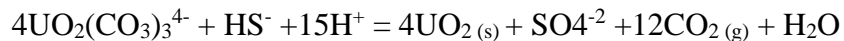
Placing this regional characterization into the context of this study, springs have been documented to discharge from the Muav Limestone, Bright Angel Shale, Tapeats Sandstone, inner-basin alluvial material, and the Proterozoic basement. The geochemistry of Horn and Salt Creek springs have been shown to be anomalous relative to other South Rim groundwaters (Beisner et al., 2020), and have been shown to have record levels of dissolved uranium for the region (Scharr, unpublished 2011; Tillman et al., 2021). This study integrates previous research with a modern data set to further characterize the hydrogeology of Horn Creek and Salt Creek with a particular focus on the behavior of dissolved uranium.

2.1.3 Uranium Hydrogeochemistry

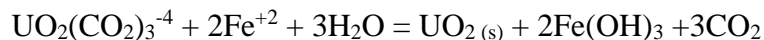
Uranium is a contaminant of concern, and currently the US EPA sets its Maximum Contaminant Level at 30 µg/L for drinking water (US EPA, 2021) while the Canadian government sets a Maximum Contaminant Level of 15 µg/L for aquatic health (CCME, 2011) and the US EPA Maximum Contaminant Level Goal (MCLG) is zero µg/L (US EPA, 2021). Uranium has 3 isotopes, U^{234} , U^{235} , and U^{238} . U^{234} and U^{238} are common, and the ratio U^{234}/U^{238} can be used as an environmental tracer for groundwater as well as age dating (Fetter et al., 2018). Uranium has 3 valence states, U^{+4} , U^{+5} , and U^{+6} . Through oxidation-reduction (redox) reactions, uranium can change valence states from U^{+4} to U^{+6} and vice versa. A common redox reaction is given in Fetter et al. 2018:



Generally, U^{+6} is more mobile in solution than U^{+4} , with U^{+6} tending to form complexes with many inorganic anions such as hydroxide, phosphate, fluoride, carbonate, and sulfate. A major control on the formation of these complexes is pH. In the presence of reduced Fe or S, U may be reduced from U^{+6} to U^{+4} resulting in the precipitation of Uranite (UO_2). Uranite is understood to be highly insoluble. Either oxidation of HS^- to SO_4^{-2} or the oxidation of ferrous iron to ferric hydroxide could create conditions that would reduce U, such that:



and



In mining environments, heavy metals are often mobilized into solution, including uranium. During flooding events in a uranium mine, uranium deposits may be flooded, and groundwater could subsequently be contaminated with extractable uranium compounds from

exposed bare rock that were oxidized due to exposure to the atmosphere during mining processes. Dissolution of precipitated salts from mining activities also occurs as a mine is inundated, with a dramatic increase in total dissolved solids in solution along with an increase in U and other associated metals (Rapantova et al., 2012). Flooding in the early stages after mine abandonment also results in the dissolution of secondary U minerals that were deposited during mining activities. Over decades, other studies have noted trends in decreasing U in solution, with some mines in the Czech Republic exhibiting trends that resulted in mines past 40 years of abandonment discharging groundwater with U concentrations less than the US EPA MCL. This phenomenon has not been observed at the Upper Horn Bedrock spring, with no discernable temporal trend in U concentrations (Beisner & Tillman 2020).

2.1.4 Stable Isotope Chemistry

Elements differ in nature with different mass numbers. These variations stem from a difference in the number of neutrons present in the nucleus and are known as isotopes. Hydrogen and Oxygen, the two elements that make up water, have corresponding isotopes ^1H and ^2H (deuterium) and ^{18}O , ^{17}O , and ^{16}O . These isotopes are referred to as stable isotopes because these isotopes do not engage in nuclear transformations and are therefore “stable” (Appelo and Postma, 2005). Other isotopes that do engage in nuclear transformations are known as radioactive isotopes and will decay over time. Examples of these elements include ^3H and ^{14}C and can be used for age dating based on their known half-lives (Appelo and Postma, 2005). The difference in mass of stable isotopes means that these isotopes will behave differently in nature. This difference is observed in a process known as isotopic fractionation, occurring during the phase change of water. As water evaporates, lighter isotopes of oxygen and hydrogen

preferentially evaporate. And vice versa, heavier isotopes of oxygen and hydrogen preferentially fall back to Earth as precipitation. These differences in stable isotopic ratios can be used as an environmental tracer to understand more about the climate at the point of groundwater recharge or the provenance of the water (Gat, 1996; Appelo and Postma, 2005).

d^2H and $d^{18}O$ represent the ratio of $^{18}O/^{16}O$ and $^2H/^1H$, and their linear relationship was first documented by Craig (1961) in the construction of a Global Meteoric Water Line (GMWL). The GMWL is defined as $d^2H = 8 * d^{18}O + 10$ and reflects the average global relationship between $d^{18}O$ and d^2H . The linear relationship of $d^{18}O$ and d^2H are a function of the isotope fractionation mentioned above and is controlled by both temperature and humidity (Putman et al., 2019). Because of this relationship with temperature and humidity, more depleted stable isotope samples (lighter in mass) or enriched (heavier in mass) allow insight into the climate at the point of groundwater recharge, with a depleted isotope sample indicating either colder recharge (winter precipitation) or recharge at higher elevations. And vice versa, an enriched stable isotope sample indicates either warmer recharge (summer precipitation) or recharge at a lower elevation. Many studies have used stable isotopes as environmental tracers for groundwater and more specifically springs in the American Southwest (Ingraham and Taylor, 1991; Zukosky, 1995; Ingraham et al., 2001, Springer et al., 2017; Beisner et al., 2020; Solder and Beisner, 2020), defining regional relationships for stable isotopes and zones of recharge.

A Local Meteoric Water Line (LMWL) represents the relationship between d^2H and $d^{18}O$ at a specific site, and although the GMWL has a slope of 8, this is a global average. Putman et al. (2019) found slopes of LMWLs range between 4.8 to 10.9, and intercepts ranged from -24‰ to +27‰. This variation in LMWLs is a function of the processes mentioned above, and the variance in humidity and temperature across different climates. Putman et al. (2019) found that

nonequilibrium processes such as sub-cloud evaporation, remoistening of the atmosphere from rain, and snow formation conditions may be responsible for the variation of LWML across the globe. Temperate regions tend to have a slope within the range of 8 and 9 with intercepts ranging from 5‰ to 20‰, subtropical arid or seasonally hot and dry regions tend to have slopes ranging from 5 to 7 with intercepts ranging from 0‰ to 15‰, while humid temperate, seasonally snow dominated regions, and cryosphere climates tend to have slopes ranging from 7 to 8 with intercepts ranging from -20‰ to 5‰ (Putman et al., 2019). Solder and Beisner (2020) characterized the LMWL of the South Rim of the Grand Canyon and Coconino Plateau as having a slope of 6.49 with an intercept of -6.2‰. Solder and Beisner (2020) also characterized the Groundwater Line (GWL) using stable isotopes collected at South Rim springs, with the GWL having a similar slope of 6.46 but with an intercept of -12‰.

2.1.5 Principles of Applied Multivariate Statistics

This section provides a brief introduction to the theory and application of three multivariate statistical analyses performed in this thesis. The first, Principal Component Analysis (PCA), is a statistical analysis that is applied to complex multivariate data sets and can be simply understood as a data reduction technique. Its application is wide ranging and is especially useful when looking at the variance of groundwater chemistry of springs (e.g., Kremer et al. 1996, Swift Bird et al. 2020). More specifically, a PCA describes the variance within a multivariate data set such that Principal Components are extracted to explain a particular linear combination between variables (Everett & Dunn, 2001). Each Principal Component that is extracted is orthogonal to other Principal Components. Principal Components are extracted based on the amount of variation they describe. As such, the first Principal Component describes the largest

amount of variation, the second component describes the second largest amount of variation, and so on. Each component captures the maximum variability not captured by the previous components, such that the sum of multiple Principal Components will account for x amount of variability (e.g., if the first Principal Component describes 38% of the variability, and the second Principal Component describes 25%, it can be said that Principal Components 1 and 2 describe 63% of the variability) (Everett & Dunn, 2001). The amount of variation each Principal Component captures is based on its eigenvalue, or the mean sum of squares from the line of best fit generated from the values for each associated variable in PCA (Everitt and Dunn, 2001). As eigenvalues are a representation of variation, the percent amount of variation explained by PC x can be determined by its eigenvalue relative to the other eigenvalues of the remaining Principal Components. PC1 will have the largest eigenvalue as it explains the largest amount of variance, PC2 considers the second most amount of variance, and so on. Thus, complex data sets with more than 3 variables (such as groundwater chemistry) can be plotted relative to one another using their Principal Component scores to graphically represent similarity and dissimilarity.

Additionally, two other multivariate statistical methods commonly applied in hydrogeochemical studies (Guler et al., 2002), Hierarchical Cluster Analysis (HCA) and K-means clustering, are applied in this thesis. Both HCA and K-means clustering group objects (for the purposes of this thesis, objects are groundwater chemistries) based on their similarity or dissimilarity, with the goal of creating groups of objects into the most distinct populations. HCA is an agglomerative clustering method, meaning that its algorithm moves from the “bottom-up” (Kassambra, 2017). Each object (or groundwater chemistry) begins in the algorithm in its own “cluster.” As the algorithm moves forward, the clusters that are the most similar are combined into a bigger cluster. The algorithm continues until one big cluster encompasses all the objects.

K-means clustering aims to accomplish a similar goal to HCA, but in a slightly different way. Before K-means clustering begins, a predefined k number of clusters is given by the user. K-means will then assign random centroids for the k clusters and compute the distances between objects and the assigned centroids, continually adjusting until the distances between items and the corresponding centroid are minimized (Hartigan and Wong, 1979; Kassambra, 2017). In doing so, K-means clustering minimizes variation within clusters while maximizing variability between each cluster.

PCA, HCA, and K-means clustering are applied in this thesis to characterize the variance and similarity of springs in Horn and Salt Creek drainage based on their aqueous chemistry. The methods section describes the chemical analytes included for each analysis, how each analysis is constructed within R studio, and how the analyses are illustrated from R studio.

2.1.6 Principles of PHREEQC

PHREEQC is a hydrogeochemical modeling software that can be used to model water-rock interactions. The software has a wide range of applications, with increasing complexity. For this study, PHREEQC is used to create inverse models of the geochemical evolution of groundwater from a “parent” spring’s chemistry to the “daughter” spring’s chemistry. PHREEQC assumes the differences between the two sampled groundwater chemistries are the result of interactions between the groundwater and minerals and gasses present as defined in the model. Inversely modeled springs are assumed to be hydrologically connected and the modeled system is assumed to be a closed system. As per the User’s Guide to PHREEQC – 07 May 1996, “the object of inverse modeling is to find sets of minerals and gases that, when reacted in appropriate amounts, quantitatively account for the differences in composition between solutions.” Preliminary modeling using data from the 2013 URS survey at the Upper Horn

Bedrock spring and Upper Horn Alluvium spring indicated that under certain conditions, the precipitation of uraninite is possible and the two springs (and their change in chemistry) are feasibly explainable. However, concerns over the quality of some groundwater data requires further modeling using samples collected in 2023. Multiple modeling scenarios were run to distinguish with the inclusion/exclusion of certain minerals if uraninite precipitation is still feasible, as well as evaluate the possibility of mixing groundwaters within Horn Creek drainage.

2.2 Hypotheses

Based on the observed variability of uranium concentrations over time and space along with the quantity of data available due to repeated sampling in the Horn Creek drainage, this site is well suited for a study investigating the controls on dissolved uranium concentrations near mineralized breccia pipes in the Grand Canyon. The hypotheses for this study are as follows:

- 1) There is a strong correlation between fluctuations in total precipitation and fluctuations in dissolved uranium content levels at UHB spring.
- 2) There is a 1- to 2-month lag time between fluctuations in total precipitation and fluctuations in dissolved uranium content levels in the Horn Creek area corresponding to the observed lag time by Goings (1985) in 1983-84.
- 3) Change in water chemistry driven by redox reactions results in the precipitation of Uraninite, explaining the decreasing concentration of U in groundwater further down the Horn Creek drainage.
- 4) Groundwater with high concentrations of uranium mix with a separate source of groundwater, explaining the decreasing concentrations of U in groundwater further down the Horn Creek drainage.

Chapter 3: Materials and Methods

3.1 Field Collection Methods

Groundwater samples were collected from 11 different sampling locations across Bright Angel drainage, Horn Creek drainage, and Salt Creek drainage across three separate 4-day backpacking trips in the months of November 2022 and March 2023 (see Fig. 2 for sampling locations). During the November 2022 groundwater surveys, samples were collected for stable isotopes (deuterium and oxygen-18), trace elements (Ag^+ , Al^{3+} , As^{3-} , B^{3+} , Ba^{2+} , Be^{2+} , Cd^{2+} , Co^{3+} , Cr^{3+} , Cu^{2+} , $\text{Fe}^{2+/3+}$, Li^+ , Mo^+ , Ni^{2+} , Pb^{2+} , Sb^{3+} , Se^{2-} , $\text{Si}^{4+/4-}$, Sr^{2+} , Ti^{4+} , U^{4+} , V^{5+} , W^{6+} , Zn^{2+}), total organic and inorganic carbon, total nitrogen, and a suite of ions (F^- , Ca^{2+} , Mg^{2+} , Na^+ , K^+ , Cl^- , Br^- , NO_3^- , NO_2^- , SO_4^{2-} , PO_4^{3-}) and then shipped to University of Nevada, Reno CORE Laboratory and University of Nevada, Reno Stable Isotope Laboratory (samples included Upper Horn Bedrock, Upper Horn Alluvium, Lower Horn Alluvium, Battleship Pools, Upper Salt Creek – East, Upper Salt Creek – West, Lower Salt Creek Vishnu, and Havasupai Gardens). For the March 2023 data set (Upper Horn Bedrock, Upper Horn Alluvium, Lower Horn Bedrock, West Horn, Upper Horn Bedrock-Below), samples were collected for stable isotopes (oxygen-18 and deuterium), trace elements (As^{3-} , Ce^{3+} , Dy^{3+} , Er^{3+} , Eu^{3+} , $\text{Fe}^{2+/3+}$, Gd^{3+} , Ho^{3+} , La^{3+} , Mn^{4+} , Nd^{3+} , Pb^{2+} , Pr^{3+} , Sb^{3+} , Se^{2-} , Sm^{3+} , Sr^{2+} , Tb^{3+} , Th^{4+} , U^{4+} , Yb^{3+}), total organic and inorganic carbon, total nitrogen, and a suite of ions (Ba^{2+} , Ca^{2+} , K^+ , Mg^{2+} , Na^+ , F^- , Cl^- , Br^- , SO_4^{2-} , NO_3^- , PO_4^{3-}). Alkalinity was also measured in November 2022 and March 2023 in the field using a Hach Titration kit following method 10244 outlined in the Hach user's manual (Hach Company, 2014).

All analytes were collected following established methods outlined in this paragraph. Stable isotopes were collected using a grab method. A 30mL HDPE plastic bottle was rinsed with spring water and then submerged as close as possible to the orifice of the spring, collecting a sample beneath the surface to minimize exposure to the atmosphere. Samples were collected with as minimal head space as possible. Trace metals were collected following USEPA method 200.7, Rev. 4.4 (USEPA, 1994). Trace metal sample bottles were acid washed prior to field work, and then double bagged. Samples were collected using a 60 mL syringe, which was rinsed 3 times with host water, before being passed through a 0.45 μ m filter in the field. Samples were double bagged, and samples were collected by personnel wearing special trace metal gloves, with a second sampler wearing nitrile gloves to help seal the outer bag and store it. Trace metal samples were kept on ice in a cooler before being transferred to a refrigerator. Acidification was done in a UNLV laboratory the Monday following field work, with the longest time between field collection and acidification not exceeding 72 hours. Total carbon/nitrogen samples were collected using a 60 mL syringe and then passed through a .45 μ m filter in the field, following USEPA SW-846 Ch. 3 guidelines (USEPA, 2018). Major ions were collected similarly, with samples collected near the orifice using a 60 mL syringe and then passed through a .45 μ m filter in the field, following USEPA SW-846 Ch. 3 guidelines (USEPA, 2018). The sampling syringe was triple rinsed between sampling sites, and a new filter was used at each sampling site. Other field collection included measuring pH, electrical conductivity (EC/SC), total dissolved solids (TDS), H₂O temperature, and air temperature using VIVOSUN Digital pH meter. The pH probe was calibrated using 4.01 pH and 7.01 pH solution every morning prior to field measurements.

Once samples were collected in November 2022, they were carried out of the canyon and transported to Las Vegas. Trace metal samples were acidified using 2% HNO₃ at UNLV

laboratory and then refrigerated. All samples were shipped to the University of Nevada, Reno (UNR) CORE Laboratory and UNR Stable Isotope Laboratory for analysis within the week. The UNR CORE Laboratory measured major ions by Ion Chromatography using a Dionex ICS-3000 (a hydroxide eluent-based system), following EPA 300.1 method (UESPA, 1997), using Dionex AS-19 column. The UNR CORE Laboratory measured trace metals using a Shimadzu 2030 ICPMS following the 200.8 USEPA method (USEPA, 1994). Total organic carbon and total nitrogen were measured using the Shimadzu TOC-L with a TNM-L module (nitrogen) and ASI-L autosampler following the US EPA 9060A method (USEPA, 2004). The UNR Stable Isotope Laboratory measured oxygen-18 and deuterium by laser spectroscopy technique, after the method of List et al. (2008). Analyses were performed using a Picarro L2130-I cavity ringdown spectrometer, using U. S. Geological Survey (USGS) water isotope standards USGS49 and USGS50 for calibration.

Once samples were collected in March/April 2023, they were carried out of the canyon and transported to Las Vegas. Trace metals were acidified using 2% HNO₃ at a UNLV laboratory and then refrigerated. All samples were either shipped to UNR CORE Laboratory or the Isotech Laboratories, Inc. in Champaign, Illinois. The trace metal samples were analyzed using ICP-MS as described previously. Stable Isotopes and a suite of ions were analyzed by Isotech. The stable isotopes were analyzed using a Picarro CRDS (cavity ringdown spectrometer) model L1102-I fitted with a Leap autosampler. Cations (Ba²⁺, Ca²⁺, Fe^{2+/3+}, K⁺, Mg²⁺, Mn⁴⁺, Na⁺, Sr²⁺) were analyzed using ICP-OES while anions (F⁻, Cl⁻, Br⁻, SO₄²⁻, NO₃⁻) were analyzed using Ion Chromatography. PO₄³⁻ was analyzed using SM 4500-P E. No further clarification was provided by Isotech regarding their specific laboratory methods (Wright personal communication, 2023).

3.2 Precipitation and Uranium Comparison Methods

Data for total dissolved uranium and rainfall were collected from historical records and then analyzed using RStudio. Data for total dissolved uranium was compiled from studies sampling as far back as 1995 (Fitzgerald, 1996), however Fitzgerald (1996) did not record total dissolved U concentrations (only U^{238}). Fitzgerald did record both U^{234} and U^{238} activities in pCi/l. As such, the period of data included for rainfall analysis begins with Liebe's data (2003) to present. Four data points were compiled from Liebe, 2003 (6/5/02, 6/25/02, 7/16/02, 7/30/02), one data point was compiled from an unpublished data set collected in 2011 by a UNLV doctoral student, Melissa Scharr (01/11/11), one data point was compiled from an unpublished data set collected by URS Inc. in 2013 (10/21/13), fourteen data points were compiled from USGS records (U.S. Geological Survey, 2022) (05/01/18, 03/14/19, 04/16/19, 04/16/19, 04/18/19, 10/08/19, 12/2/19, 1/21/20, 6/2/20, 4/27/21, 11/3/21, 12/22/21, 3/22/22, 4/20/22), and two data points were included from this study's sampling conducted in November of 2022 (11/11/22) and March of 2023 (3/31/23). The result of this compilation is 22 data points collected across the past two decades.

To compare historical precipitation to dissolved uranium, an established weather station is required. There is no weather station situated in Horn Creek drainage or directly above it on the Rim. Consequently, The National Climatic Data Center's *Climate Data Online* (CDO) portal (<https://www.ncdc.noaa.gov/cdo-web/>) was used to locate nearby weather stations to the Horn Creek drainage. The three closest weather stations are Phantom Ranch weather station (GHCND:USC00026471), approximately 5.5 km (3.4 mi) to the east north east, with a period of record from 1966 to present (36.1066°, -112.0947°; elevation 771.1 m AMSL (2529.9 ft AMSL)), Grand Canyon Airport weather station (GHCND:USW00003195), approximately 13.3

km (8.26 mi) to the south, with a period of record from 1996 to present (35.94581°, -112.15536°; elevation 1993.3 m AMSL (6539.7ft AMSL)), and two weather stations in Grand Canyon Village, approximately 2.5 km (1.55 mi) to the south east, that combined together provide a period of record that matches the period of record of the dissolved uranium data set (Fig. 6). The first weather station is the Grand Canyon Visitor Center (GHCND:USC00023582) with a period of record from October of 2011 to present (36.05931°, -112.10943°; elevation 2,158.9 m AMSL) and the second weather station is Grand Canyon National Park 2 (GHCND:USC00023596) with a period of record from 1976 to March of 2012 (36.0527°, -112.1502°; elevation 2,068.1 m AMSL).

Each weather station has a monthly record of Climatological Observations, with 24-hour totals of “rain, melted snow, etc.” and “snow, ice pellets, and hail” recorded in inches at each weather station. All precipitation data were compiled from these NOAA records for 120 days prior to the sampling date for each data point for dissolved uranium at UHB spring. Once precipitation data were compiled, some data gaps were present where no precipitation had been recorded. In these instances where data was missing, precipitation data from the day prior and the day following the missing precipitation data point were averaged and inserted to complete the climate record. To account for snowpack that had not melted, measured snowpack was reduced by a ratio of 10:1 to replicate snowmelt, and was then added to the “rain, melted snow, etc.” recorded for that day.

Once all precipitation and dissolved uranium data were compiled, bivariate analysis was conducted using RStudio. Plots were generated with total dissolved uranium concentrations recorded on the y-axis and total rainfall plotted on the x-axis. Plots were generated by summing precipitation data at various intervals of Days Prior to Sampling (DPS). Weekly intervals (1-7

DPS, 8-14 DPS etc.), bi-weekly intervals (1-14 DPS, 15-28 DPS etc.), staggered bi-weekly intervals (7-21 DPS, 22-35 DPS), three-week intervals (1-21 DPS, 22-42 DPS), four-week intervals (1-28 DPS, etc.), and at eight-week intervals. Initial patterns in conjunction with Spearman's rho correlation coefficients were used to determine further time intervals to investigate. Plots that had the highest Spearman's rho correlation coefficients prompted further linear regression, this time using different time intervals of sums of DPS (e.g. 62-72 DPS, 62-73 DPS, 62-74 DPS, etc.). This comparison was repeated using Phantom Ranch precipitation data, Grand Canyon Airport precipitation data, and Grand Canyon Visitor Center data. In total, 93 plots were generated for precipitation data from each weather station (279 total plots), with correlation analysis performed on each plot comparing dissolved uranium to precipitation data at varying time intervals.

3.3 PHREEQC Inverse Modeling Methods

PHREEQC Interactive version 3.7.3.15968 (Parkhurst and Appelo, 2013) was used to investigate the geochemical evolution of groundwater in Horn Creek drainage. More specifically, the evolution in groundwater chemistry between UHB spring and UHA spring. Inverse models were created using major ion chemistries of UHB spring, UHA spring (sampled in April 2023) and EHC-BS (sampled in October 2013). Two scenarios were modeled, one scenario with UHB as the sole parent spring and a second scenario with EHC-BS and UHB both as parents. Considerations were made regarding the minerals present in the system based on literature review from other studies conducted in the Grand Canyon.

First, considerations were made for which springs should be used for the inverse model and which data from which study should be chosen. To reduce temporal variability, chemistries

of UHB and UHA springs were sampled on the same day in the Spring of 2023 and used in these modeling scenarios. The springs are inferred to be hydrologically connected (a necessary characteristic of any springs used in an inverse model) based on several factors. First, the primary source of U in the drainage is understood to be the Uraninite hosted in the breccia pipe directly above UHB spring (Tillman et al., 2021). The presence of dissolved U at UHA spring is one indication that just like UHB spring, groundwater discharging from the spring previously interacted with a uranium bearing mineral, likely uraninite situated in the nearby breccia pipe. A second spring, EHC-BS, has been sampled once on record in the eastern sub-drainage of the Horn Creek drainage. The sample was collected in October of 2013 (URS Inc., 2014). Both UHB spring and EHC-BS springs are situated further up drainage from UHA spring and are therefore inferred to be “parent” springs to UHA spring in the modeling scenario where two “parents” are included.

Next, considerations were made regarding which minerals to include in the input file to indicate which minerals were present in the system. UHB spring discharges from the Muav Limestone and UHA spring discharges from inner basin alluvial material. Due to not being able to take field samples, minerals were selected based on geologic unit descriptions taken from Beus and Morales (1990), Snelling (2021) which looked at mineral compositions in the Bright Angel Shale, and from Chenoweth (1986) which describes in detail the minerals present in the breccia pipe. Kaolinite, hematite, and dolomite were included (Beus and Morales, 1990). Quartz, potassium-feldspar, dolomite, and illite were included from the Bright Angel Shale (Snelling, 2021). Halite was included in some modeling scenarios but was only allowed to precipitate out of solution as an evaporite. Exploratory modeling included uraninite, gypsum, and pyrite based on their documentation in the mined breccia pipe (Chenoweth, 1986). It is highly unlikely that

these minerals would be present under normal circumstances, it is possible that during mining operations exposed tailings may have been transported into the inner-basin alluvial material directly below the mine. It is important that exploratory modeling considers these minerals when considering changing concentrations of uranium as they may allow for reduction-oxidation reactions to occur as a mechanism for uraninite precipitation.

Once considerations were made for springs to be modeled, the source of the water quality data and the minerals present, the input files for each modeling scenario were constructed. The uncertainty was set to the lowest possible value that would still yield models. The range section was left blank. The Lawrence Livermore National Laboratory (LLNL) database in PHREEQC was used as all the minerals included in the inverse model were also present in the LLNL database. In some scenarios, input files were able to run, but 0 models were returned. When the input files ran without error but produced 0 models, it was because too few minerals had been included or the uncertainty was too low. Uncertainty was increased until models were returned.

PHREEQC Modeling Scenarios

Water-rock interactions were modeled for two scenarios. Scenario 1 (S1) models the hydrogeochemical evolution of groundwater from Upper Horn Bedrock (UHB) to Upper Horn Alluvium (UHA). In this scenario it is assumed that only water-rock interactions control the change in chemistry between the sampling locations. Scenario 2 (S2) models the hydrogeochemical evolution of groundwater from Battleship spring (EHC-BS) and Upper Horn Bedrock (UHB) spring to Upper Horn Alluvium (UHA) spring. In S2, it is assumed that water-rock interactions and mixing between EHC-BS spring and UHB spring are the two controls on the observed change in chemistry at UHA spring.

Scenario 1

Within S1, six separate modeling “runs” were conducted with each run differentiated by the minerals included and the inclusion or exclusion of dissolved uranium. Scenario1-Run1 (S1.R1) included minerals documented in the literature from the known lithology and excluded dissolved uranium in the chemistries of UHB and UHA springs. S1.R1 models the change in major ion chemistry from UHB to UHA via water-rock interactions. Scenario1-Run2 (S1.R2) includes the same minerals as in S1.R1 plus uraninite and the measured dissolved U at UHB and UHA. S1.R2 models the change in major ion chemistry and dissolved uranium concentrations via water-rock interactions with the known lithology. Scenario1-Run3 (S1.R3) includes the same minerals as in S1.R2 plus Pyrite, a mineral found in the breccia pipe, but not documented in the literature in the typical lithology of the region. S1.R3 models the change in major ion chemistry and dissolved uranium chemistry from UHB to UHA via water-rock interactions if pyrite were present in the inner basin alluvial material. Scenario1-Run4, Scenario1-Run5, and Scenario1-Run6 all mirror the input parameters S1.R1, S1.R2, and S1.R3, respectively, with the addition of the mineral halite which was told to precipitate out of solution. S1.R4 corresponds to modeling parameters of S1.R1 plus halite, S1.R5 corresponds to S1.R2 plus halite, and S1.R6 corresponds to S1.R3 plus halite.

Scenario 2

Within Scenario 2 are five separate modeling “runs” with each run differentiated by the minerals included and the inclusion or exclusion of dissolved uranium in the spring chemistry, similar to Scenario 1. Scenario2-Run1 (S2.R1) includes the known minerals in the lithology along the flow path and excludes the sampled dissolved uranium at UHB, EHC-BS, and UHA

springs. Scenario2-Run2 (S2.R2) has the same minerals inputs as S2.R1 and includes the mineral halite, which was told to precipitate. Scenario2-Run3 (S2.R3) included the same minerals as S2.R2, except hematite was excluded from the inputs. Scenario2-Run4 and Scenario2-Run5 had identical inputs to S2.R1 and S2.R2, except that dissolved uranium is included in the groundwater chemistry inputs for UHB, EHC-BS, and UHA springs. S2.R4 corresponds with the inputs of S2.R1 and S2.R5 corresponds to S2.R2.

3.4 Multivariate Statistical Methods

Three multivariate statistical methods are performed in this thesis: Principal Component Analysis (PCA), Hierarchical Clustering Analysis (HCA), and K-means clustering. The three multivariate analytical methods are performed on three separate data sets, with each data set including certain analytes and groundwater chemistries to compare variance over time, spatial variance in overall groundwater chemistry, and spatial variance in uranium correlated analytes. The following section discusses how each analytical method is constructed using R studio and the data included in each analysis.

Correlation Matrices Design

Correlation matrices were created using R studio. Data was standardized using the `scale()` function from the base R studio package. Pearson's r coefficients were calculated using the `cor()` function for the `corrplot` package (Wei and Simko, 2021) in R studio and the `rcorr()` function from the `Hmisc` package (Harrell, 2023) in R studio. The `rcorr()` function was also used to yield p-values for the Pearson's r coefficients. Only coefficients with p-values $<.05$ were included in

the final correlation matrix figures. Coefficients with p-values >0.05 were left “blank” in the correlation matrices (fig. 7).

Principal Component Analysis Design

To perform the Principal Component Analysis (PCA), the `prcomp()` function from the base package R was used to perform PCA on the input matrix. Variables were standardized about a mean of zero, scaled to have unit variance take place before the analysis, and rotated (Guler et al., 2002; Zhang and Castello, 2017). The results of the `prcomp()` function were run in the `fviz_eig()` function from the “factoextra” package (Kassambra and Mundt, 2020) to create an eigenvalue plot displaying the variance against the number of dimensions (Principal Components). Several functions from the “factoextra” package in R were used to create biplots illustrating the relationships between analytes and groundwater chemistry with Principal Components 1-4. The `fviz_pca_var()` function was used to plot vectors of the analytes. A 3-dimensional plot displaying the relationship of groundwater chemistry to PC1, PC2, and PC3 was created using `scatterplot3d()` from the “scatterplot3d” package (Ligges and Mächler, 2003). Inputs from the `prcomp()` function were put into the `ggplot()` function and `stat_ellipse()` function from the “ggplot2” package (Wickham, 2016) to create biplots where the springs were grouped by their geology (bedrock/alluvium and their specific geologic units) .

Hierarchical K-means Clustering Design

Hierarchical cluster analysis (HCA) and K-means cluster analysis were combined using R-studio to classify distinct groups of sampling locations based on their chemistry. Data were first standardized using the `scale()` function from the base package of R. Next, an optimal number of clusters was determined using the `fviz_nbclust()` function from the factoextra package

in RStudio (Kassambra and Mundt, 2020). Then, standardized data were input into the `hkmeans()` function from the `factoextra` package in RStudio. The linkage rule applied is Ward's method (Ward, 1963), which calculates the error sum of squares, or the sum distance from each individual sample to the center of its respective cluster (Judd, 1980). Euclidean distances are used to measure similarity/dissimilarity (Guler et al., 2002; Kassambra, 2017), and the Hartigan-Wong (1979) algorithm is used for the K-means algorithm. The results from the `hkmeans()` are then plotted in a hierarchical dendrogram using the `fviz_dend()` from the `factoextra` package in RStudio and a K-means biplot using the `fviz_cluster()` functions from the `factoextra` package in RStudio.

Data Selection and Analytical Scenarios for Multivariate Analyses

Both PCA and HK-means clustering are performed on three separate data sets in this thesis. The first data set compares variation in groundwater chemistry between springs sampled in Horn and Salt Creek drainage in 2013. The second data set compares variation in groundwater chemistry over time in Horn Creek drainage between 2013 to 2023. The third data set compares variation in groundwater chemistry associated specifically with dissolved uranium and correlated analytes across Horn and Salt creek drainage using data collected in 2013.

The first data set comparing variation in groundwater chemistry across Horn and Salt Creek drainage includes fifteen groundwater chemistries collected by URS, Inc. (2014) in October of 2013. All variables denoted (T) for total in URS, Inc. (2014) were excluded from the data set. Additionally, Sb^{3+} , Be^{2+} , Cd^{2+} , Cr^{3+} , $\text{Fe}^{2+/3+}$, Re^{+7} , Ag^{+} , and W^{6+} were excluded because they were consistently below the minimum laboratory reporting limit. The first data set includes 27 analytes (Al^{3+} , As^{3-} , Ba^{2+} , B^{3+} , Ca^{2+} , Co^{3+} , Cu^{2+} , Li^{+} , Mn^{4+} , Mo^{+} , Ni^{2+} , Se^{2-} , $\text{Si}^{4+/4-}$, Na^{+} , Sr^{2+} ,

Th⁴⁺, U⁴⁺, V⁵⁺, Zn²⁺, Cl⁻, F⁻, SO₄²⁻, TIC, Total Alk., U²³⁴, U²³⁵, δ¹⁸O) after correlated variables were removed (e.g. Wilson et al., 2022). TDS (strong correlations with Ca²⁺, Mg²⁺, K⁺, and SO₄²⁻), U²³⁸ (strong correlation with U), Mg²⁺ (strong correlations with TDS, Ca²⁺, and K⁺), K⁺ (strong correlations with Li⁺ and Mg²⁺), and δ²H (strong correlation with δ¹⁸O) were all removed from the comprehensive PCA .csv input file to avoid redundancy in the PCA. No substantial differences were noted between the PCA of all chemical analytes and the PCA removing correlated variables.

A second data set comparing groundwater chemistries sampled in 2013 and 2023 included nine samples. Five spring chemistries from 2023 were included (UHB, UHA, WHC, LHB, and UHB-below) and four spring chemistries from 2013 were included (UHB, UHA, WHC, and LHB). The two data sets had 19 analytes in common (As³⁻, Ba²⁺, Ca²⁺, K⁺, Mg²⁺, Mn⁴⁺, Na⁺, Se²⁻, Th⁴⁺, U⁴⁺, TIC, Sr²⁺, F⁻, Cl⁻, SO₄²⁻, Alkalinity, δ²H, δ¹⁸O, and TDS), and these were included in the PCA input file. Highly correlated analytes were not removed from this PCA.

A third data set included five analytes: uranium, analytes with a high correlation with uranium (As³⁺, Se²⁻, Mo⁺), and sulfate. The data set included groundwater chemistries collected in October 2013 by URS Inc. (2014). Only springs were included in this analysis (no sampling locations at the end of reaches), totaling 11 groundwater chemistries. SO₄²⁻ did not have a significantly strong correlation with U within the data set, however when LHB is removed a stronger correlation emerges. Additionally, SO₄²⁻ is the only major ion that has drastic change in concentration between UHB and UHA, a flow path of primary interest for this study due to the drastic change in dissolved U also observed between these two springs. LHB has elevated U, and

has extremely elevated SO_4^{2-} , in accordance with elevated concentrations of many of the other major ions in its chemistry. It is possible that the elevated SO_4^{2-} is due to both the springs lithology, as well as potential influence from interactions with the U ore body, and thus SO_4^{2-} was included.

3.5 Stable Isotopes and Water Chemistry Interpretation Methods

Stable isotopes collected in October of 2013 (URS Inc., 2014) from across the drainage were compiled. Stable isotopes were also compiled from Zukosky (1995) and the USGS for both UHA and UHB (U.S. Geological Survey, 2022). Stable isotopes were plotted using Microsoft Excel to compare trends in seasonality and elevation across springs. The GWML (Global Water Meteoric Water Line) was plotted from Craig (1961), and the LMWL and GWL (Local Meteoric Water Line and Groundwater Line, respectively) for the South Rim of the Grand Canyon region were plotted from Solder and Beisner (2020). A line of best fit was calculated using Microsoft Excel's linear regression tool for the stable isotopes collected by URS in 2013 and samples collected for this study. Microsoft Excel was also used to evaluate correlations between dissolved U at UHB and $\delta^2\text{H}$ and $\delta^{18}\text{O}$, $\delta^2\text{H}$ and elevation, $\delta^{18}\text{O}$ and elevation. To evaluate relationships between elevation and stable isotopes, data from URS (2014) was compiled. To evaluate correlations between dissolved U and $\delta^2\text{H}$ and $\delta^{18}\text{O}$, data were compiled from the URS report (2014), the USGS (U.S. Geological Survey, 2022), and data collected during this study.

Chapter 4: Results

4.1 General Results of Field Sampling

Springs in November of 2022 and April of 2023 were sampled for basic water quality parameters, major ions, trace metals, and stable isotopes. This first section will describe the general trends observed in the water quality parameters, major ions, and trace metals. A full suite of major ions was not analyzed in samples collected in November of 2022 due to a complication with the CORE Laboratory's ICP-MS. However, a complete suite of major ions were analyzed for samples collected in 2023. These water chemistries are plotted in a Piper diagram (Fig. 8). UHB and UHB-B plot very similarly and can be characterized as Mg-Ca-SO₄-HCO₃ type while UHA and WHC plot very similarly and can be characterized as Mg-Ca-HCO₃-SO₄ type water. LHB plots separately and can be characterized as Na-Cl-SO₄ type water. Samples collected in 2023 had major ion chemistries very similar to samples collected in October 2013 by URS Inc. All samples collected in 2023 had a charge balance of less than 2%, indicating an accurate data set (Appelo and Postma, 2005). No charge balance or piper diagram were created for November 2022 data due to the absence of SO₄²⁻ in the data set.

pH across the sampling sites ranged from slightly acidic to slightly basic (6.65 at LHB to 7.82 at UHB-B), and water temperatures ranged from 4°C to 14.7°C (39.2°F to 58.46°F), slightly colder than the range of air temperatures observed while sampling (8.4°C to 18.7°C or 47.1°F to 58.5°F). TDS ranged from 650.6 ppm (WHC) to 3360.1 ppm (LHB), with sites sampled in Nov. 2022 having a lower TDS than in April 2023. Dissolved uranium was elevated in March 2023 relative to Nov. 2022 samples, with UHB sampled at 332.5 ppb (201 ppb in Nov. 2022) and

UHA sampled at 71 ppb (5.41 ppb in Nov. 2022) (Fig. 3b, Fig. 3c). While comparing samples collected in 2022 and 2023, no samples exceeded the USEPA MCL for Arsenic in 2022. However, in 2023 samples collected at UHB had elevated As concentrations (16.8 ppb), exceeding the USEPA MCL of 10 ppb. No other contaminants analyzed were above their respective USEPA MCL. Although flow measurements were not collected during sampling, significantly higher flow was observed in both the east and west Horn Creek sub-drainages during the 2023 sampling. A canyon guide offered a qualitative assessment during the March/April survey, stating that the drainages had some of the highest flows he had observed during the time he had worked in the canyon (10+ years).

4.2 Stable Isotopes

Stable isotopes were compiled from USGS (U.S. Geological Survey, 2022), Zukosky (1995), URS (2014), and this study to tabulate data for 9 sites within Horn and Salt Creek drainage, as well as at Havasupai Gardens for comparison. Salt Creek-Top (SC-TOP) had the lightest mean and median $\delta^2\text{H}$ and $\delta^{18}\text{O}$ of the dataset (-89.358‰ and -11.971‰ respectively for mean and -89.6‰ and -12.01‰ respectively for median). East Horn – Battleship (EHC-BS) had the heaviest mean and median $\delta^2\text{H}$ and $\delta^{18}\text{O}$ of the dataset (-58.15‰ and -7.205‰ respectively for mean and median (n=2)). Upper Horn Bedrock (UHB) had the largest range for $\delta^2\text{H}$ and $\delta^{18}\text{O}$ of the data set (13.3‰ and 2.19‰ respectively). Values for stable isotope data within Horn and Salt Creek drainages were compared with values collected by the USGS for 28 groundwater sampling locations across the South Rim region of the Grand Canyon (Beisner et al., 2020) and values collected by Zukosky (1995). Groundwater sampled within Horn and Salt Creek drainages from URS and this study had a $\delta^2\text{H}$ range of 14.3‰ and a $\delta^{18}\text{O}$ range of 2.46‰, while

the 28 groundwater sampling locations from Beisner and others (2020) had a $\delta^2\text{H}$ range of 14.1‰ and a $\delta^{18}\text{O}$ range of 2.57‰. UHA spring has the longest sampling record over time for stable isotopes, with the earliest stable isotopes collected in April of 1993 (Zukosky, 1995). Stable isotopic samples spanning from 1993 to 2023 have no temporal trend and have remained relatively consistent.

Groundwater sampled within Horn and Salt Creek drainages from URS and this study had a slight offset in the median and average value of the 28 groundwater sites included in Beisner and others (2020) and the 11 groundwater sites included in Zukosky (1995), with data from this study and URS having heavier median and mean stable isotopes. Additionally, several of the samples collected by URS and this study had heavier stable isotopic ratios than any samples in Beisner and others (2020) (UHB, LSC, LHB, and WHC). A line of best fit for the stable isotopes from URS and this study was created using Microsoft Excel's Linear Regression function. The line of best fit is $d^2\text{H}=5.7054*d^{18}\text{O} - 21.424\text{‰}$, with an R^2 value of .9454 ($n=19$) (Fig. 9).

Relationships between dissolved uranium and stable isotopes, stable isotopes and elevation, and $\delta^2\text{H}/\delta^{18}\text{O}$ and month collected were plotted in Excel. There was no correlation between dissolved uranium at UHB spring and $\delta^2\text{H}$ ($R^2=.0822$, $n=10$) and a weak negative correlation between dissolved uranium at UHB spring and $\delta^{18}\text{O}$ ($R^2=.3433$, $n=10$). No relationship was found between $\delta^2\text{H}$ and spring elevation ($R^2=.0007$, $n=15$) and no relationship was found between $\delta^{18}\text{O}$ and elevation ($R^2=.0026$, $n=15$) at springs in Horn and Salt Creek drainages. No relationship between sampling date (seasonality) and $\delta^2\text{H}$ ($R^2=.0532$, $n=14$) and $\delta^{18}\text{O}$ ($R^2=.0769$, $n=14$) was found for the sampling record at UHB spring.

4.3 Multivariate Statistics

Correlation Matrix

A correlation matrix was created from groundwater chemistry data collected from 15 sites in October of 2013 by URS, Inc. Only significant correlations ($p < .05$) are shown in Fig. 7. Heavy metals of concern include U and As, and both are recorded over their USEPA MCL at springs in this drainage. Uranium exhibits positive correlations with Se, Mo, As, U^{234} , U^{235} , and U^{238} and has no strong negative correlations. Arsenic has positive correlations with Mo^+ , Ni^{2+} , Se^{2-} , U^{4+} , U^{234} , U^{235} , and U^{238} and has negative correlations with Total Inorganic Carbon and Total Alkalinity (as $CaCO_3$). Other trends to note in the data include δ^2H and $\delta^{18}O$ being highly correlated, Li^+ being highly correlated with the major ions and TDS, and a general relationship that major ions are correlated with one another. The initial mining claim for Orphan Lode Mine was for copper, and a small amount of copper was extracted before uranium mining ever began (Chenoweth, 1986). Cu^{2+} exhibits strong correlations with Co^{3+} , Mn^{4+} , V^{5+} , Zn^{2+} , δ^2H , and $\delta^{18}O$ and exhibits a strong negative correlation with F, however no strong correlation exists between Cu^{2+} and U^{4+} .

Multivariate Analyses for Complete GW Chemistry

A PCA and H-Kmeans cluster analysis were performed on 15 sampling locations in Horn and Salt Creek drainages sampled in October of 2013 by URS, Inc. Spring chemistries were graphed in 2-dimensional and 3-dimensional space based on their relation to Principal Components 1, 2, and 3. Principal Component 1 captured the largest amount of variability (30.6%), Principal Component 2 captured the second largest amount of variability (24.3%), and Principal Component 3 captured the third largest amount of variability (18.4%). Fig. 10 offers

the most insight into grouping spring chemistries, with PC1-PC3 capturing 73.3% of the variance in the data. Squared cosines compute the significance of a component on the observation to the origin (Abdi and Williams, 2010). We can see that PC1 is dominated by Sr^{2+} , B^{3+} , Li^+ , Cl^- , and Na^+ while PC2 is dominated by U^{4+} , Mo^+ , Se^{2-} , U^{234} , and U^{235} (Fig. 11). PC3 is dominated by Zn^{2+} , Mn^{4+} , Cu^{2+} , Co^{3+} , V^{5+} , and $\delta^{18}\text{O}$. When plotting the PCA in 3-dimensional space, a central grouping of sampling locations emerges with four other sampling locations plotting in their own respective grouping.

The H-Kmeans identified 4 clusters (Fig. 12), with the largest cluster including all the alluvial sampling locations, all the sampling locations in West Horn, all the sampling locations in Salt Creek, and NEHC-TOP. This is the same central cluster observed in the 3-dimensional PCA plot (Fig. 10). EHC-BS grouped in its own group and was determined to be more similar to the larger cluster than either of the sampling locations below Lost Orphan Mine or LHB. UHB and UHB-B were more similar to the larger cluster than LHB, resulting in LHB plotting alone in its own group.

Multivariate Analyses for Time Comparison PCA

A PCA and H-Kmeans cluster analysis were performed on a data set composed of samples from October 2013 and March 2023 from Horn Creek drainage. UHB spring, UHA spring, LHB spring, and WHC spring were sampled in 2013 and then again by UNLV researchers in 2023. A ninth data collection point, UHB-Below (2023) was collected at the end of the reach of the creek flowing from UHB spring and was also included in the PCA. Of note, total dissolved U were elevated for each sampling site in 2023 compared to 2013, except at LHB, which observed a decrease in dissolved U from 46 ppb to 36 ppb. The PCA captures 78% of the

variability in its first 3 Principal Components, with the first Principal Component capturing 50% of the explained variability, the second Principal Component capturing 15.7% of the explained variability, and the third component capturing 12.3% of the explained variability (Fig. 13). PC1 is dominated by Cl^- , Na^+ , TDS, Sr^{2+} , SO_4^{2-} , K^+ , and Mg^{2+} while PC2 is influenced strongly by $\delta^2\text{H}$, $\delta^{18}\text{O}$, As^{3-} , and U^{4+} (Fig. 14). The biplot of PC2 and PC3 indicates that $\delta^2\text{H}$, $\delta^{18}\text{O}$, and U^{4+} dominate PC2 the most while PC3 is dominated by Se^{2-} , Alkalinity, Th^{4+} , and U^{4+} (Fig. 15). When plotted in 3-dimensional space, LHB-2013 and LHB-2023 plot in similar regions as do UHA-2013 and UHA-2023, while there is a little more separation between WHC samples (Fig. 13).

Hierarchical K-means clustering indicates that the optimal number of clusters is two, with all groundwater sites clustered together as most similar, and LHB clustered together. The next best number of clusters is four. When separated into four clusters, a general trend emerged that 2013 and 2023 springs clustered together, except for UHB-2013 and UHB-2023 (Fig. 16). The variation between UHB-2013 and UHB-2023 can be observed in the 3-dimensional PCA plot, with significant differences between UHB-2013 and UHB-2023 along the axes of PC2 and PC3 (dominated by U, $\delta^2\text{H}$, $\delta^{18}\text{O}$, Se, Alkalinity, and Th).

Multivariate Analyses of U correlated analytes

Both Principal Component and clustering analyses were performed on a small subset of data from the 2013 URS report that included 11 sampling sites (all spring orifices) and included analytes found to have strong correlations with dissolved U^{4+} (As^{3-} , Se^{2-} , Mo^+ , and U^{4+}) and SO_4^{2-} . PC1 and PC2 captured 80.4% of the explained variance (50.5% and 29.9%, respectively), while PC3 captured 13.7% of the explained variance, for a sum of 94.1% of the explained

variance captured in the first three Principal Components (Fig. 17). PC1 is dominated by U^{4+} and Mo^+ , while SO_4^{2-} and As^{3-} dominate PC2, and PC3 is dominated by Se^{2-} (Fig. 18 and 19). When observing the PC1 and PC2 biplot, UHB is a clear outlier, while WHC and LHB group together.

The Hierarchical K-means clustering analysis performed on the U-specific data set yielded some interesting results. Although the optimal number of clusters is 2, the average silhouette is still relatively high for assigning up to 5 or 6 clusters (Appendix D). When 6 clusters are assigned, it is observed that UHB groups by itself and is the most different compared to the 10 other springs (Fig. 20). WHC and LHB group together, LSC-V and SC-Tonto group together, and LHA-Tonto and LHA group together, NEHC-TOP and SC-TOP group together, and lastly EHC-BS and UHA group together. When the K-means clusters are plotted in 2-D space and only 2 clusters are assigned, we see that UHB is observed to be significantly different from the other springs in the study area (Fig. 21).

4.4 PHREEQC Inverse Modeling

This section describes the general results of PhreeqC inverse modeling as well as the trends in mixing ratios and phase mole transfers observed in the produced models (see Appendix B for specific phase mole transfer values). In total, the PhreeqC modeling scenarios described in the methods section produced 235 models (87 models for Scenario 1 and 148 for Scenario 2). Some models were excluded from analysis due to issues with the solution fractions used in modeling not summing to 100%. In Scenario 1, which simulated the hydrogeochemical evolution of groundwater from Upper Horn Bedrock (UHB) to Upper Horn Alluvium (UHA), models were excluded from further analysis when the solution fraction for UHB was not 100%. As UHB was

the only defined “parent” groundwater source in Scenario 1, 100% of the solution must be used in the modeling to isolate water-rock interactions as the control used to explain changes in chemistry between UHB and UHA. In Scenario 2, simulating hydrogeochemical evolution from two parent springs, EHC-BS and UHB to downgradient UHA, models were excluded from further analysis when the solution fractions for the two input “parent” chemistries did not sum to 100% or when a mixing model only used one “parent” spring in the modeling. Of the 235 models, 88 did not meet the required solution fraction and were excluded from further analysis. The following paragraphs describe the trends observed in the models, broken down into sections by the modeling scenario and then more specifically each modeling run (e.g. S2.R1).

Scenario 1 – Modeling chemical evolution of groundwater between UHB and UHA

Scenario 1-Run 1 (S1.R1)

The modeling parameters of S1.R1 (that excluded dissolved uranium in simulating rock-water interactions from the known formational lithologies between UHB and UHA), produced 16 model outputs, with 13 of those 16 models meeting the required solution fraction for UHB. The phase mole transfers for those 13 models has the following trends. Gypsum is the only mineral to consistently precipitate, while Calcite, Quartz, and Kaolinite consistently dissolve into solution. The behavior of Potassium Feldspar, Dolomite, Illite, and CO_{2(g)} vary across the modeling scenarios. The modeling run required an uncertainty of 5.5% to produce the 16 models.

Scenario 1-Run 2 (S1.R2)

The modeling parameters of S1.R2, (that simulated major ion chemistry changes while including dissolved uranium concentrations between UHB and downgradient UHA), produced 8

model outputs. While no models produced meet the required solution fraction of 100% for UHB, 6 models did return a solution fraction of 99.97%. The phase mole transfers for those 6 models have the following trends. Calcite, Illite, and $\text{CO}_{2(g)}$ precipitate out of solution when present while Potassium Feldspar, Quartz, Dolomite, and Kaolinite dissolve into solution when present. The only mineral with varying behavior across models is Gypsum. The modeling run required an uncertainty of 64.8% to produce the 8 models.

Scenario 1-Run 3 (*S1.R3*)

The modeling parameters of S1.R3, (that modeled the change in major ion chemistry and dissolved uranium chemistry from UHB to UHA if pyrite were present in the inner basin alluvial material), produced 18 models. Of those 18 models, 15 models produced a solution fraction of 100% for UHB. The phase mole transfers for those 15 models have the following trends. Hematite, Gypsum, and Uraninite all precipitate out of solution when present, while Calcite, Quartz, Kaolinite, and Pyrite dissolve into solution when present. The behavior of Potassium Feldspar, $\text{CO}_{2(g)}$, Dolomite, and Illite varies across the 15 models. In S1.R3, reduction-oxidation reactions occur, with Fe^{3+} and U^{4+} decreasing in solution, while SO_4^{2-} increases in solution. The modeling run required an uncertainty of 5.7% to produce the 18 models.

Scenario 1-Run 4 (*S1.R4*)

The modeling parameters of S1.R4, (that excluded dissolved uranium in simulating rock-water interactions from the known formational lithologies between UHB and UHA, but included halite), produced 17 models. Of those 17 models, 15 models have a 100% solution fraction for UHB. The phase mole transfers for those 15 models have the following trends. Gypsum and Halite precipitate out of solution across all models when present while Calcite, Quartz, and

Kaolinite dissolve into solution across all models when present. The behavior of Potassium Feldspar, $\text{CO}_{2(g)}$, Dolomite, and Illite vary across the models. The modeling run required an uncertainty of 5.5% to produce the 17 models.

Scenario 1-Run 5 (*S1.R5*)

The modeling parameters of S1.R5, (that modeled the change in major ion chemistry and dissolved uranium chemistry from UHB to UHA if halite were present in the inner basin alluvial material), produced 11 models. Zero models produced a solution fraction of 100% for UHB, however, similar to S1.R2, 10 models produced a solution fraction of 99.97%. The phase mole transfers for those 10 models have the following trends. $\text{CO}_{2(g)}$, Calcite, Illite, and Halite precipitate out of solution across all models when present while Potassium Feldspar, Quartz, Dolomite, and Kaolinite dissolve into solution across all models when present. The behavior of Gypsum varies across the produced models. Of note, Uraninite is told to precipitate in the modeling parameters, however no models included phase changes for Uraninite. The modeling run required an uncertainty of 64.8% to return the 11 models.

Scenario 1-Run 6 (*S1.R6*)

The modeling parameters of S1.R6 (that modeled the change in major ion chemistry and dissolved uranium chemistry from UHB to UHA if both pyrite and halite were present in the inner basin alluvial material), produced 17 models. 15 of the 17 models have a solution fraction of 100% for UHB. The phase mole transfers for those 15 models have the following trends. Across all models Hematite, Gypsum, Uraninite, and Halite precipitate out of solution when

present. Across all models, Calcite, Quartz, Kaolinite, and Pyrite dissolve into solution when present. The behavior of Potassium Feldspar, $\text{CO}_{2(g)}$, Dolomite, Illite varies across models. In S1.R6 reduction-oxidation reactions occurred, with Fe^{3+} and U^{4+} decreasing in solution while SO_4^{2-} increases in solution. The modeling run required an uncertainty of 5.7%.

Scenario 2 - Modeling hydrogeochemical evolution with two parent springs sources, UHB and EHC-BS, to downgradient UHA

Scenario 2-Run 1 (S2.R1)

The modeling parameters of S2.R1 (included only the documented minerals in the lithology and excluded dissolved uranium concentrations for UHB, EHC-BS, and UHA), produced 34 models. Of those 34 models, 18 models had sufficient mixing between UHB and EHC-BS. The phase mole transfers for those 18 mixing models have the following trends. Quartz, Dolomite, and $\text{CO}_{2(g)}$ dissolve into solution when present while all other minerals have variable behavior across the produced models. Models in Scenario 2 produced mixing ratios in addition to phase mole transfers. 18 models have significant contributions from both “parent” groundwaters, while 16 models only have contributions from one “parent” groundwater. In all 16 of those models, the one parent groundwater is UHB. The greatest contribution of EHC-BS to UHA groundwater in any modeling scenario is 77.2%. Only one model produced this mixing ratio, with 16 out of 18 models having a mixing ratio dominated by UHB groundwater (UHB contribution greater than 50%). The modeling run required an uncertainty of 5.1%.

Scenario 2-Run 2 (S2.R2)

The modeling parameters of S2.R2 (included the documented minerals in the lithology plus halite and excluded dissolved uranium concentrations for UHB, EHC-BS, and UHA) produced 18 models. Of those 18 models, 7 models had sufficient mixing between UHB and EHC-BS while the other 11 models only had contributions from UHB groundwater. The phase mole transfers for those 7 mixing models have the following trends. Gypsum consistently precipitates out of solution when present while $\text{CO}_{2(g)}$, Calcite, Quartz, Dolomite, and Kaolinite dissolve into solution when present. Potassium Feldspar and Illite had variable behavior across models when present. All 7 mixing models are dominated by UHB groundwater, with 28.7% being the highest contribution from EHC-BS in any of the models produced in S2.R2. The modeling run required an uncertainty of 3.8% to produce the 18 models.

Scenario 2-Run 3 (S2.R3)

Hematite was included in all modeling scenarios in Scenario 1, however hematite phase mole changes only occurred in modeling scenarios when pyrite was included (S1.R3 and S1.R6). S2.R3 included known lithologies and halite but removed hematite, testing whether including hematite in a modeling run where pyrite was not present would have an impact on the models. The modeling parameters of S2.R3 produced the same 18 models S2.R2 produced (where hematite was still included). The removal of hematite had no impact on the modeling run, as hematite's exclusion is the only difference between the parameters of S2.R2 and S2.R3.

Scenario 2-Run 4 (*S2.R4*)

The modeling parameters of S2.R4 (included known minerals from the lithology and included the total dissolved uranium concentrations for UHA, UHB, and EHC-BS) produced 48 models. Of those 48 models, 23 models have sufficient mixing between UHB and EHC-BS. The phase mole transfers for those 23 models have the following trends. CO_{2(g)} and Quartz dissolve into solution when present, while all other minerals have variable behavior across the models. While the majority of models (17 out of 23 mixing models) have a mixing ratio dominated by UHB, 6 models return a mixing ratio dominated by EHC-BS. The highest mixing ratio of EHC-BS was 77.2%, present in 5 models. The modeling run required an uncertainty of 5.1% to produce the 48 models.

Scenario 2-Run 5 (*S2.R5*)

The modeling parameters of S2.R5 (included known minerals from the lithology plus halite and included the total dissolved uranium concentrations for UHA, UHB, and EHC-BS) produced 30 models. Of those 30 models, 18 models have sufficient mixing between UHB and EHC-BS. The phase mole transfers for those 18 models have the following trends. Gypsum and Halite precipitate out of solution when present while CO_{2(g)}, Quartz, and Dolomite dissolve into solution when present. Potassium Feldspar, Calcite, Kaolinite, and Illite all have variable behavior across models when present. The mixing ratio is dominated by UHB in all mixing models, with EHC-BS's highest mixing ratio being 27.8%. The modeling run required an uncertainty of 3.8% to produce the 30 models.

4.5 Precipitation and Dissolved Uranium

This section outlines the results of bivariate analysis of recent precipitation (120 days prior to sampling) and dissolved uranium over a period of approximately 20 years. Both the time window (e.g. precipitation falling two weeks prior to sampling) and the climatic record (weather station on the rim versus at the base of the canyon) were compared in this analysis. The range of total dissolved uranium at Upper Horn Bedrock Spring varies greatly over its sampling record, with a minimum of 151 $\mu\text{g/L}$ recorded on January 21st, 2020 (U.S. Geological Survey, 2022) and a maximum recorded of 509 $\mu\text{g/L}$ recorded in January of 2011 (Scharr 2011, unpublished). The average dissolved uranium value is 264.80 $\mu\text{g/L}$, a median value of 238 $\mu\text{g/L}$, and a standard deviation of 83.10 $\mu\text{g/L}$. The data ranges from Summer of 2003 to Spring of 2023. The distribution of dissolved uranium sampling over time is shown in Fig. 22, with no significant linear correlation ($R^2 = .3994$) found between dissolved uranium and time. Upper Horn Bedrock Spring has been sampled in 10 of the 12 calendar months (no samples were collected in February or August), and no relationship between seasonality and dissolved uranium is present, with both the highest and lowest recorded concentrations of dissolved uranium occurring in the month of January.

Comparing the data of the three weather stations, Grand Canyon Airport had the most consistent record of hydroclimatic data (99.81% of days recorded), however snowpack was never measured at this weather station. Phantom Ranch has the second most consistent record of coverage, with both snowfall and rainfall recorded when data was collected (98.41% of days recorded). The two weather stations located in the South Rim Village were stitched together to create a continuous record, however significant gaps in the record are present at this weather station during 2019 and for most of 2020 and early 2021 likely due to the COVID-19 global

pandemic (83.33% of days recorded). These climate data were adjusted as described in the methods section, but it is probable that the length of data gap may result in biased data. Bivariate correlation analysis was replicated for all 3 data sets (the resulting spearman's rho correlation coefficients can be found in Appendix C). Precipitation data at Phantom Ranch yielded the highest spearman's rho correlation coefficients with dissolved uranium and consequently are described in much greater detail in the following paragraphs relative to the other two weather stations' data.

Spearman's rho correlation coefficients range from 1 to -1, with values ranging closer to either extreme exhibiting greater strength of relationship. The most significant observed Spearman's rho correlation coefficient were present for the relationship between Phantom Ranch (PR) and dissolved uranium 57 to 77 days prior to sampling ($R = -0.72$) and 57 to 70 days prior to sampling ($R = -0.71$). Across all three data sets, all elevated rank coefficients tended to be negative. The strongest rank coefficients for GRCA-AP and GRCA-VC rainfall data were present in the period of 57-63 days prior to sampling ($R = -0.63$ and $R = -0.66$ respectively). Negative coefficients indicate the general relationship that as rainfall increases, uranium decreases.

In examining trends, it is important to note that precipitation measured at GRCA-VC in the period of 22 to 28 DPS yielded a correlation coefficient of -0.063 , while the precipitation measured at GRCA-AP in the period of 29 to 35 DPS yielded a correlation coefficient of -0.62 . Although elevated relative to other weekly sampling periods, the elevated ranking scores did not correspond with a qualitative relationship in the data. In the GRCA-VC data for 22 to 28 DPS, the highest dissolved uranium sample corresponds to the third highest rainfall sample, negating a trend of increasing rainfall results in less dissolved uranium at UHB spring. Similarly, in the

GRCA-AP data for 29-35 DPS, the lowest dissolved uranium sample corresponds to minimal rainfall while the third highest dissolved uranium sample corresponds to significant rainfall in the 29-35 DPS window, negating a trend of increasing rainfall results in less dissolved uranium at UHB spring.

R-values less than -0.7 or greater than 0.7 indicate a significant result (Royal Geographic Society, 2005). The only two time periods across any of the three meteorological data sets to yield R coefficients less than -0.7 were 57-77DPS and 50-70DPS for precipitation records at Phantom Ranch. Both plots (Fig. 23) depict a non-linear relationship, with general trends that in dry periods there is relatively high variation in dissolved uranium, while in wetter periods there are consistently low dissolved uranium values, with the lowest dissolved uranium sample corresponding to the wettest period in both 57-77 DPS and 57-70 DPS. More specifically, in the 57-70 DPS period, no values above 200 ppb dissolved uranium were recorded when precipitation exceeded 1 in. As described previously, no significant results were found when comparing GRCA-VC and GRCA-AP meteorological data with dissolved uranium at UHB.

Chapter 5: Discussion

5.1 Multivariate Analyses

A correlation matrix, multiple Principal Component Analyses, and a combination of hierarchical and k-means clustering techniques were used to explore the similarity and dissimilarity of groundwater chemistries across Horn and Salt Creek drainages. The results from the correlation matrix indicate that dissolved U behaves differently in Horn and Salt Creek when compared with previous regional studies. Additionally, three separate multivariate analyses support three separate inferences. When isolating groundwater chemistry over time, UHB is the only groundwater chemistry to vary significantly from itself in samples collected ten years apart. When the variance of groundwater chemistry including all analytes is considered, both proximity to the mineralized breccia pipe and the bedrock lithology of groundwaters emerge as major controls on the variation in chemistry. And finally, when considering only the variance of analytes that behave similarly to dissolved U across groundwater in the drainages, new clusters emerge, highlighting the distinct chemistry of UHB, as well as the similarity between UHA and EHC-BS and the similarity between LHB and WHC. Some of these relationships, in addition to other lines of evidence, may support a conclusion that defunct mine workings play a significant role in the variable chemistry both spatially and temporally in Horn and Salt Creek drainage.

2013 Correlation Matrix

The correlation matrix considered the correlation of all analytes measured in groundwater collected in October 2013. The purpose of this method was to identify which analytes were

correlated with one another, with a specific interest in analytes that behave similarly to dissolved U across springs in the two drainages.

The correlation matrix created using analytes collected in 2013 revealed several strong correlations between analytes and dissolved uranium at springs in Salt and Horn Creek drainage (Fig. 7). However, these relationships differed slightly with other studies examining correlations between dissolved U and other analytes in groundwater in the Grand Canyon region. While positive correlations with U^{4+} were observed for As^{3-} , Mo^+ , Se^{2-} , U^{234} , U^{235} , and U^{238} in this study, Beisner and others (2017) observed statistically significant Kendall's Tau values between U^{4+} and Li^+ , Mo^+ , Se^{2-} , Sr^{2+} , and Zn^{2+} in groundwater discharging along the North Rim of the Grand Canyon. Additionally, Beisner and others (2020) observed statistically significant Kendall's Tau values between U^{4+} and Mo^+ , Se^{2-} , Sr^{2+} , SO_4^{2-} , Ba^{2+} , and As^{3-} in groundwaters discharging on the South Rim of the Grand Canyon, although chemistry for UHB spring was not included in their study of South Rim springs.

The differences in correlated variables between this study and analytes observed on the North Rim by Beisner and others (2017) could be attributed to a difference between environmental controls at the local versus regional scale. While the presence of elevated U in groundwater chemistry was determined to be independent of proximity to known uranium ore bodies and or uranium mining activities in North Rim waters (Beisner et al., 2017), anomalous groundwater chemistries in Horn and Salt creek drainages (Beisner and Solder, 2020) are likely due to their proximity to the mineralized breccia pipe of Lost Orphan Mine (Beisner et al., 2023). In addressing the difference in correlations between this study and Beisner and others' study (2020) of South Rim groundwater, one explanation could be the inclusion of LHB in this study's analysis. Beisner and others (2020) found relationships between U^{4+} and SO_4^{2-} and Sr^{2+} . While

LHB does have elevated dissolved U (46 ppb) relative to any other basement springs sampled (Liebe, 2003), it also has extremely elevated levels of SO_4^{2-} and Sr^{2+} . These elevated values are unique to other springs in the Horn and Salt Creek drainages and could explain why no correlation between U^{4+} and SO_4^{2-} and Sr^{2+} is present in the 2013 data set.

PCA-1: All 2013 analytes included

The first set of multivariate analyses considers all analytes measured in groundwater collected in October 2013. The aim of this analysis was to understand the variance of groundwater chemistry in Horn and Salt Creek drainage broadly.

In the first set of multivariate analyses, where all chemical analytes were included from 2013 sampling, 4 distinct groups emerged (Fig. 10). The central cluster was poorly defined by both PC1 and PC2, while the two sampling locations beneath Orphan Lode Mine (UHB and UHB-B), EHC-BS, and LHB were all distinct and well defined by PC1 and PC2. LHB has anomalous major ion chemistry comparatively to other springs in the subset, with elevated TDS, major ions, and some elements (Li^+ and B^{3+}) associated with mixing of deeper fluids (Crossey et al., 2009). LHB's position in the PC1-PC2 plot (Fig. 11) corresponded with the vectors of the elevated analytes mentioned previously, supporting the conclusion that this spring groups by itself due to water-rock interactions from a deeper flow path significantly affecting its chemistry relative to other sampling locations in the data set. The two sampling locations discharging from the Muav Limestone directly below Lost Orphan Mine (UHB and UHB-B) correspond with vectors for U^{4+} and analytes that were found to have a strong correlation with U (As^{3-} , Se^{2-} , U^{234} , U^{235} , and Mo^+), supporting the conclusion that the groundwater flow path interacts with the Lost

Orphan ore body, resulting in anomalous groundwater chemistry relative to other springs in Horn and Salt Creek.

Also grouping alone is EHC-BS, a Muav Limestone spring located in the eastern sub-drainage of East Horn Creek, opposite to UHB and UHB-B. EHC-BS is characterized by having significantly low concentrations of U^{4+} and its correlated analytes as well as having a moderate positive correlation with Mn^{4+} , Co^{3+} , Ba^{2+} , and $\delta^{18}O$. EHC-BS grouping alone is significant, in that it may support the conclusion that its chemistry is the least impacted by the Lost Orphan ore body in comparison to other springs sampled in Horn and Salt Creek drainages. While inner-basin alluvial springs cluster together, the four Muav Limestone springs (UHB, NEHC-TOP, SC-TOP, and EHC-BS) do not, with significant variation occurring along the axes of PC2 and PC3 across the four springs. This supports the conclusion that both lithology and proximity to and interaction with the orebody are controls on the variation in groundwater chemistry in Horn and Salt Creek drainage.

PCA-2: 2013 versus 2023 Time Comparison

The second set of multivariate analyses included groundwater chemistry collected at five springs roughly ten years apart (October 2013 and March 2023), exploring any variation in groundwater chemistry over time. The most interesting result of the Time Comparison multivariate analyses is that only UHB varied significantly between time series (Fig. 13). Monroe and others (2005) noted that most South Rim springs sampled had consistent chemistries when sampled multiple times, albeit on a shorter time scale than this comparison. The variability at UHB spring occurs predominantly along the PC2 and PC3 axes of the Time Comparison PCA (Fig. 15). We see this variability corresponds to δ^2H , $\delta^{18}O$, As^{3-} , F^- , and U^{4+} along the PC2 axis

and a difference in Se^{2-} values along the PC3 axis. The 2023 UHB sample was collected at a period of unusually high flow in the Horn Creek drainage after a recent precipitation event, which could account for the variability in stable isotopes. While these two samples have similar U^{4+} relative to the observed variance historically at this site, it is interesting that variability in As^{3-} and Se^{2-} separate these two sampling locations given both elements had a positive correlation with U^{4+} in the 2013 URS data set. The observed variation in UHB chemistries may support the hypothesis that the source of groundwater for this spring is not consistent, and that inconsistent mixing of two separate sources may drive the change in chemistry observed over the previous two decades. A mechanism for this mixing may be the introduction of a modern component of groundwater infiltrating rapidly during storm events. A mechanism for this rapid infiltration could be a vertically collapsed mine shaft open to the atmosphere situated stratigraphically in the Coconino Sandstone (Chenoweth, 1986) (Fig. 5).

PCA 3: Uranium correlated analytes

The third set of multivariate statistical analyses focused on a subset of the data that only included analytes that behaved similarly to dissolved uranium. By only including these analytes, the influence of bedrock lithology on the variation of groundwater chemistry across the two drainages was greatly reduced.

The 5 analytes included in the multivariate analyses were As^{3-} , Mo^+ , Se^{2-} , U^{4+} and SO_4^{2-} . As^{3-} , Mo^+ , and Se^{2-} were all found to have positive correlations with U^{4+} , while SO_4^{2-} had a positive correlation with U excluding LHB (high TDS). After PCA and cluster analysis was performed, the optimal grouping based on average silhouette was 2, separating UHB from the 10 other springs included (Fig. 20). The average silhouette value was still relatively high for up to 6

groupings, and thus springs were grouped in further detail to understand similarity and differences between the remaining 10 springs (Fig. 20).

The most interesting of the six clusters is arguably WHC and LHB. These two springs group together as the most similar to one another, are the second and third highest concentrations of dissolved U in the 2013 data set, however they are also the furthest apart in the stratigraphic column. Dominated by their SO_4^{2-} signature, they are also the only two springs besides UHB to plot positively with U^{4+} , Mo^+ , As^{3-} , and Se^{2-} along the PC1 axis, albeit minorly (Fig. 18). This clustering may support the conclusion that these two springs are the most influenced by interactions with the ore body of the mineralized breccia pipe after UHB. WHC is geographically close to the mineralized breccia pipe, and logically would likely be under some influence from the breccia pipe given its proximity. LHB, however, is situated the furthest away from the mineralized breccia pipe of any spring in the data set. For this spring to be heavily influenced by the mineralized breccia pipe, a mechanism must be present to allow for groundwater to interact with the mineralized breccia pipe and then infiltrate through the regional aquitard, the Bright Angel shale. One mechanism could be an exploratory drill hole (P-13) created while Orphan Lode Mine was active (Chenoweth, 1986) (Fig. 5). This drill hole was drilled 583m (1,914 feet) from the 550 level of the mine, drilling through the Redwall Limestone, Muav Limestone, and Bright Angel Shale, reaching the top of the Tapeats sandstone. The drilling could allow for vertical connectivity between groundwater interacting with the mineralized breccia pipe and groundwater discharging out of the Vishnu schist. In further support for the unique chemistry observed at LHB, four springs (Blue, Havasu, Warm, and Ferns springs) with unique chemistry were characterized to be potentially mixing with deeper fluids along the South Rim in Beisner and others (2020), however none had elevated dissolved U concentrations.

A second cluster is also of interest. EHC-BS and UHA cluster together, even though EHC-BS has the lowest U concentration in the data set. EHC-BS and UHA grouping together may support the hypothesis that EHC-BS may be a significant parent source, mixing with groundwater from UHB to result in the chemistry of UHA spring. Further investigation of the relationship between EHC-BS and UHA spring is discussed in the PhreeqC inverse modeling portion of this thesis, evaluating the potential mixing ratios between EHC-BS spring and UHB spring that could result in the sampled chemistry of UHA spring.

All these analyses considered together demonstrate the complex chemical evolution of the groundwater found in Horn and Salt Creek drainages, a drainage with springs that were already found to have anomalous chemistry relative to the rest of the region. The multivariate statistical analyses demonstrate that the change in spring lithology coupled with a localized orebody drive the changes in observed groundwater chemistry. The multivariate analysis of groundwater chemistry at UHB ten years apart further explores the nature of the variation in overall chemistry at UHB, while also demonstrating that the variation is unique to UHB when compared to other springs in Horn Creek drainage. The temporal variation of dissolved uranium concentrations at UHB spring is investigated further in the precipitation bivariate analysis portion of this thesis. Finally, the multivariate analyses isolating uranium correlated analytes produce clusters that reduce the influence of the regional stratigraphy and highlight the variation of analytes associated with the mined orebody. These analyses expose an expected similarity between EHC-BS and UHA and an unexpected similarity between LHB and WHC, prompting further investigation into a mechanism that could feasibly explain such a similarity. All the multivariate analyses expose patterns in a complex and highly variable data set of groundwater chemistry, with each subset of data focusing on a targeted aspect of temporal or spatial variation.

5.2 PHREEQC Analyses

A drastic change in concentrations of dissolved uranium along a relatively short flow path between UHB and UHA spring has been documented, with a general pattern of roughly an order of magnitude change in concentrations from UHB (elevated dissolved U) to UHA (lower dissolved U). Recent modeling approaches (Beisner and others, 2023) along with this thesis, characterize the observed change in chemistry through modeled water-rock interactions using the modeling software, PHREEQC. Unique to this thesis' modeling approach, is the use of a groundwater sample of UHA that contains the highest dissolved uranium concentration on record (71 ppb). Additionally, the potential for a new parent chemistry, EHC-BS, is considered in a scenario where the chemistry of UHB mixes with another groundwater chemistry. This section will discuss the results of the modeling conducted to answer a fundamental question: How can we quantitatively explain the observed change in major ion chemistry and dissolved uranium chemistry at Upper Horn Alluvium spring? Two separate modeling “scenarios” are considered to answer this question. The first, Scenario 1, models the change in chemistry between UHB and UHA if water-rock interactions are the only mechanism allowed to explain this chemistry change. Six separate runs within this scenario are conducted, each run slightly tweaking the modeling inputs to explore different geochemical reactions that may be taking place. The second, Scenario 2, models the change in chemistry between UHA and a combination of both UHB and EHC-BS. In this scenario, water-rock interactions and mixing combine to explain the changing chemistry. Five separate runs within Scenario 2 are conducted, with small adjustments made to the modeling inputs to explore different geochemical reactions and mixing scenarios that may be taking place.

Scenario 1 assumes a closed system between UHB spring and UHA spring to evaluate if water-rock interactions could quantitatively explain the observed changes in major ion chemistry between UHB and UHA springs. The first modeling run, S1.R1, included only known minerals and excluded uranium from the input solutions. PHREEQC calculations show that the minerals documented in the rock lithology along the UHB to UHA flow path can explain the change in major ion chemistry (Appendix B). S1.R4 approached the same question, except with the inclusion of the mineral halite precipitating out of solution. Halite was included to provide a sink for the decrease in Cl⁻ from UHB to UHA. The inclusion of Halite allowed for more models (17 total) to be produced with a lower sum of residuals compared to S1.R1. This demonstrates that in this scenario (S1.R4), the inclusion of halite allows for a greater number of combinations of phase mole transfers that could generate the observed hydrogeochemical evolution of groundwater from UHB to UHA. Although more models were produced, the introduction of halite did not change the trends in which other minerals consistently dissolved or precipitated in models.

The second run (S1.R2) once again assumed a closed system between UHB and UHA and included dissolved U in the input solutions. This modeling run evaluated the potential for water-rock interactions to feasibly account for the observed changes in major ion chemistry and concentrations of dissolved uranium. The PHREEQC calculations show that the change in groundwater chemistry between UHA and UHB is feasible with an extremely elevated minimum uncertainty of 64.8%. Indicating that for PHREEQC to quantitatively explain the observed changes in chemistry, the concentration of each element was allowed to vary up to 64.8%. Additionally, none of the returned models have a solution fraction of exactly 100% for UHB, instead PHREEQC required UHB to be 99.97%. PhreeqC requiring a much higher minimum

uncertainty and solution fraction deficiencies support that closed system with the modeled inputs for UHB and UHA could likely not account for the observed changes in groundwater chemistry with the documented lithologies. A notable gap in the modeled inputs is the absence of dissolved oxygen in the data set. Other modeling approaches in Beisner and others (2023) included dissolved oxygen, and under those modeled inputs reduction-oxidation reactions were feasible, resulting in the precipitation of uranium in a closed system between UHB and UHA.

If UHB to UHA is once again assumed to be a closed system, and minerals present in the breccia pipe (specifically pyrite) were also present along the flow path in the inner-basin alluvial material (S1.R3), PhreeqC calculations show that water-rock interactions could explain the observed changes in groundwater chemistry at UHA spring with much lower uncertainties. The third run (S1.R3) of modeling for Scenario 1 returned 8 models. Several trends are important to note. Although Hematite and Uraninite are included in every modeling run, Hematite and Uraninite only undergo phase mole transfers when reduction-oxidation reactions occur. With the inclusion of the mineral Pyrite (unique to the mineralized breccia pipe), reduction-oxidation reactions are enabled. Across all 18 models of S1.R3, Uraninite, Pyrite, and Hematite as well as Fe^{3+} , U^{4+} , and SO_4^{2-} behave identically. Uraninite and Hematite precipitate out of solution ($-1.1\text{e-}6$ and $-7.34\text{e-}8$ moles respectively) while Pyrite dissolves into solution ($1.47\text{e-}7$ moles). Both Fe^{3+} and U^{4+} decrease in solution ($-1.47\text{e-}7$ and $-1.1\text{e-}6$ moles respectively) while SO_4^{2-} increases in solution ($2.57\text{e-}7$ moles). S1.R3 required a minimum uncertainty of 5.7%, significantly lower than the minimum uncertainty required for S1.R2 and reasonably close to the default minimum uncertainty set for PhreeqC of 5%. Given that uranium's chemistry can be a function of reduction-oxidation reactions (Appelo and Postma, 2005; Fetter et al., 2018) it is reasonable to assume that if Pyrite is present and enabling reduction-oxidation reactions, water-rock

interactions could explain the observed changes in groundwater chemistry. It is also important to note that Fe was below laboratory detection levels at UHA when sampled in March of 2023, and that samples at UHA had the lowest Fe concentration sampled during that survey.

Two more modeling runs (S1.R5 and S1.R6) replicated the modeling parameters of S1.R2 and S1.R3, with the addition of precipitating halite. The addition of halite to S1.R2 did not result in changes in the solution fraction issues for UHB of 99.97%, nor did it change the anomalously high minimum uncertainty of 64.8% required to produce models. The addition of halite to S1.R3 had no impact on the minerals and ions involved in the reduction-oxidation modeled in S1.R3 and the addition of Halite did not change the minimum uncertainty to return models.

Scenario 2 investigated mixing, and assumed a closed system between EHC-BS, UHB, and UHA groundwaters to evaluate the potential for mixing between EHC-BS spring and UHB spring to produce the observed chemistry at UHA spring. Due to the decrease in dissolved uranium present at UHA relative to UHB, dilution via mixing with a second source of groundwater could be a possible mechanism explaining the significant decrease in dissolved uranium at UHA spring. If mixing between EHC-BS and UHB is expected to account for the change in dissolved U, then the mixing ratio would have to be dominated by EHC-BS. More specifically, a mixing ratio of 79.94% EHC-BS and 20.06% UHB would result in the observed concentration of 71 ppb collected in March of 2023 at UHA spring.

Although no mixing models returned the predicted mixing ratio of 79.94% EHC-BS and 20.06% UHB, the first and fourth modeling runs of Scenario 2 returned a total of 6 models with mixing ratios close to the predicted mixing ratio. The first modeling run, S2.R1, returned one mixing model with a ratio of 77.2% EHC-BS and 22.8% UHB while the fourth modeling run,

S2.R4, returned five mixing models with the ratio of 77.2% EHC-BS and 22.8% UHB. Both modeling runs modeled mixing between EHC-BS and UHB with the known minerals present, with S2.R4 also including dissolved U in the input solutions. Using the modeled mixing ratios in S2.R1 and S2.R4, we would expect to see a dissolved U at UHA of 79.98 ppb rather than the observed concentration of 71 ppb, collected in March of 2023. This discrepancy in modeled versus observed may indicate that a third source is mixing to create the observed chemistry at UHA. A third source contributing towards dilution could be rainwater infiltrating into the inner-basin alluvial material or potentially groundwater from a deeper flow path. Overall, the mixing ratios in S2.R1 and S2.R4 support the conclusion that EHC-BS could be a parent groundwater source to UHA, with models displaying that mixing and water-rock interactions could explain the observed change in major ion chemistry as well as the change in dissolved U chemistry. Of note, all the models produced by S2.R2, S2.R3, and S2.R5 did not produce any models with the necessary mixing ratio as all modeling outputs produced mixing ratios dominated by UHB.

In summary, the PHREEQC modeling scenarios in this thesis suggests that for water rock interactions to be a likely primary control on the observed change in dissolved uranium concentrations, pyrite would need to be present in trace amounts in the alluvial material down gradient from UHB spring. If pyrite and dissolved oxygen are not present, then it is much less likely that water-rock interactions could be the driver of the observed change in dissolved uranium concentrations. In a scenario in which water rock interactions are not the primary environmental control on the change in dissolved uranium concentrations, mixing modeling (Scenario 2) suggests that EHC-BS could mix with UHB groundwater resulting in the observed change in groundwater chemistry at UHA spring. Even so, it is likely some further dilution from

rainfall and/or runoff seeping into the inner-basin alluvial material would be necessary to reach the precise concentrations of dissolved uranium observed in March of 2023.

In comparing this modeling scenario with those modeled in Beisner and others (2023), Beisner and others were able to show that observed changes in dissolved uranium are possible in a separate scenario, with the precipitation of uraninite if dissolved oxygen is present in groundwater and surface waters, and reducing conditions are present in the subsurface. Dissolved oxygen was not measured in samples collected in 2023 for this study, and consequently were not defined in the modeling parameters of this study. It is also important to note that the reducing or oxidizing conditions of the subsurface are undefined along this flow path, a limitation highlighted in Beisner and others (2023), and that for uraninite to precipitate it would require reducing conditions in the subsurface.

Finally, in evaluating EHC-BS as a 'parent' groundwater, Beisner and others (2023) identified two other potential parent groundwaters: Pumphouse spring and Valle Groundwater Well. The mixing ratios in Beisner and others (2023) indicate that the ratio of Pumphouse (as high as 83% PH to 17% UHB) could be a feasible mixing partner with the observed chemistries of UHB and UHA in this study. It is important to note that Beisner and others (2023) used data collected by the USGS from 2019-2022, and observed much lower dissolved uranium concentrations at both UHB and UHA than were observed in samples collected in this study.

5.3 Stable Isotopes Analysis

In discussing the stable isotopic data from this study, data from Salt and Horn Creek drainages must be placed in context of the larger South Rim/Coconino Plateau region first. Most

springs in Horn and Salt Creek drainage have stable isotopic signatures resembling groundwater dominated by high-elevation, winter recharge possibly sourced from the San Francisco peaks with a minor component of lower-elevation, summer recharge mixing along the flow path, consistent with other groundwater sampled from the regional R-aquifer across the South Rim (Solder and Beisner, 2020). Solder and Beisner calculated a Local Meteoric Water Line (LMWL) with a slope of 6.49 and an intercept of -6.2‰ and calculated a Groundwater Line (GWL) with a slope of 6.46 and an intercept of -12‰. The line of best fit for data from URS (2013) and this study had a slope of 5.7054 and an intercept of -21.424‰ (Fig. 9). The variation between the line of best fit and the GWL may be explained through processes such as evaporation, as waters within the drainage are more enriched than the GWL would predict. An interesting phenomenon is that springs in Horn and Salt Creek drainages have a large range of stable isotopes, with the range of all 28 groundwater sites compiled by Solder and Beisner (2020) for the South Rim region being comparable to the range of stable isotopes within Horn and Salt Creek drainages. One explanation for the variance in stable isotopes between springs in the drainages could be the influence of intense, localized summertime (isotopically enriched) precipitation events mixing with deeper flow paths of the regional R-aquifer (less isotopically enriched). LHB, WHC, LSC, and EHC-BS springs have samples with stable isotopic signatures that have a heavier isotopic signature and thus may have a larger component of a more local summer recharge relative to other springs in the drainage. Additionally, some inner-basin variation is likely due to evapoconcentration (an evaporative signal is present between groundwater sampled at the emergence point and groundwater sampled at the end of the reach of the spring's flow at UHB spring, LHA spring, and WHC spring in 2013).

Springs discharge from three aquifers in Horn and Salt Creek drainages: local inner-basin alluvial aquifers of Salt and Horn Creek, the regional R-aquifer, and the deeper bedrock aquifer. However, there is no clear relationship between aquifer and stable isotopic signature (Fig. 24). With Upper Horn Bedrock spring having both a larger range of stable isotopic signatures (less significant if UHB2023 is excluded), and a large range of dissolved uranium values, it was hypothesized that if variation in volume of recent precipitation is a control on dissolved uranium, then there may be a correlation between dissolved uranium and stable isotopes. However, no relationship between $\delta^2\text{H}$ and dissolved U ($R^2=.198$, $n=11$) nor $\delta^{18}\text{O}$ and dissolved U ($R^2=.192$, $n=11$) was found (Fig. 25). Other lines of evidence in this study support the hypothesis that precipitation events act as a control on dissolved U via dissolution. The lack of a relationship between stable isotopic signatures and dissolved U warrant explanation given this context. It is possible that a significant precipitation event could occur in either winter or summer, and although similar volumes of flow would enter the system and impact dissolved U at UHB spring, they would likely have different stable isotopic signatures, yielding no correlation. The absence of significant correlation may support the characterization that seasonality of groundwater recharge is not a dominant control on dissolved U at UHB spring.

Additionally, a key component of this study is characterizing the connectivity between Upper Horn Bedrock Spring and Upper Horn Alluvium. The variance in stable isotopic signatures can help characterize potential differences in zones of recharge. Data compiled for this study show that the mean $\delta^2\text{H}$ at UHA spring is -87.98‰ , and the mean $\delta^{18}\text{O}$ is -11.813‰ , while data compiled for this study show that the mean $\delta^2\text{H}$ at UHB spring is -87.029‰ , and the mean $\delta^{18}\text{O}$ is -11.68‰ . Previous sampling by Zukosky (1995) at UHA had a slightly heavier average signature of -11.87 $\delta^{18}\text{O}$ and -90.3 $\delta^2\text{H}$, but in general there is minimal change in stable isotopic

signatures across 3 decades of sampling at UHA spring. Given that UHB spring discharges from the regional R-aquifer, and that UHA spring discharges from inner-basin alluvium, a distinct change in the stable isotopic signature might be expected. Both springs however have similar signals and are distinctly more isotopically depleted than mean summer precipitation ($\delta^2\text{H}$: $-46.8\text{‰} \pm 25$, d^{18}O : $-6.5\text{‰} \pm 3.9$ (Solder and Beisner, 2020)). The absence of variation supports the characterization that UHA and UHB springs are both sourced from similar sources of winter dominated recharge, and both springs have signals consistent with other springs sourced from the regional R-aquifer, indicating they may both be sourced from the regional R-aquifer. Another explanation could be that UHA spring and UHB spring have different sources of recharge but have similar stable isotopic signatures. This could be possible if, for example, UHA spring was primarily sourced from local snowmelt run-off while UHB spring was sourced from a deeper flow path from the regional aquifer, but both had depleted stable isotopes characteristic of high-elevation and/or winter recharge.

While several springs exhibit similar stable isotopic signatures to UHB (UHA, SC-TONTO, SC-TOP, NEHC-TOP, and LHA), others including WHC, LHB, LSC, and EHC-BS have heavier signatures. LSC is the only alluvial spring sampled significantly down drainage (furthest from the Redwall and Muav Limestones), and thus it is possible the warmer signature is evidence of larger component of this spring's recharge coming from summer rainfall infiltrating into the alluvium. EHC-BS is an outlier in the data set. This spring has a much more enriched isotopic signature relative to other springs across the two drainages (mean $\delta^2\text{H}$: -59.3‰ , mean $\delta^{18}\text{O}$: -6.31‰), and its signature closely resembles summer rainfall described in Solder and Beisner (2020). This spring is in the East Fork of East Horn Creek drainage and is higher in elevation than UHB spring. The stable isotopic signature of this spring could support the

characterization that summertime precipitation is a much more significant component of its recharge and that this spring may be separate from the regional aquifer. While multivariate analysis clustered EHC-BS and UHA when considering analytes correlated with dissolved uranium, supporting the potential for EHC-BS to be a significant contributor to UHA groundwater, the lighter signature of UHA coupled with the heavy signature of EHC-BS would not support EHC-BS being a significant contributor to UHA groundwater.

In discussing the heavier signatures of WHC, LHB, and UHB it is important to discuss potential error introduced in the data. WHC and UHB were both sampled at the base of the Redwall Limestone, and during sampling a significant overflow was pouring down the cliff and mixing to some degree with groundwater. It is likely that this mixing component could undergo evaporation and subsequent fractionation, explaining the heavier signatures for these samples. WHC was sampled in 2013 not at the base of the Redwall, but rather further down drainage due to accessibility. Evaporation and subsequent fractionation may have also influenced the stable isotopic signature of this sample as the water would have flowed from the Muav Limestone through the drainage before being sampled. Alternatively, a heavier stable isotopic signature was attributed to a degree of separation from the regional aquifer in Solder and Beisner (2020) which is dominated by a lighter signature. Thus, the heavier signature of LHB and WHC could also support a characterization that the flow emerging from these springs has a greater component sourced from summer monsoonal events. Both springs have also been sampled to have elevated uranium. Therefore, it is possible both springs could be sourced in part by run off from summer monsoons infiltrating directly into old mine workings and exploratory drill holes. Within this interpretation, mixing with groundwater from the regional aquifer would have to be minimal.

5.4 Precipitation and Dissolved Uranium at UHB Analysis

Previous portions of this thesis focused on the spatial variation in dissolved uranium between UHB and UHA springs, with some minor analysis in the temporal variation of dissolved uranium at UHB spring (e.g. Time PCA, stable isotopes vs. dissolved U at UHB). This section contains the bulk of the analysis for temporal variation of dissolved uranium, specifically focusing on the relationship between precipitation and dissolved uranium. The high Spearman's Rho correlation coefficients present in the relationship between dissolved uranium and precipitation as recorded at the Phantom Ranch weather station support the hypothesis that precipitation events are a control on the temporal variation of dissolved uranium at Upper Horn Bedrock Spring (Fig. 23). However, the times where the correlations are present do not fully support the hypothesis that there is a 1–2-month lag time. Rather, the evidence supports that there is a lag time of around two to two and a half months (9 to 10 weeks or 57-70 DPS) between rainfall events and an observed change in the groundwater chemistry at UHB spring. The negative coefficients may support the conclusion that rainfall events are impacting the groundwater chemistry via the process of dilution. A pattern resembling an exponential distribution can be seen for the 57-77 DPS and 57-70 DPS periods. As precipitation increases between 57 to 70 days prior to sampling, there is a general decrease in dissolved uranium concentrations discharging from the spring. Additionally, drier periods 57 to 70 days prior to a sampling event yielded higher observed dissolved uranium concentrations, with significant variation amongst these data points.

In discussing the relationship present, the evidence can be characterized by two extremes. During extreme wet periods 57 to 70 days prior to sampling, the lowest concentrations of dissolved uranium are observed (151 ppb to 200 ppb), while during extreme dry periods 57 to 70

days prior to sampling, the highest concentrations of dissolved uranium are observed (300 to 500 ppb). The bulk of the dissolved uranium concentrations fall within 200-280 ppb dissolved uranium, corresponding to periods of moderate to low rainfall. This relationship may suggest that precipitation events act as a control on the system. Runoff from an intense precipitation event could infiltrate into the system at higher rates, mixing with groundwater contaminated with high levels of dissolved uranium, resulting in lower concentrations of dissolved uranium discharging at the terminus of its flow path (UHB spring).

While the spearman's rho yielded significant correlations, linear regression analysis yielded weak to no significant correlations. This is due to the fact that during drier periods, significant variability of dissolved uranium is observed while summed precipitation values are similar. The nature of the observed relationship could indicate that larger precipitation events have a significant role in lowering concentrations of dissolved uranium via dilution. However, when precipitation is absent, a second environmental control must be present to explain the observed variability of the higher dissolved uranium concentrations. Time cannot be isolated as a control based on the evidence, given that Liebe (2003) observed dissolved uranium concentrations ranging from 300 to 400 ppb of uranium during periods of no rainfall 57 to 70 days prior, and then nine years later Scharr (2011) observed the regional maximum of 511 ppb, also during a period of no rainfall 57 to 70 days prior. A potential explanation for the variation could be that dilution is still a primary control, except it could be dilution from recharge via longer flow paths through the regional aquifer. Average residence times for groundwater on the South Rim of the Grand Canyon vary from less than 100 years to over 10,000 years (Solder et al., 2020). Solder and others (2020) found that Horn Spring (unclear if Lower Horn Alluvium or Upper Horn Bedrock) had an average residence time of 356 years. It is plausible that these

deeper flow paths and changes in seasonal recharge are also controls on changes in groundwater chemistry. These controls may have less influence when recent precipitation is present and can dilute the system significantly, affecting the groundwater's chemistry.

The period of 57 to 70 days prior to sampling yielding significant correlation coefficients would indicate a rapid average response time to precipitation events relative to typical residence times of groundwater along the South Rim if a relationship is present (Solder et al., 2020). This rapid average response time could be explained via the capture of runoff into an old, collapsed mine shaft situated in the Coconino Sandstone, and still presently open to the atmosphere. This shaft (~10 m in diameter) could funnel large amounts of runoff directly into old mine workings, allowing the system to behave similar to karst systems in the region, where rapid response times to recent precipitation can be common (Jones et al. 2018, Tobin et al. 2018).

The nature of the observed relationship indicates that as rainfall events significantly increase, dilution also significantly increases. This relationship could be understood in the context of runoff. As rainfall increases, infiltration will reach a threshold, at which point run-off drastically increases and flooding occurs. This would normally not impact dilution in a typical groundwater system as infiltration would reach a ceiling when soils become saturated. However, if the system in question had a tunnel (such as the open adit) that could increase infiltration by catching extra run-off, it is possible that we might see a dramatic dilution effect in groundwater during more significant rainfall events as seen for data during the 57 to 70 DPS period.

Another point of discussion is the presence of a significant relationship between dissolved uranium and precipitation records at Phantom Ranch weather station while no such relationship is present between dissolved uranium and precipitation records at the Grand Canyon Visitor Center weather station and the Grand Canyon Airport weather station. Distance may be a

factor when comparing the Airport weather station to the Visitor Center and Phantom Ranch weather stations, however the distance between Phantom Ranch and the Visitor Center weather stations and Horn Creek is similar. A key difference between the Visitor Center and Phantom Ranch is elevation, with the Visitor Center weather station located on the South Rim while Phantom Ranch is located at the bottom of the Grand Canyon. Storms in the region are often intense and very localized. It is possible that Phantom Ranch captured weather patterns similar to Horn Creek because it is situated within the canyon. Another difference between the weather stations was the frequency of snowfall and therefore the application of adjusting recorded snowpack at a ratio of 10:1 to account for snowmelt infiltration. Grand Canyon Airport did not report snowpack, while Phantom Ranch and the Visitor Center did. Phantom Ranch rarely received snowfall, while the Visitor Center did due to its much higher elevation on the Rim. There are two limitations of adjusting daily precipitation to include snow with the ratio of 10:1 snow water equivalent. The first limitation is that the snow water equivalent is assumed to be 10%, however that is just a standard average, and snow water equivalents can vary seasonally and interannually (Trujillo and Molotch, 2014). The second limitation is that the snow water equivalent was added to the total precipitation that fell on that day. In many instances it is likely that snow fall would accumulate and potentially take several days or weeks to infiltrate as snowmelt. The variability in the time for snowpack to become snowmelt is not accounted for in the methodology. These limitations could influence the correlations between precipitation records and dissolved uranium at a site where significant snowpack is observed, such as the Grand Canyon Visitor Center weather station.

Chapter 6: Conclusion

The goal of this study is to further understand environmental controls on the variation of dissolved uranium in groundwater in Horn and Salt Creek drainages, integrating modern sampling with older, previously unpublished groundwater chemistries. Through hydrogeochemical data collection and subsequent multivariate statistical analyses, PHREEQC inverse modeling, bivariate analysis, and isotopic analysis using these data, further insight into the processes present at Horn and Salt creek drainage is provided. Results from PHREEQC modeling and hierarchical cluster analysis support the interpretation that mixing between groundwater from UHB spring and EHC-BS spring may be the driver of the observed decrease in dissolved uranium at UHA spring. In this scenario, mixing ratios indicate a roughly 4 to 1 ratio of EHC-BS to UHB, with an undefined influence from precipitation recharging directly into alluvial material likely impacting the mixing ratio. However, stable isotopes collected at EHC-BS in 2013 do not support the conclusion that EHC-BS is a major contributor to UHA spring. With a 4 to 1 mixing ratio, we would expect to see UHA bear a stable isotopic signature similar to EHC-BS, however UHA's signature is significantly lighter than EHC-BS. A groundwater with a similar major ion chemistry to EHC-BS but sourced from the regional aquifer (consistent with the lighter stable isotopic signature) could explain a 4 to 1 mixing ratio. However, no such groundwater chemistry with the associated major ion chemistry and stable isotopic signature was present in these data. The competing hypothesis is that water-rock interactions drive the observed change in chemistry from UHB to UHA. Results from PHREEQC modeling in this study suggest that water-rock interactions could feasibly explain the significant decrease in dissolved uranium

if minerals from the mineralized breccia pipe, such as pyrite, are present in inner-basin alluvial deposits and reducing conditions are also present. Other modeling approaches in Beisner and others (2023) indicate that reduction-oxidation reactions could also occur along the flow path from UHB to UHA if dissolved oxygen is present along with reducing conditions.

Temporal variation in the groundwater chemistry at UHB spring is clear, and multivariate analyses and stable isotopes highlighted that UHB's variation is greater than other springs in the drainage. Rainfall analyses indicate that recent precipitation events (two to two and a half months prior to sampling UHB spring) have a correlation with lower dissolved uranium concentrations. The relationship indicates a general trend of dilution, with wetter periods corresponding to lower dissolved uranium concentrations, and drier periods corresponding to higher dissolved uranium concentrations. The exponential nature of the relationship also indicates that other controls on the dissolved uranium are present, with significant variation in dissolved uranium concentrations observed in dry periods two to two and a half months prior to sampling. The rapid response time between precipitation and observed groundwater chemistry is significant and may indicate that previous mining activities (excavation and drilling) maintain a strong influence on the flow path groundwater discharging at UHB spring.

An additional point of interest is the elevated dissolved uranium observed at LHB spring, discharging from the Proterozoic basement lithology. While other springs of interest, such as UHB and UHA, have a significant record of sampling, LHB spring has been sampled once prior to this study, in October of 2013 (elevated dissolved uranium was also recorded). The high dissolved uranium supports the conclusion of recent interaction with a uranium ore body. Influence of groundwater discharging out of the basement would require vertical connectivity between groundwater from the regional aquifer and groundwater in the basement lithology,

beneath the Bright Angel shale (aquitarde). One explanation could be the P-13 drill hole drilled while Orphan Lode mine was in operation and could be a further example of the impact on groundwater chemistry in Horn Creek drainage from prior mining activity. Further investigation is warranted to better understand the relationship between precipitation and dissolved uranium at UHA, the influence of mine excavation on the flow path of Horn and Salt Creek springs, and a broader characterization of EHC-BS and LHB springs, which have never been sampled for certain radiogenic isotopes such as tritium, that could provide greater insight into their groundwater flow paths. Of specific interest may be a dye-tracer study, similar to Tobin and others (2018), specifically tracing groundwater's path from the open shaft at the defunct Orphan Lode Mine.

Appendix A: Figures Referenced in Text

Fig. 1 Study Area

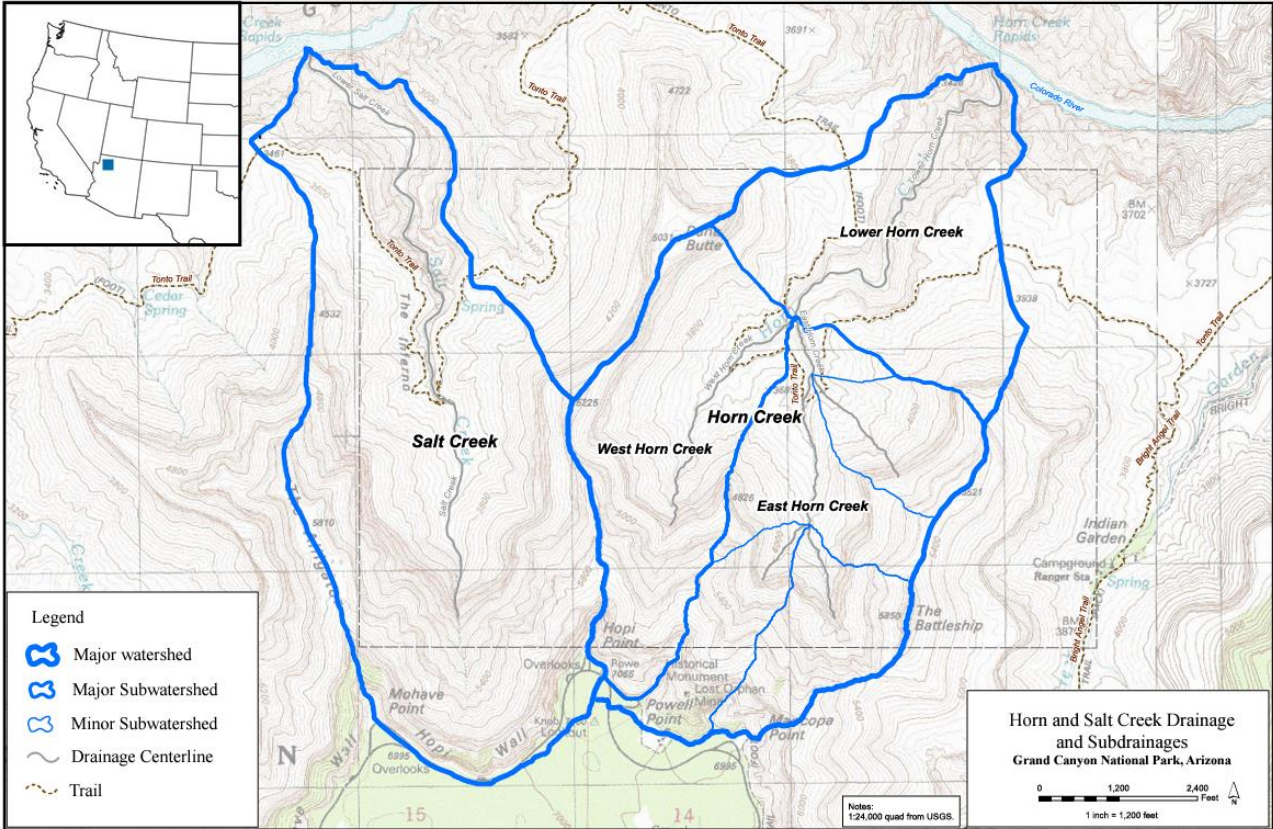


Fig. 1 Topographic map featuring Horn Creek and Salt Creek drainage and subdrainage boundaries. Inset map to the top left depicts location of the study area relative to the Western United States. Figure adapted from URS Inc. (2014).

Fig. 2 Sampling Sites

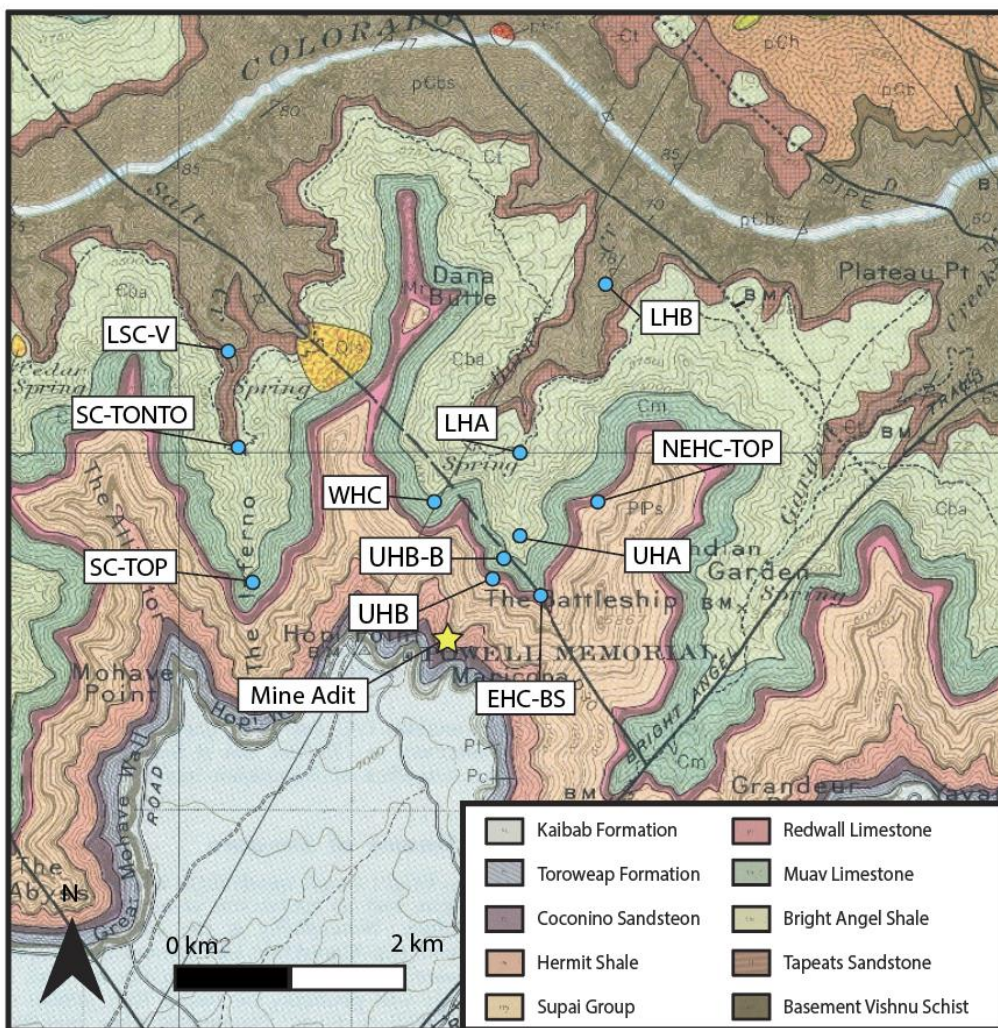


Fig. 2 Geologic map (Maxon, 1961) of the Bright Angel quadrangle in Grand Canyon National Park. Springs are designated with blue dots and labeled with their abbreviated name. The adit of Orphan Lode Mine is designated with a yellow star.

Fig. 3a Distribution of Total Dissolved Uranium in October 2013

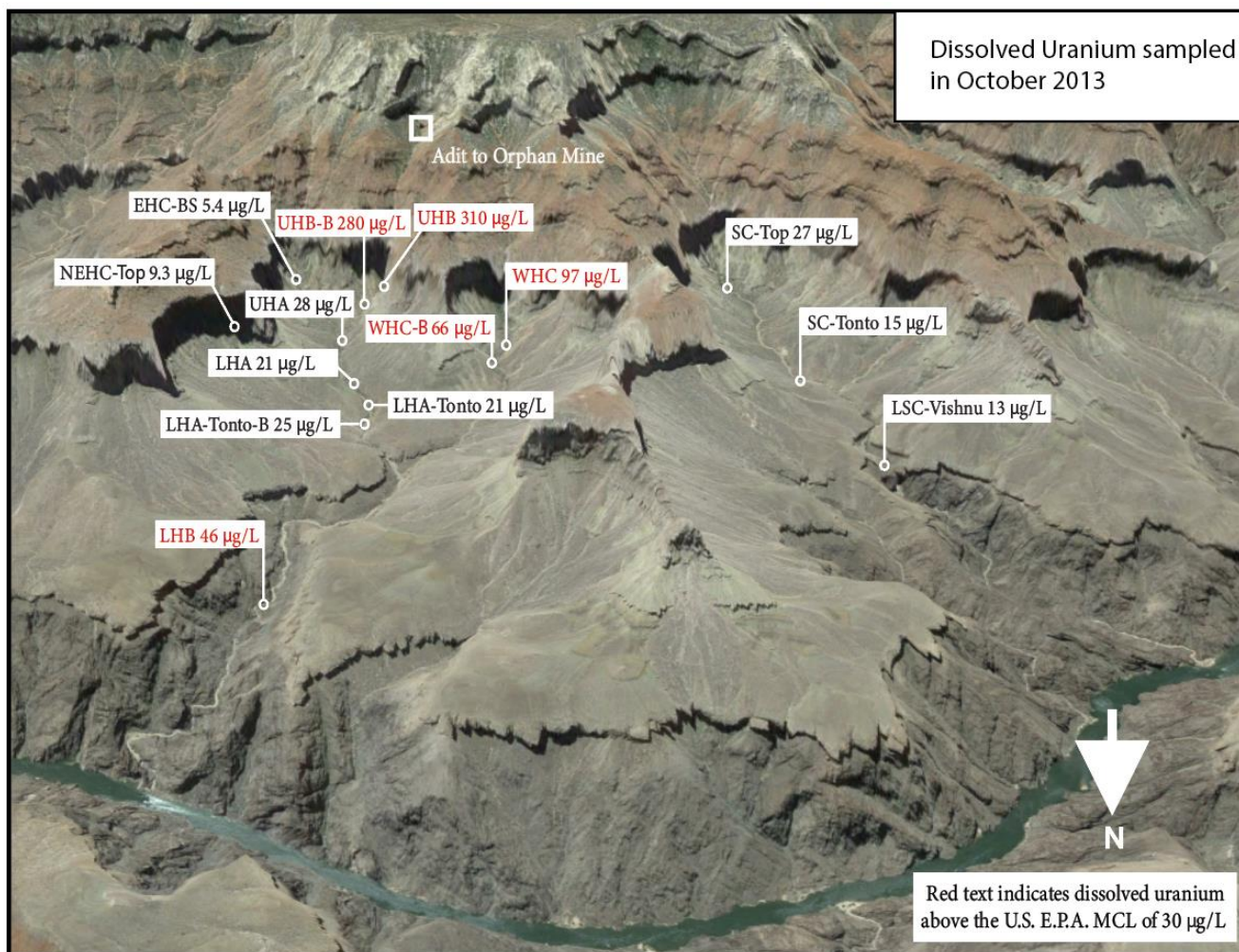


Fig. 3a Satellite imagery of Horn and Salt Creek drainages from Google Earth, with sampling locations and recorded dissolved uranium displayed. Red text indicates dissolved uranium concentrations greater than the US EPA drinking water MCL of 30 µg/L. Data were collected over two weekends in October of 2013 by URS Inc.

Fig. 3b Distribution of Total Dissolved Uranium in November 2022

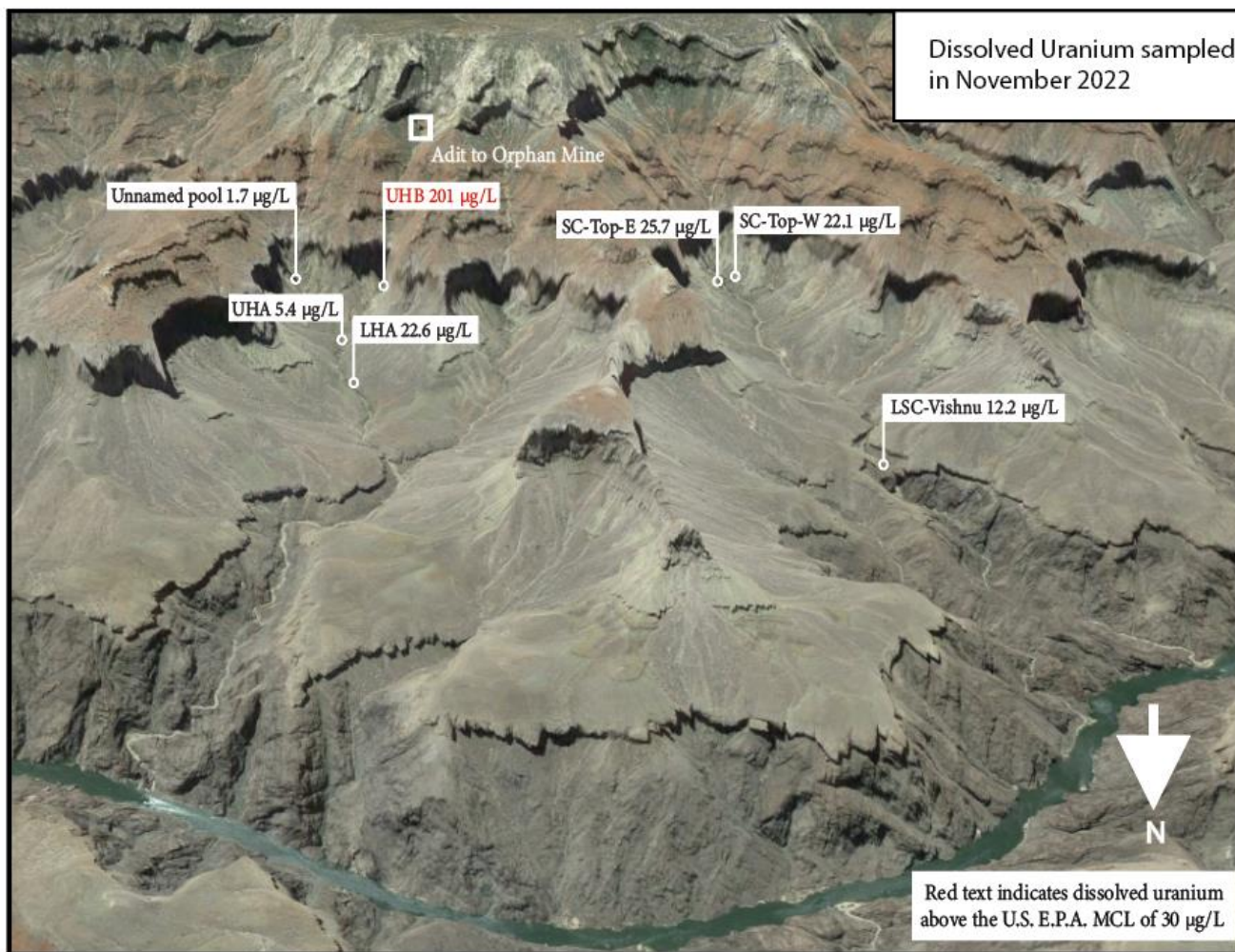


Fig. 3b Satellite imagery of Horn and Salt Creek drainages from Google Earth, with sampling locations and recorded dissolved uranium displayed. Red text indicates dissolved uranium concentrations greater than the US EPA drinking water MCL of 30 µg/L. Data were collected over two weekends in November of 2022 by UNLV researchers.

Fig. 3c Distribution of Total Dissolved Uranium in March 2023

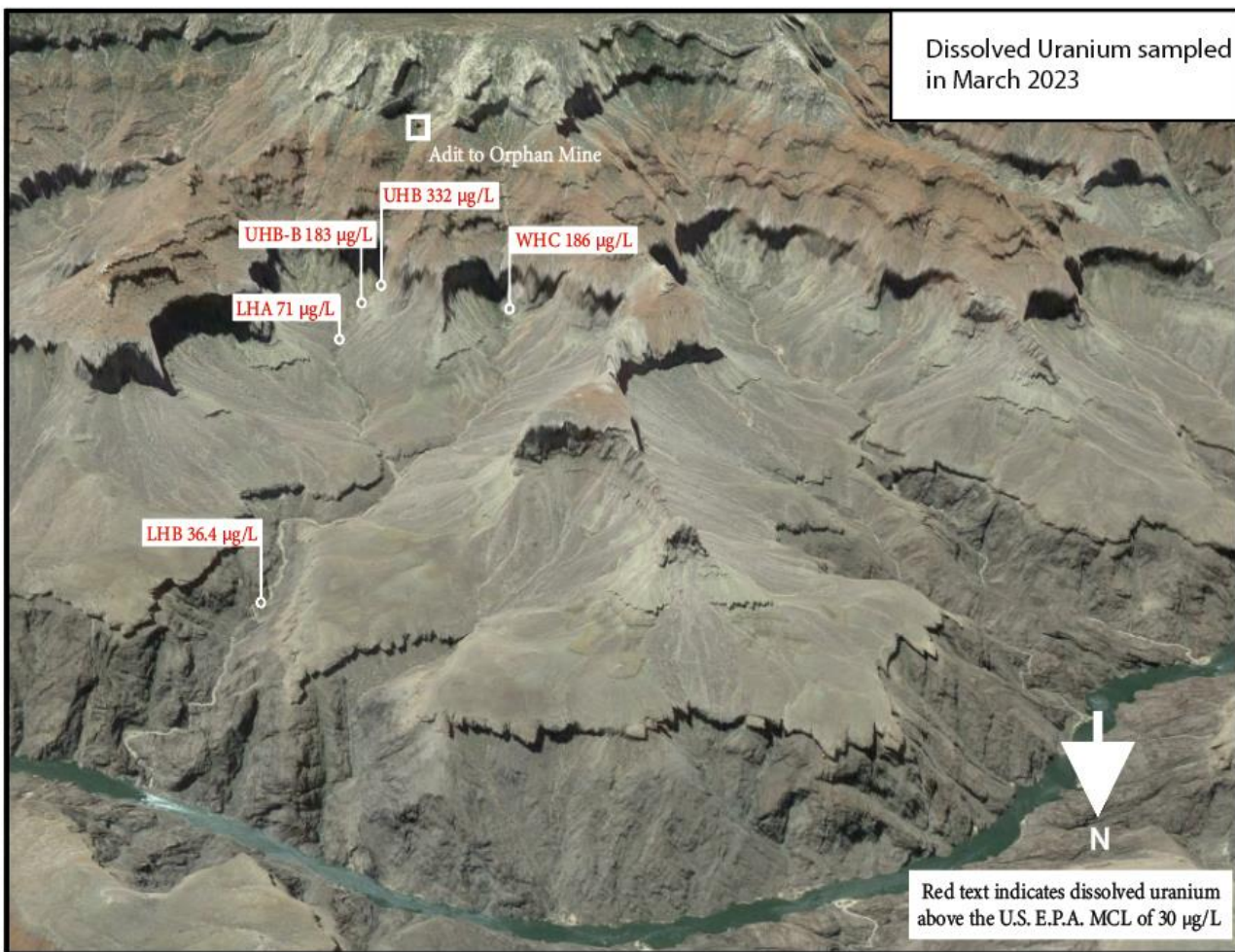


Fig. 3c Satellite imagery of Horn and Salt Creek drainages from Google Earth, with sampling locations and recorded dissolved uranium displayed. Red text indicates dissolved uranium concentrations greater than the US EPA drinking water MCL of 30 µg/L. Data were collected in one weekend in March of 2023 by UNLV researchers.

Fig. 4 Stratigraphic Column of Grand Canyon Lithology

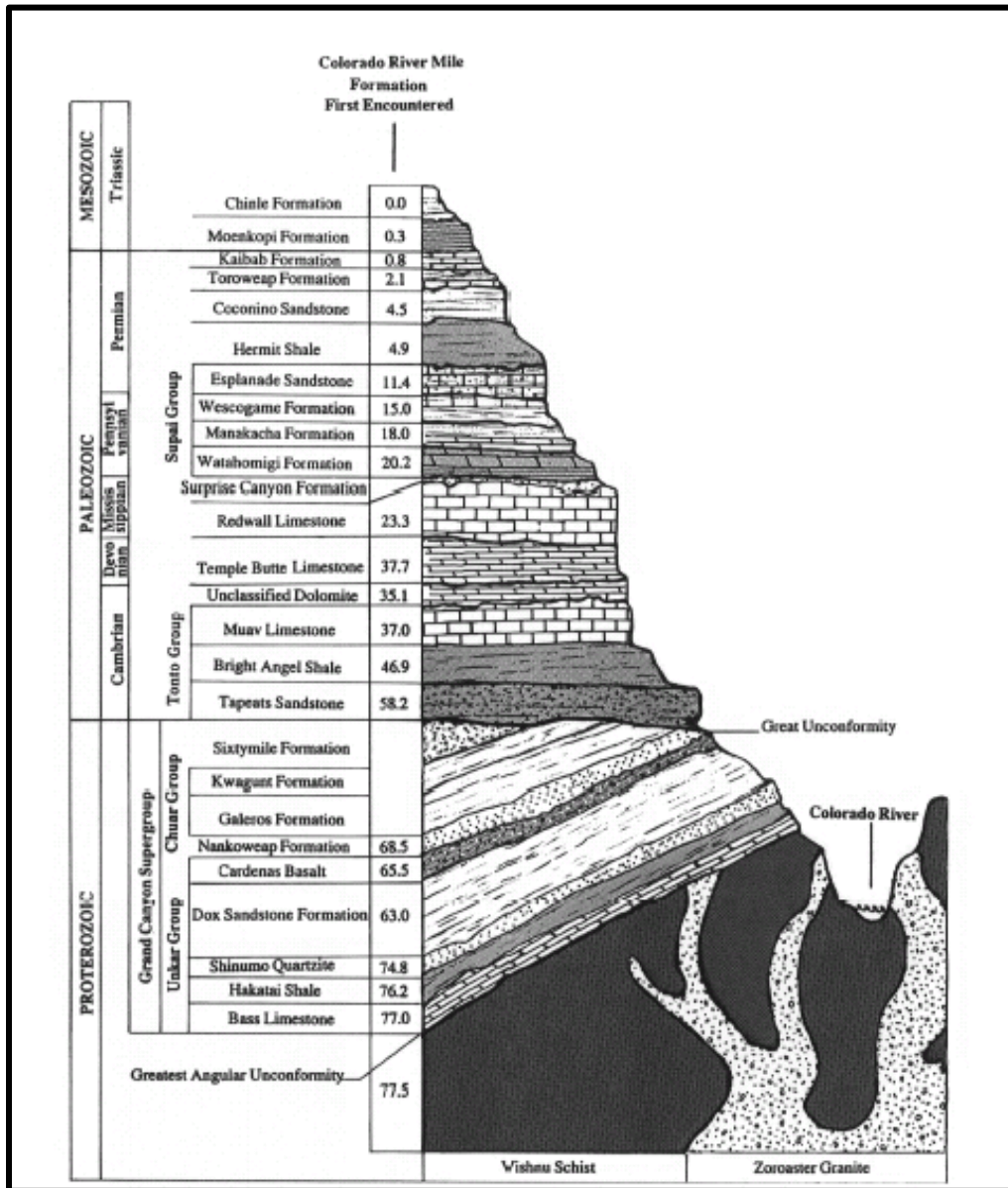


Fig. 4 A general stratigraphic column of Grand Canyon stratigraphy from Billingsley and Elston (1989). Of note, the Grand Canyon Supergroup is not exposed at the surface in the Horn and Salt Creek drainage, with the Tapeats Sandstone overlying the Proterozoic basement of the Vishnu Schist and Zoroaster Granite.

Fig. 5 Horn Creek Cross-section

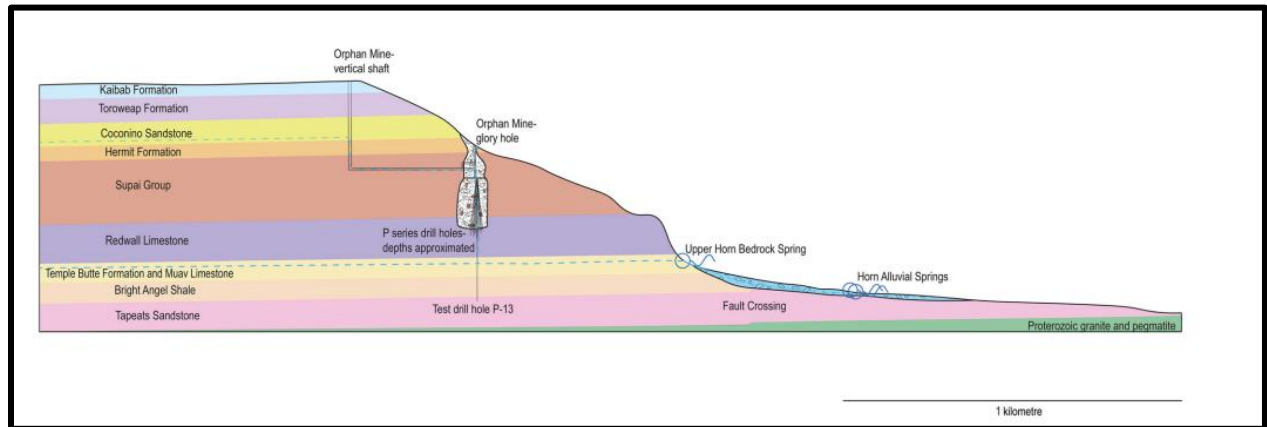


Fig. 5 Cross section of Horn Creek drainage from Beisner and others (2023). Cross section includes old mine shafts and drill holes, breccia pipe, and location of Upper Horn Bedrock spring and Upper Horn Alluvium spring.

Fig. 6 Locations of weather stations relative to UHB spring

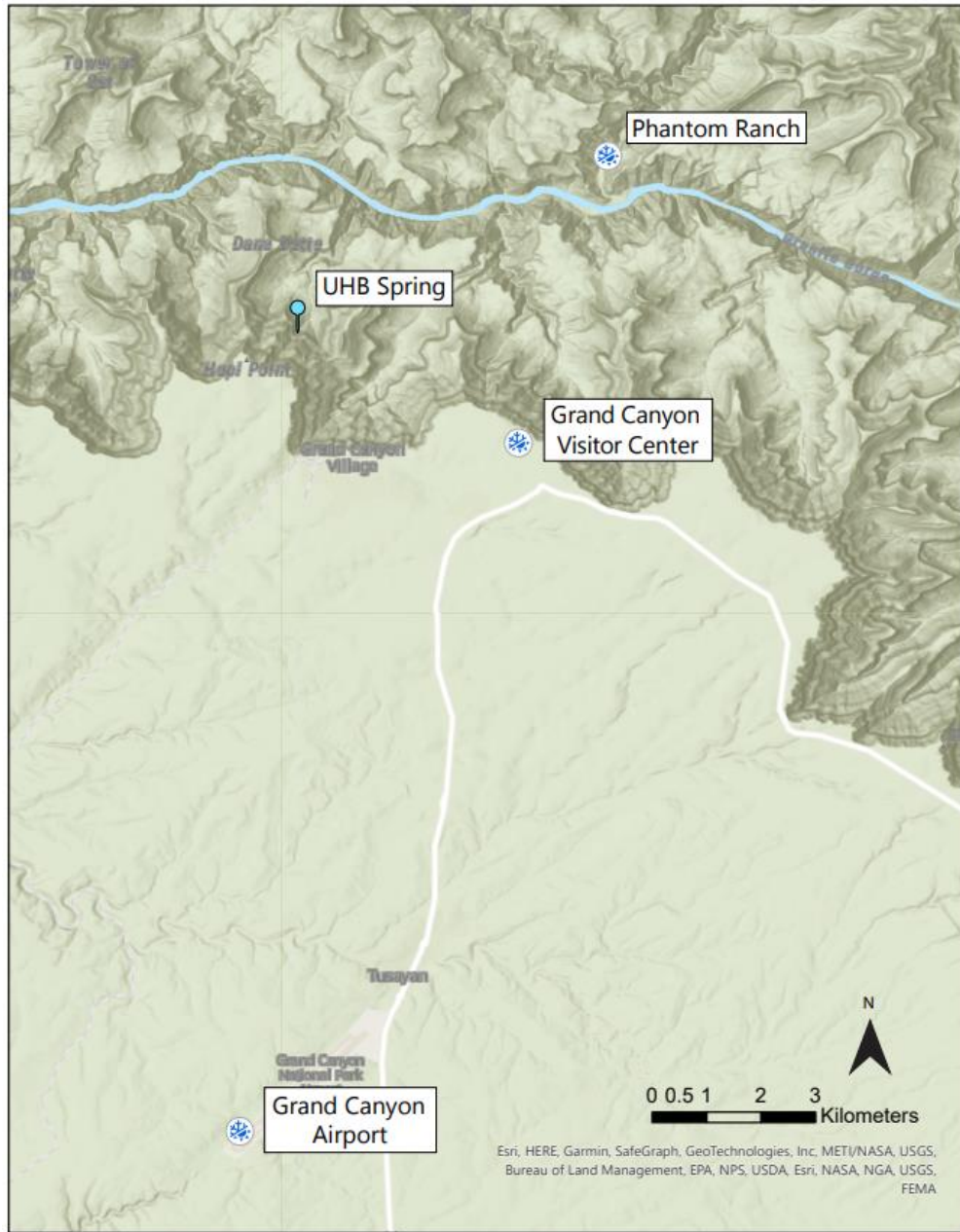


Fig. 6 Topographic map displaying the locations of three weather stations, Grand Canyon Airport (GRCA-AP), Phantom Ranch (PR), and Grand Canyon Visitor Center (GRCA-VC) in relation to UHB spring. Note that GRCA-VC and GRCA-AP are situated on the rim while PR is situated within the canyon near the Colorado River.

Fig. 7 Correlation Matrix

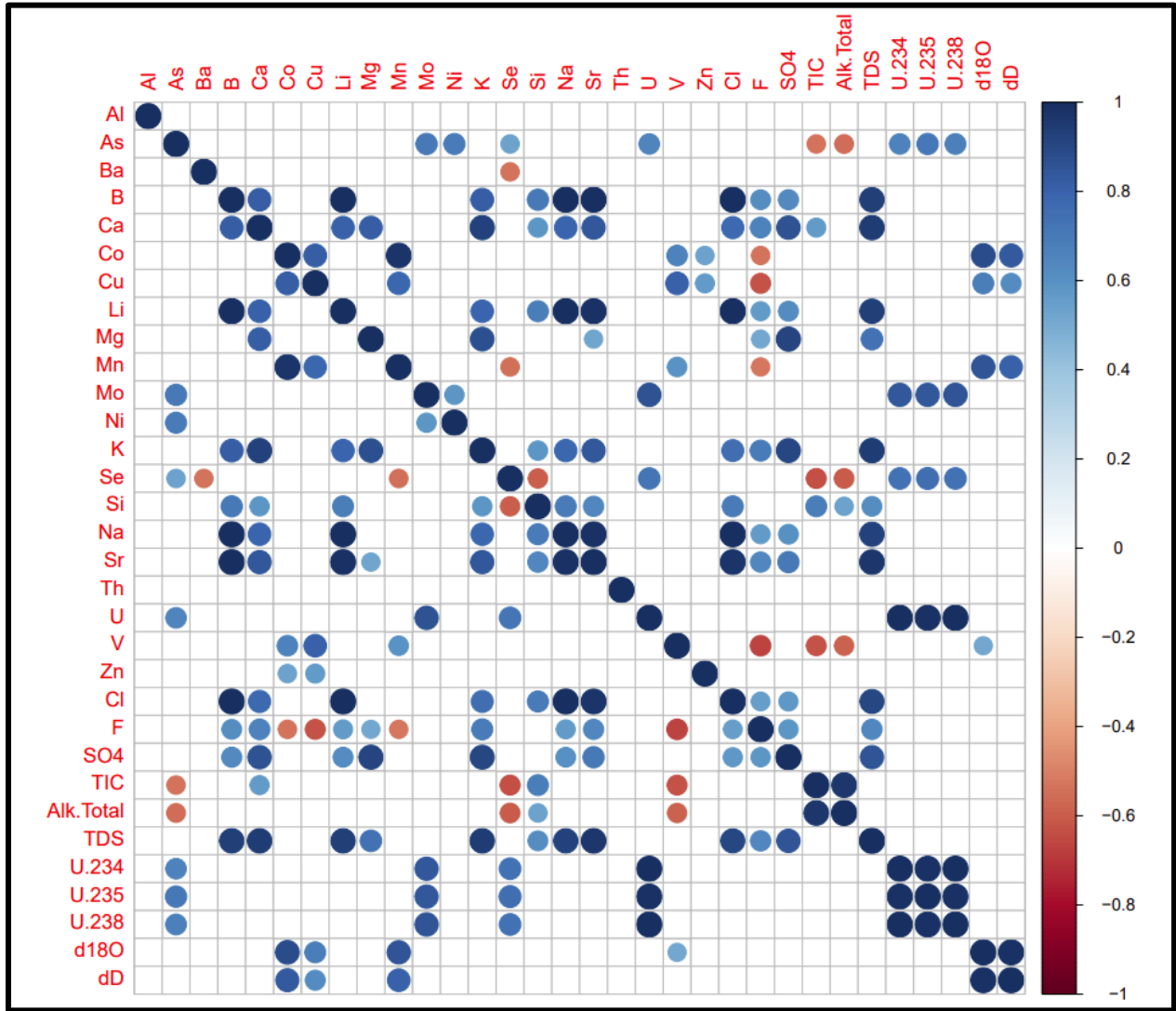


Fig. 7 Correlation matrix of data collected in October 2013 by URS, Inc. All values present returned a p-value < 0.05, and empty squares represent correlations that returned p-values greater than 0.05. Blue values indicate a positive correlation, and red values indicate a negative correlation.

Fig. 8 Piper Diagram of 2013 and 2023 data

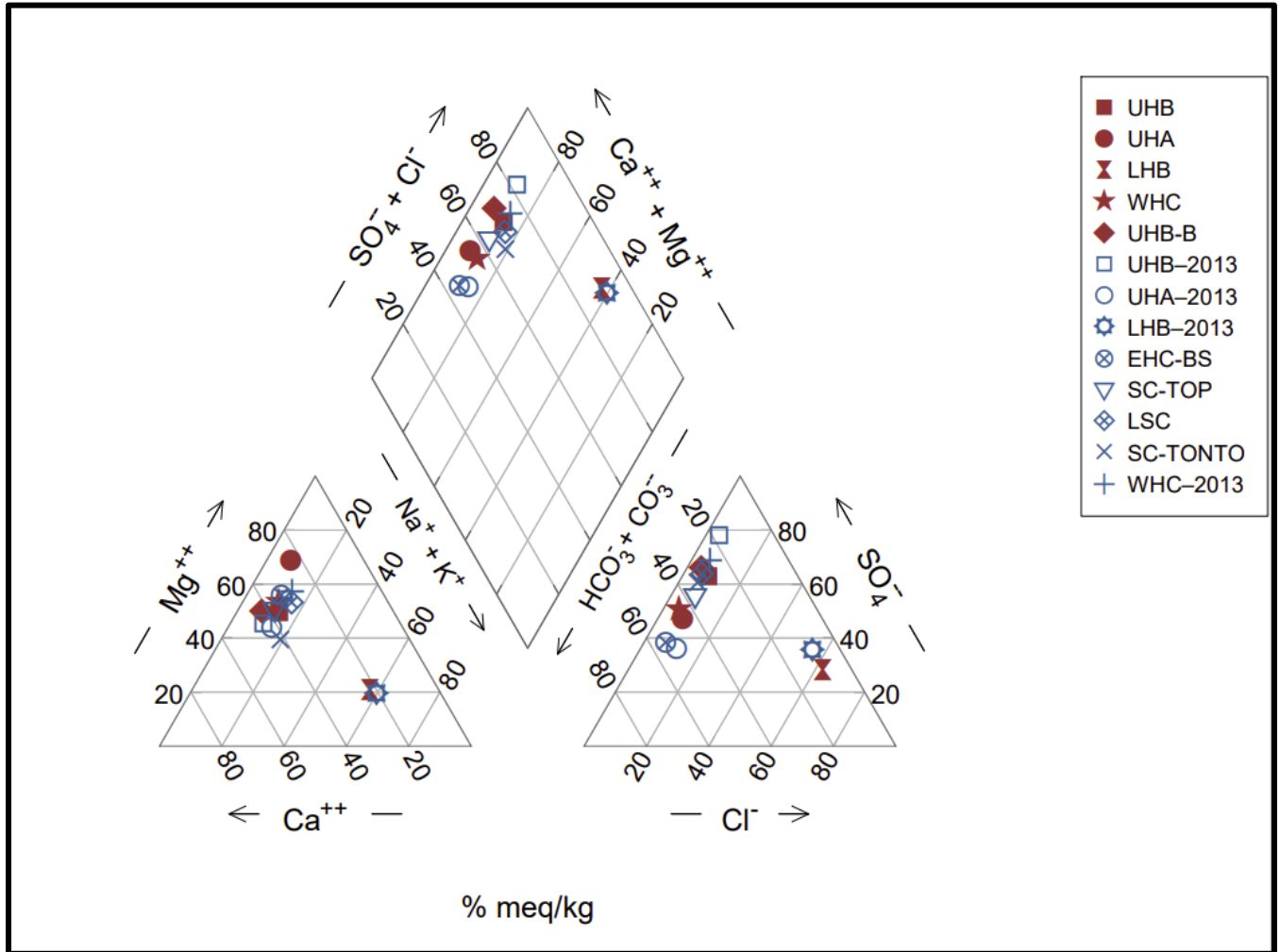


Fig. 8 Piper diagram displaying the chemistry of groundwater sampled in 2022 and 2023 (red) and groundwater samples collected in 2013 (blue). The piper diagram displays the ratio of major ions within a sample, not the total sum (TDS).

Fig. 9 Horn and Salt Creek Stable Isotopes

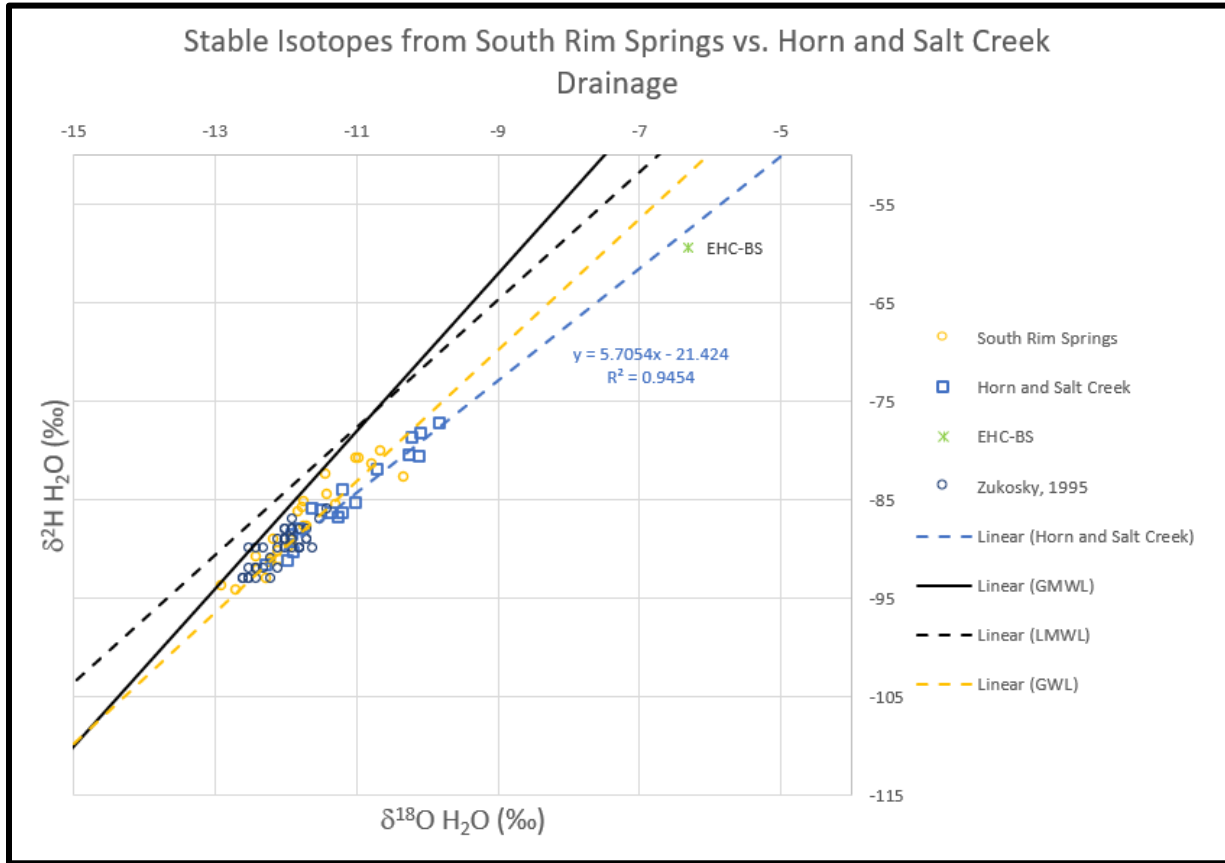


Fig 9. Stable isotopes from Horn and Salt Creek drainages from URS Inc. (October 2013) and this study (November 2022 and April 2023) plotted as blue, hollow squares. Data includes all samples collected at spring orifices, including one outlier, EHC-BS spring, which was significantly enriched relative to other springs in the drainage. Yellow circles represent stable isotopic data compiled from groundwater sources within the South Rim/Coconino Plateau in Beisner and Solder (2020) and Zukosky (1995). The line of best fit (blue-dashed) was calculated using excel linear regression, and did not include EHC-BS. The GWL and LMWL were calculated in Solder and Beisner (2020) and the GMWL was calculated in Craig (1961).

Fig. 10 3-D PCA of all analytes collected in 2013

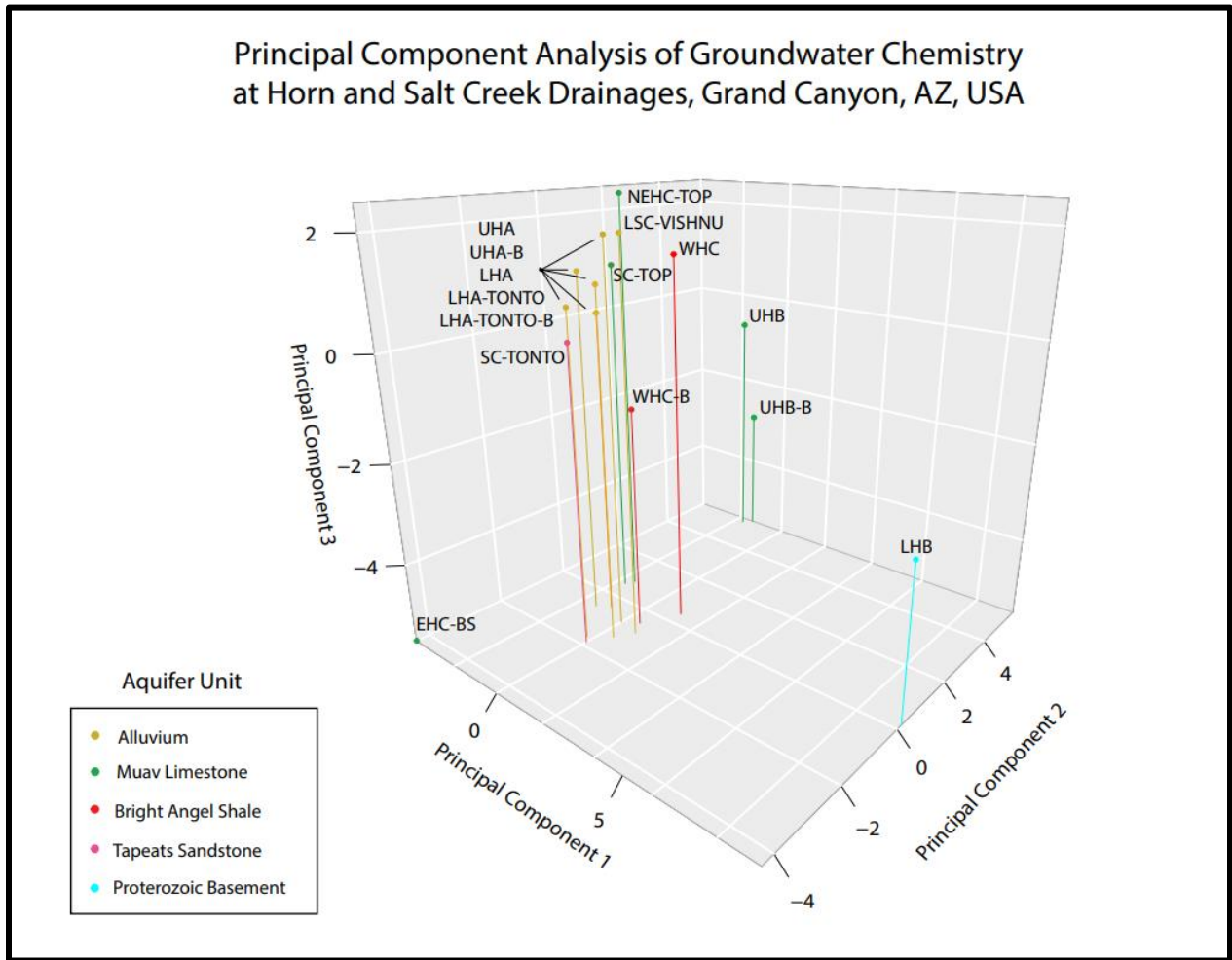


Fig. 10 A 3-dimensional plot displaying the results of the Principal Component Analysis for all groundwater samples collected in October of 2013. The chemistries are plotted in relation to PC1, PC2, and PC3. The color of the samples in the figure correspond to the lithology of the sample location as described by URS Inc. (2013).

Fig. 11 All Analytes PCA: PC1-PC2 Biplot

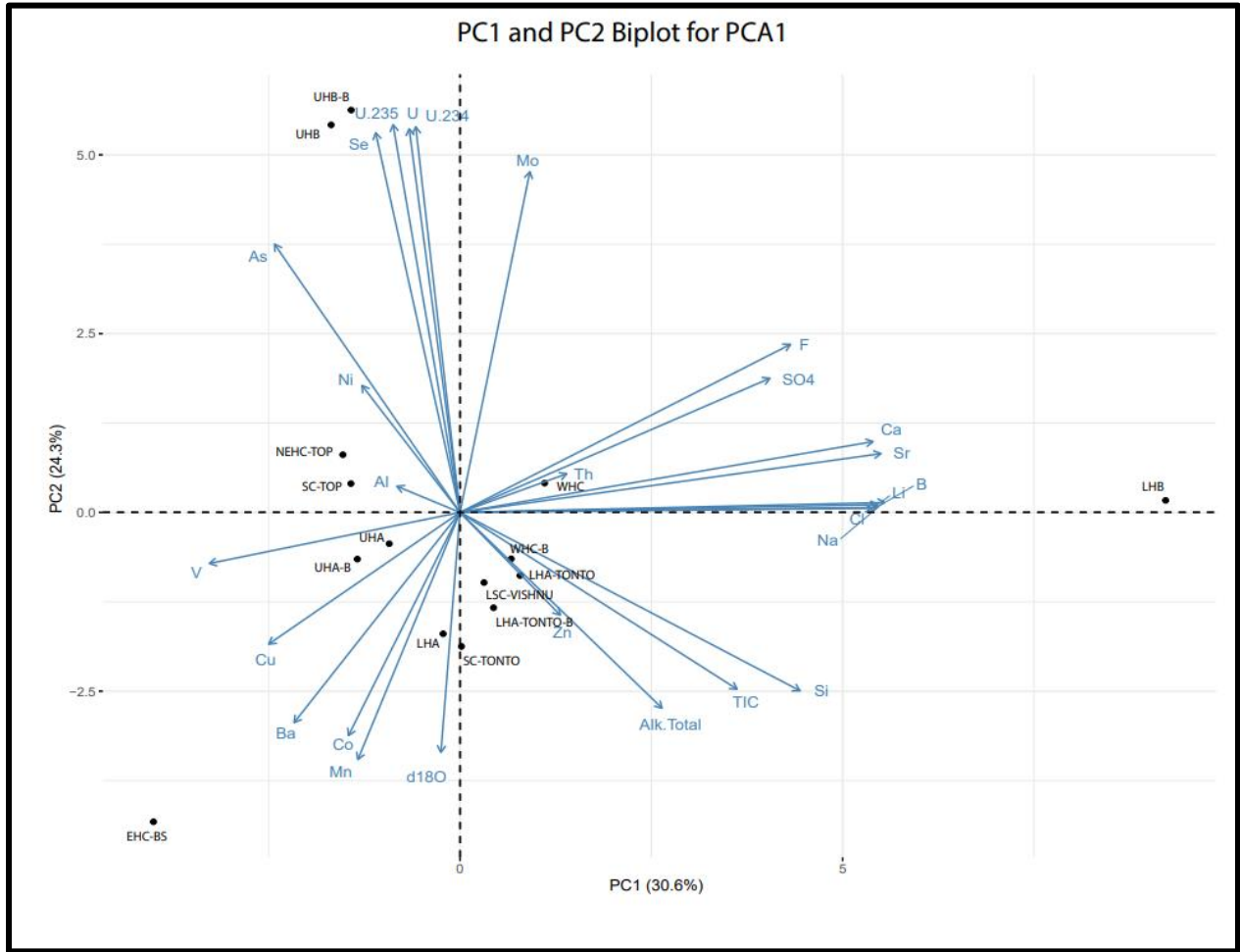


Fig. 11 A 2-dimensional plot displaying the results of the Principal Component Analysis for all groundwater samples collected in October of 2013. The chemistries are plotted in relation to PC1 and PC2, as are the vectors for each analyte included in the PCA. Longer vectors indicate a more significant relationship between an analyte and PC1 and/or PC2.

Fig. 12 H-Kmeans for Multivariate Analysis of All Analytes Collected in 2013

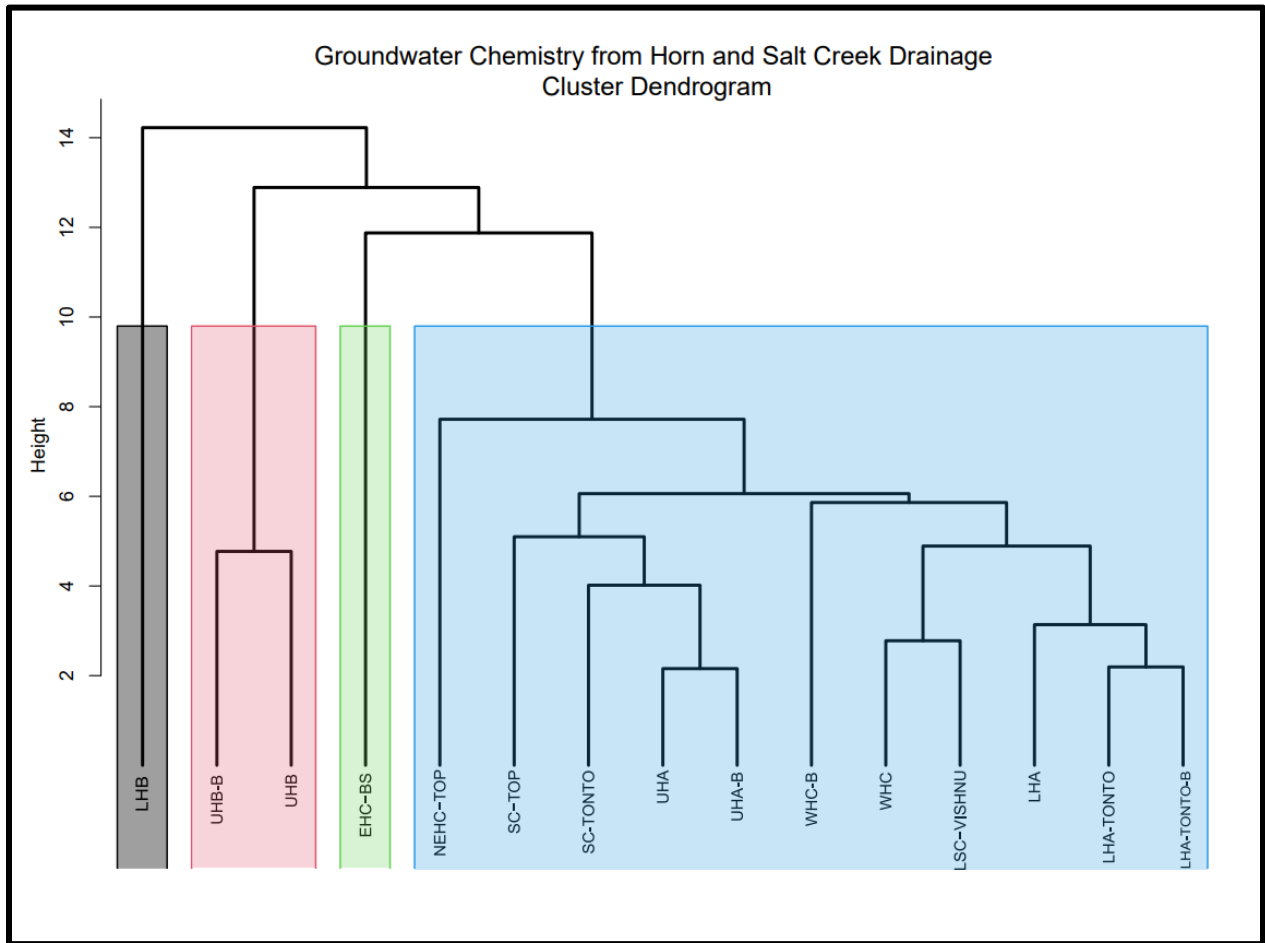


Fig. 12 Shows groundwater chemistries sampled in October of 2013 in the Horn and Salt Creek drainages. The dendrogram portrays the similarity and dissimilarity between chemistries. At each height, more similar sites are grouped together, such that eventually all sites are in one group. The H-Kmeans analysis indicated four clusters, portrayed in this figure using color.

Fig.13 Time PCA: 3-D Plot

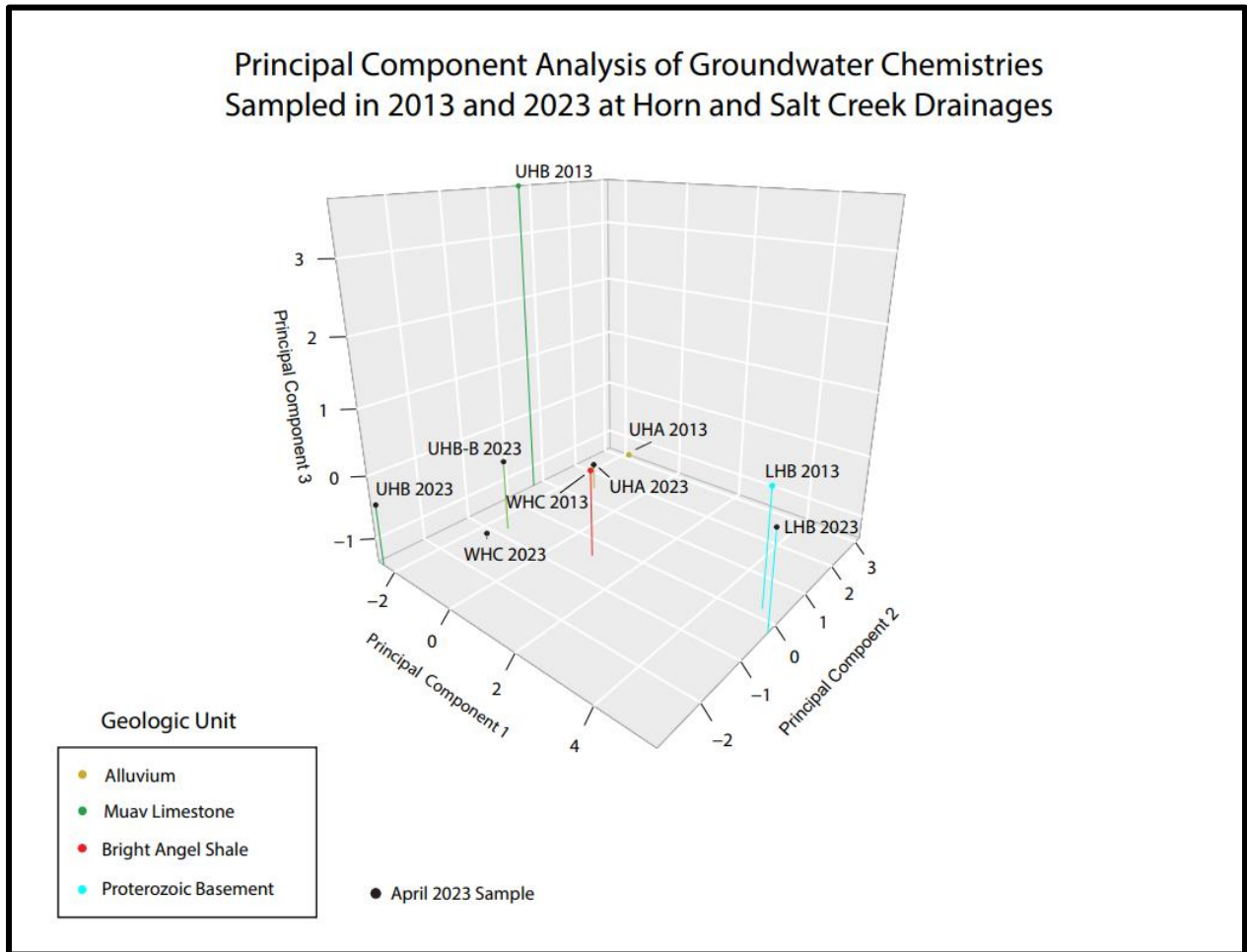


Fig. 13 A 3-dimensional plot displaying the results of the Principal Component Analysis for groundwater samples collected in October of 2013 and then again in March of 2023. The chemistries are plotted in relation to PC1, PC2, and PC3. The color of the samples in the figure correspond to the lithology of the sample location as described by URS Inc. (2013) and field observations in 2023. Black dots indicate a 2023 sample.

Fig. 14 Time PCA: PC1-PC2 Biplot

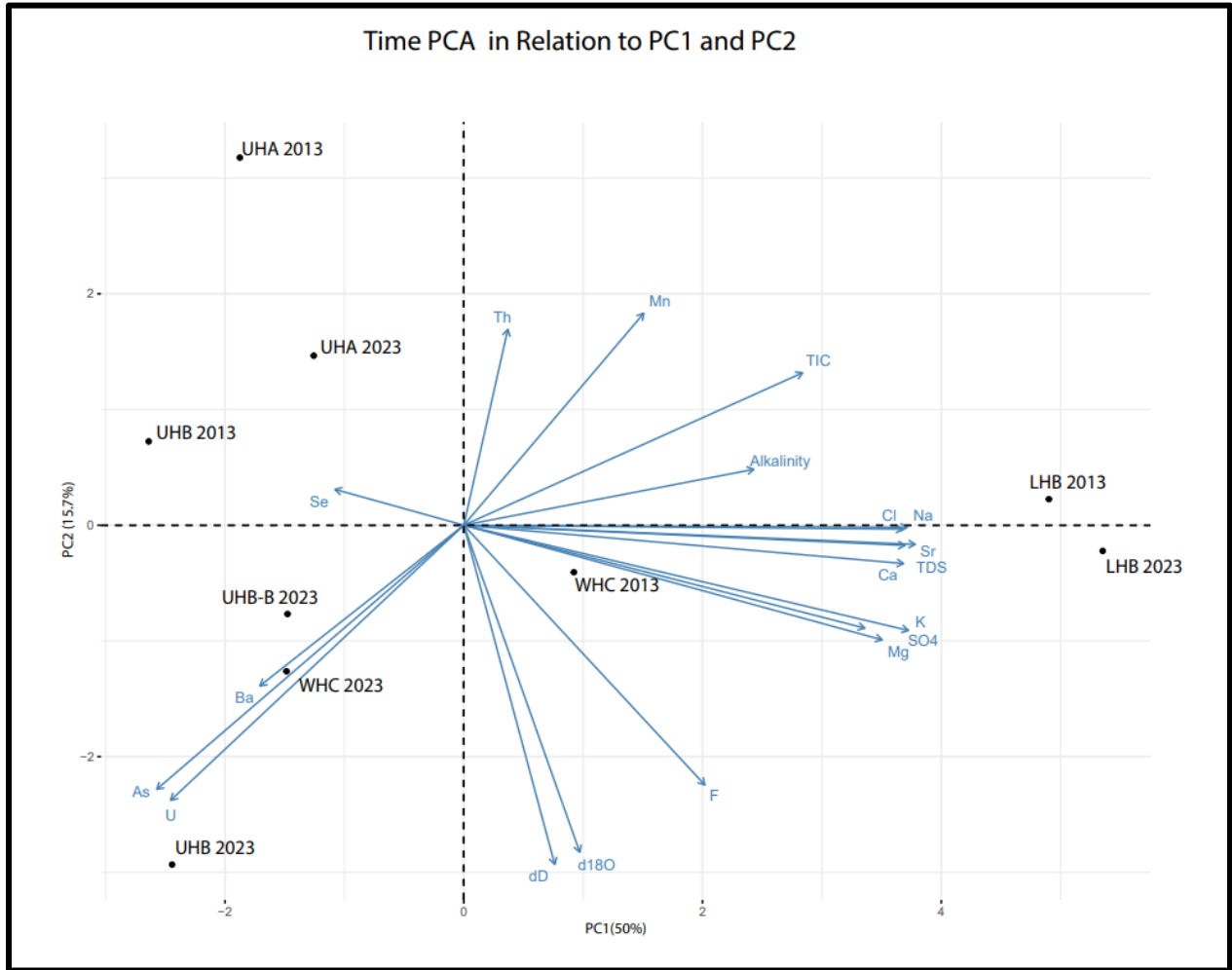


Fig. 14 A 2-dimensional plot displaying the results of the Principal Component Analysis for groundwater samples collected in October of 2013 and again in March 2023. The chemistries are plotted in relation to PC1 and PC2, as are the vectors for each analyte included in the PCA. Longer vectors indicate a more significant relationship between an analyte and PC1 and/or PC2.

Fig. 15 Time PCA: PC2-PC3 Biplot

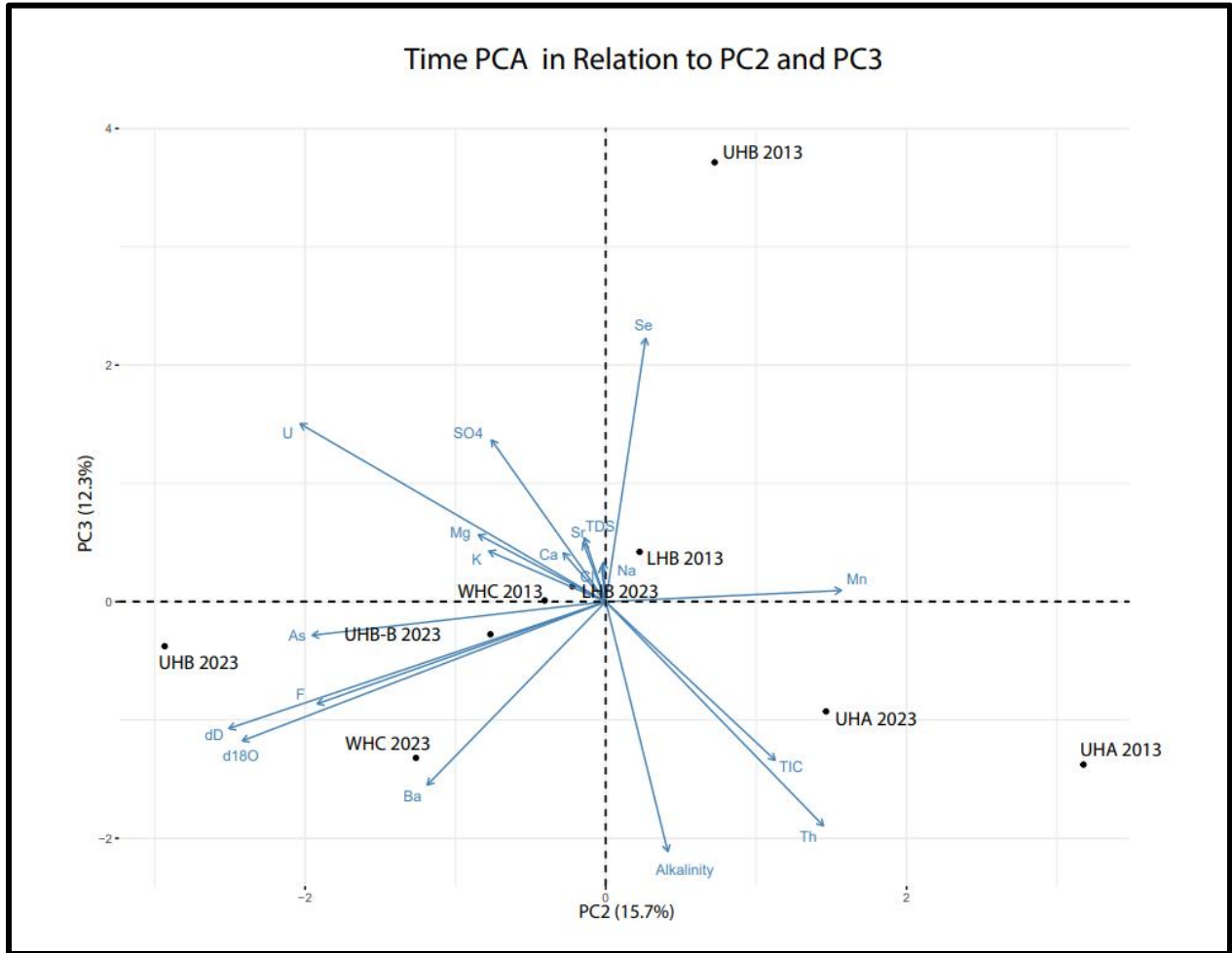


Fig. 15 A 2-dimensional plot displaying the results of the Principal Component Analysis for groundwater samples collected in October of 2013 and again in March 2023. The chemistries are plotted in relation to PC2 and PC3, as are the vectors for each analyte included in the PCA. Longer vectors indicate a more significant relationship between an analyte and PC2 and/or PC3.

Fig. 16 Time PCA: Cluster Plot

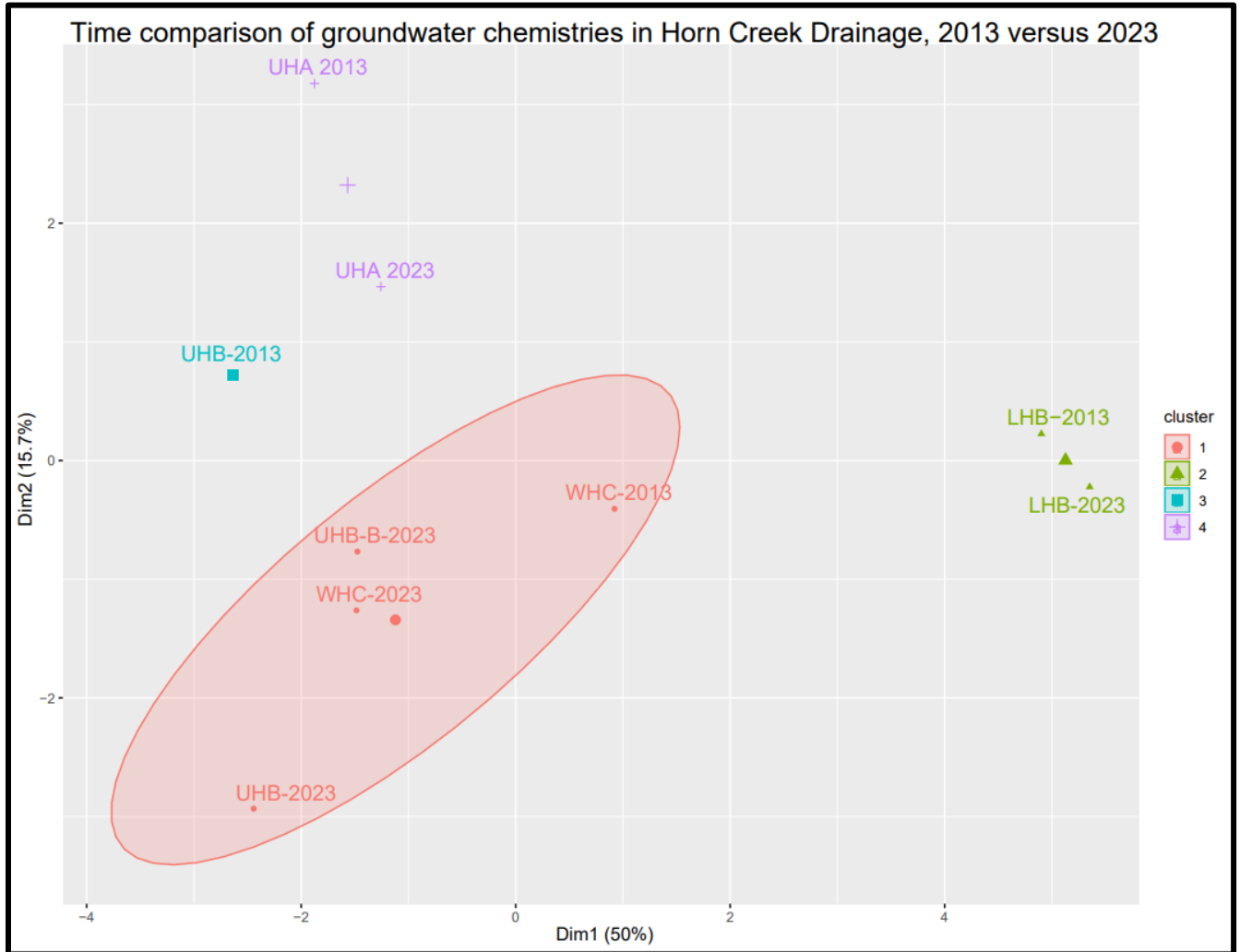


Fig. 16 H-Kmeans plot displaying the springs sampled in October 2013 and again in March 2023. The spring's chemistries are displayed in a PCA biplot, with colors indicating the four clusters identified in the H-Kmeans clustering analysis. OU2-TMS clusters alone.

Fig. 17 Uranium Analytes PCA: 3-D Plot

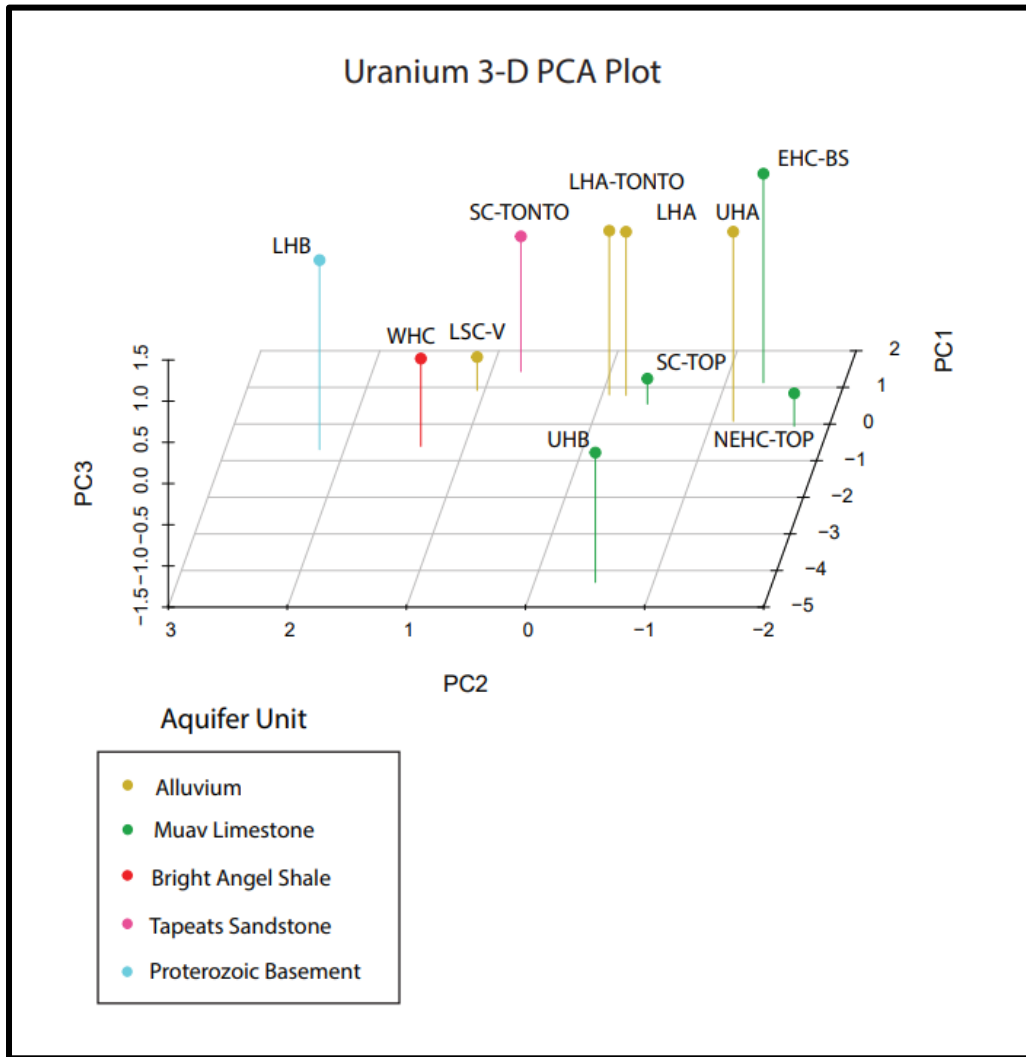


Fig. 17 A 3-dimensional plot displaying the results of the uranium-focused Principal Component Analysis for groundwater samples collected in October of 2013. Only analytes associated with dissolved uranium were included. The chemistries are plotted in relation to PC1, PC2, and PC3. The color of the samples in the figure correspond to the lithology of the sample location as described by URS Inc. (2013).

Fig. 18 Uranium Analytes PCA: PC1-PC2 Biplot

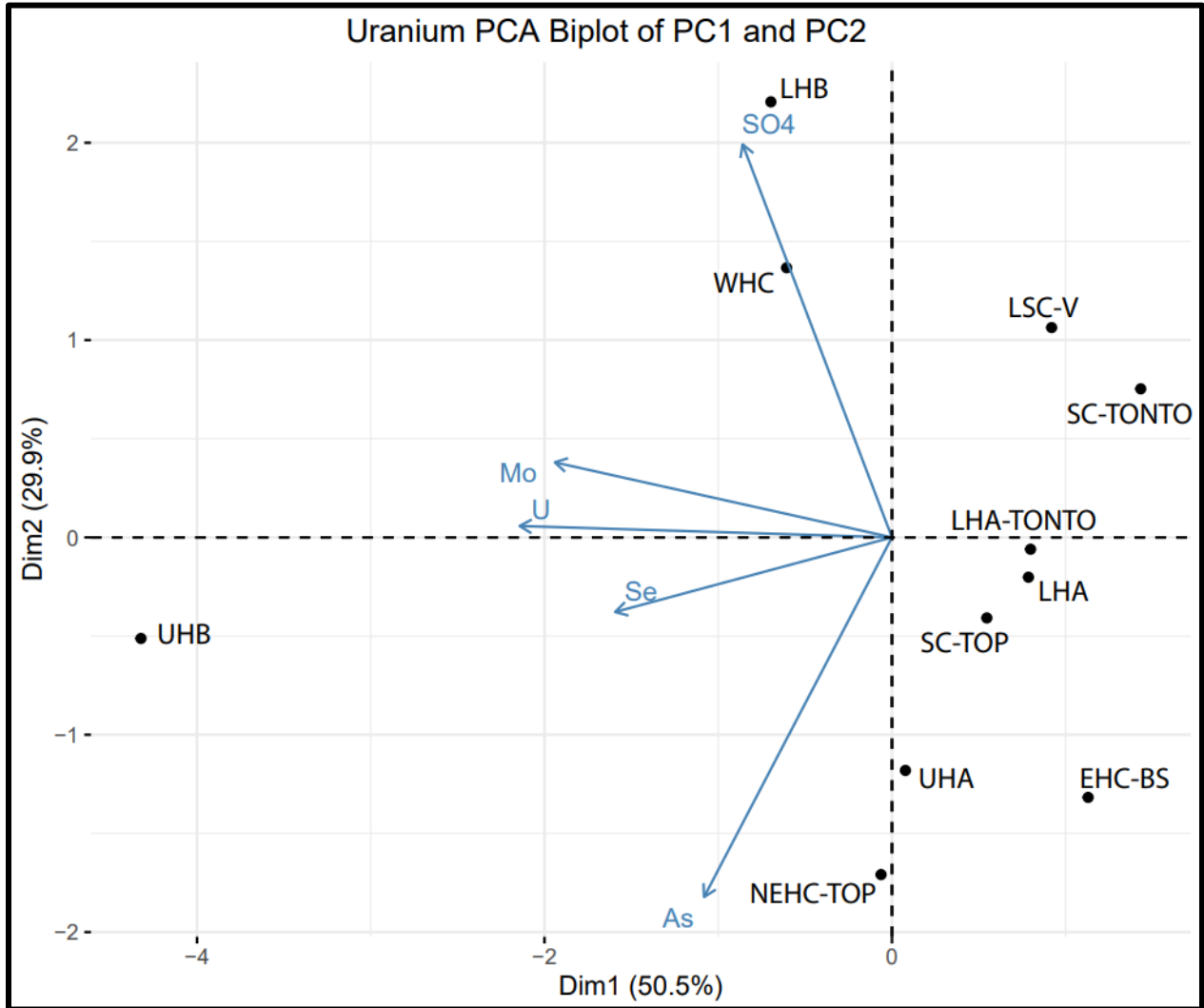


Fig. 18 A 2-dimensional plot displaying the results of the uranium focused Principal Component Analysis for groundwater samples collected in October of 2013 in the Horn and Salt Creek drainages. Only analytes associated with dissolved uranium were included. The chemistries are plotted in relation to PC1 and PC2, as are the vectors for each analyte included in the PCA. Longer vectors indicate a more significant relationship between an analyte and PC1 and/or PC2.

Fig. 19 Uranium Analytes PCA: PC2-PC3 Biplot

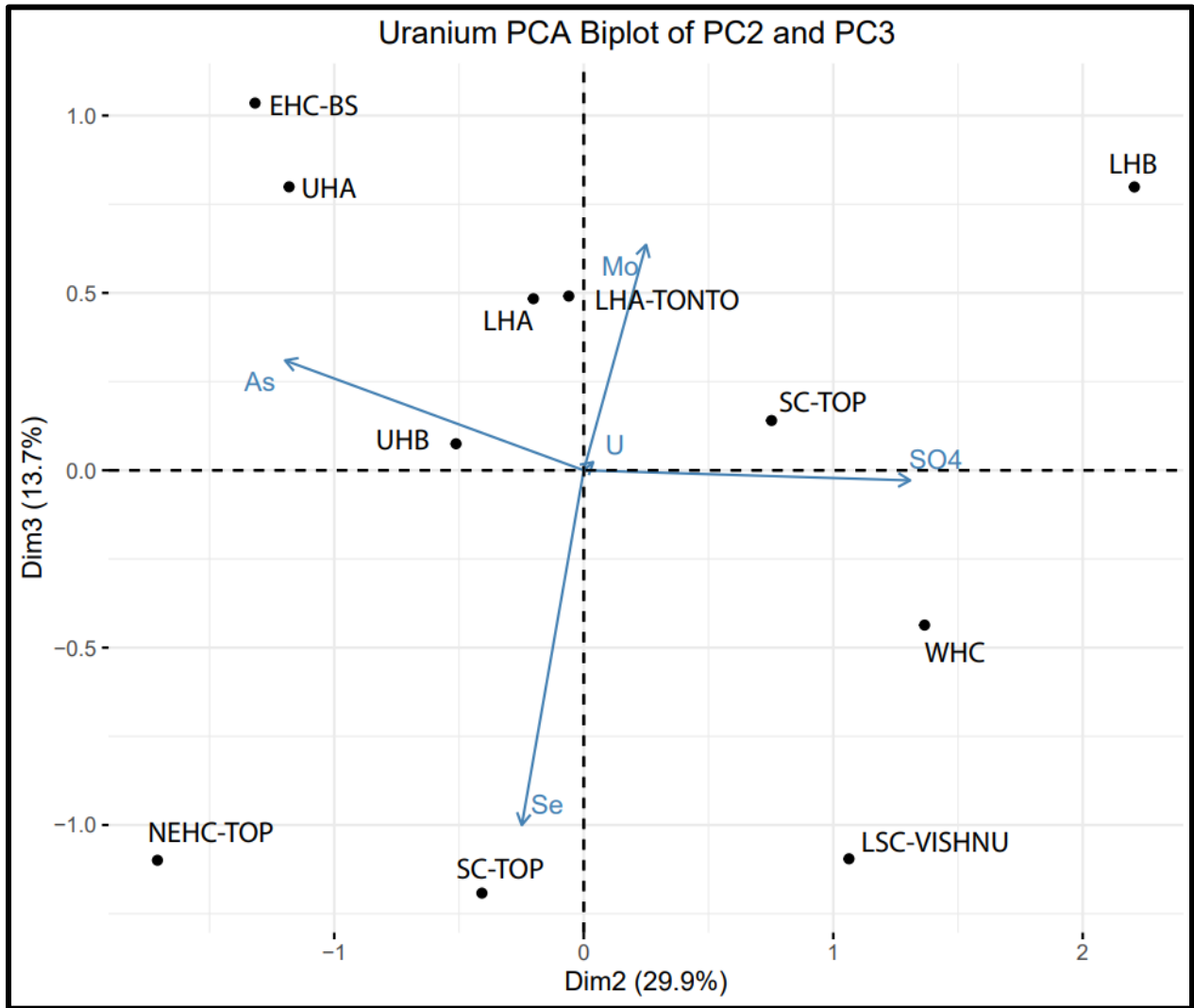


Fig. 19 A 2-dimensional plot displaying the results of the uranium focused Principal Component Analysis for groundwater samples collected in October of 2013 in the Horn and Salt Creek drainages. Only analytes associated with dissolved uranium were included. The chemistries are plotted in relation to PC1 and PC2, as are the vectors for each analyte included in the PCA. Longer vectors indicate a more significant relationship between an analyte and PC1 and/or PC2.

Fig. 20 Uranium Analytes H-Kmeans Chart

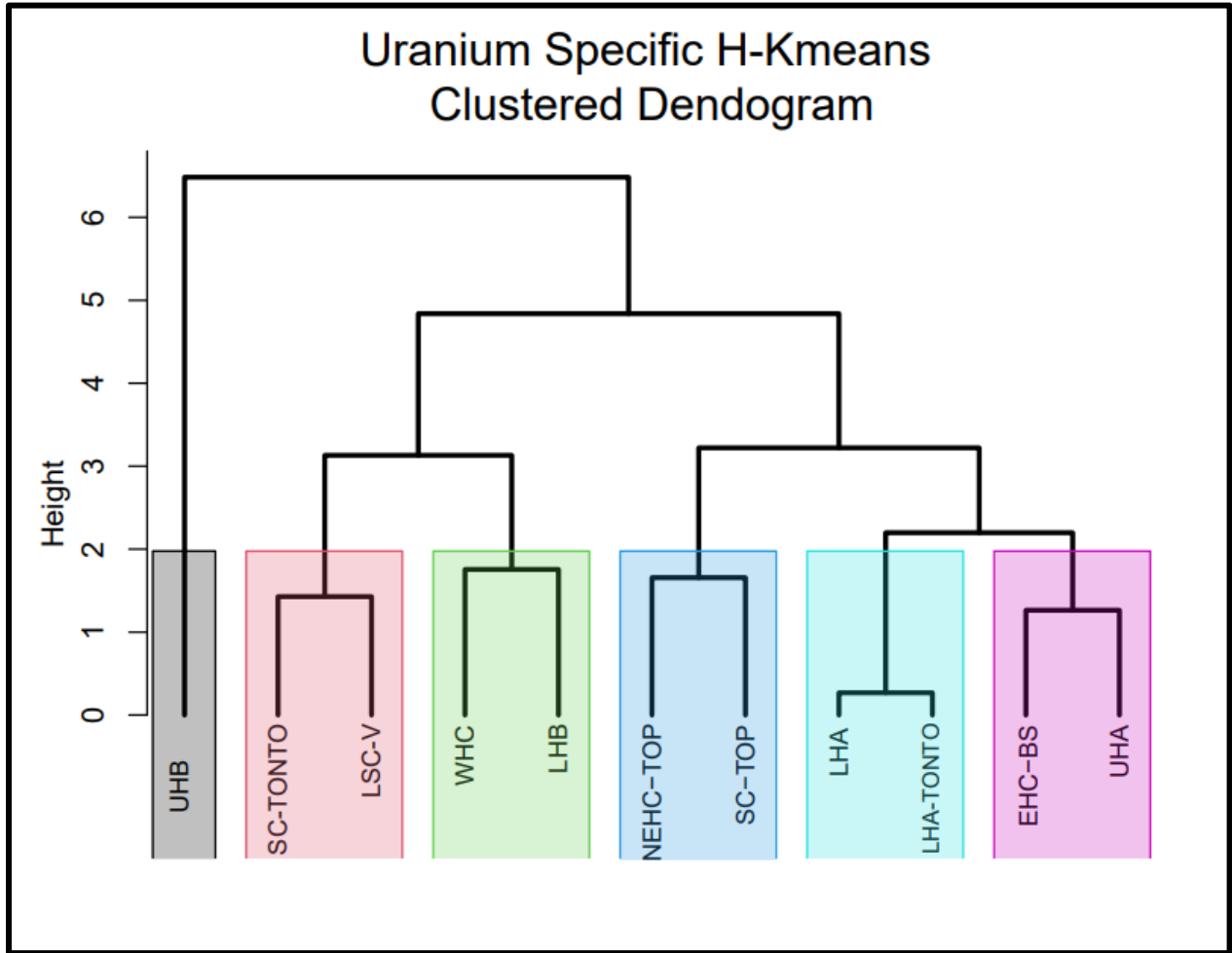


Fig. 20 Shows groundwater chemistries sampled in October of 2013 in the Horn and Salt Creek drainages. This H-Kmeans analysis only included uranium specific analytes (SO₄, U, As, Mo, and Se). The dendrogram portrays the similarity and dissimilarity between chemistries. At each height, more similar sites are grouped together, such that eventually all sites are in one group. The H-Kmeans analysis indicated six clusters, portrayed in this figure using color.

Fig. 21 Uranium Analytes K-means Plot

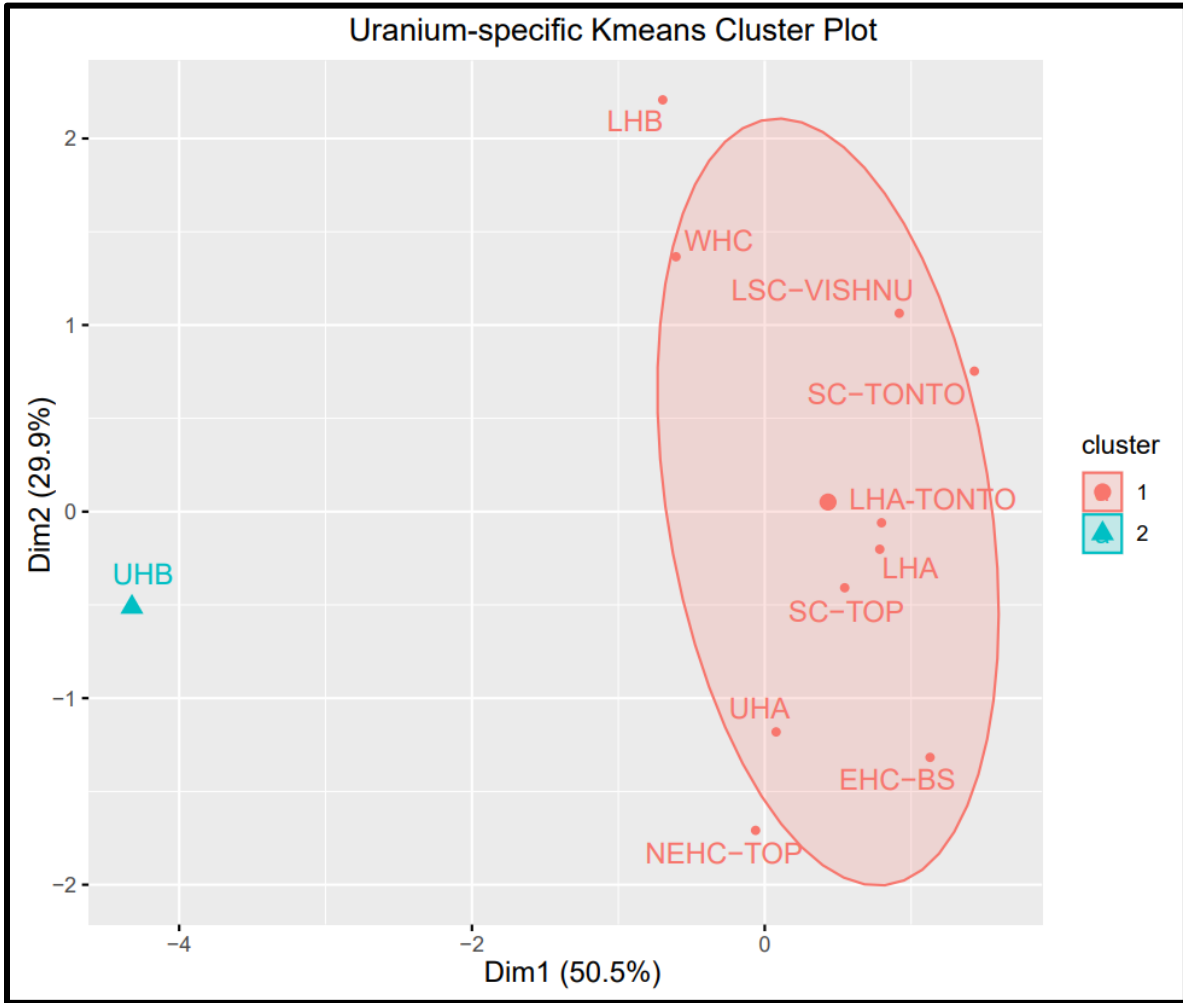


Fig. 21 H-Kmeans plot displaying the springs sampled in October 2013 in Horn and Salt Creek drainage. Only analytes associated with dissolved uranium were included in the analysis. The spring's chemistries are displayed in a PCA biplot, with colors indicating the two clusters identified in the H-Kmeans clustering analysis. OU2-TMS clusters alone.

Fig. 22 Total Dissolved Uranium Over Time at Upper Horn Bedrock

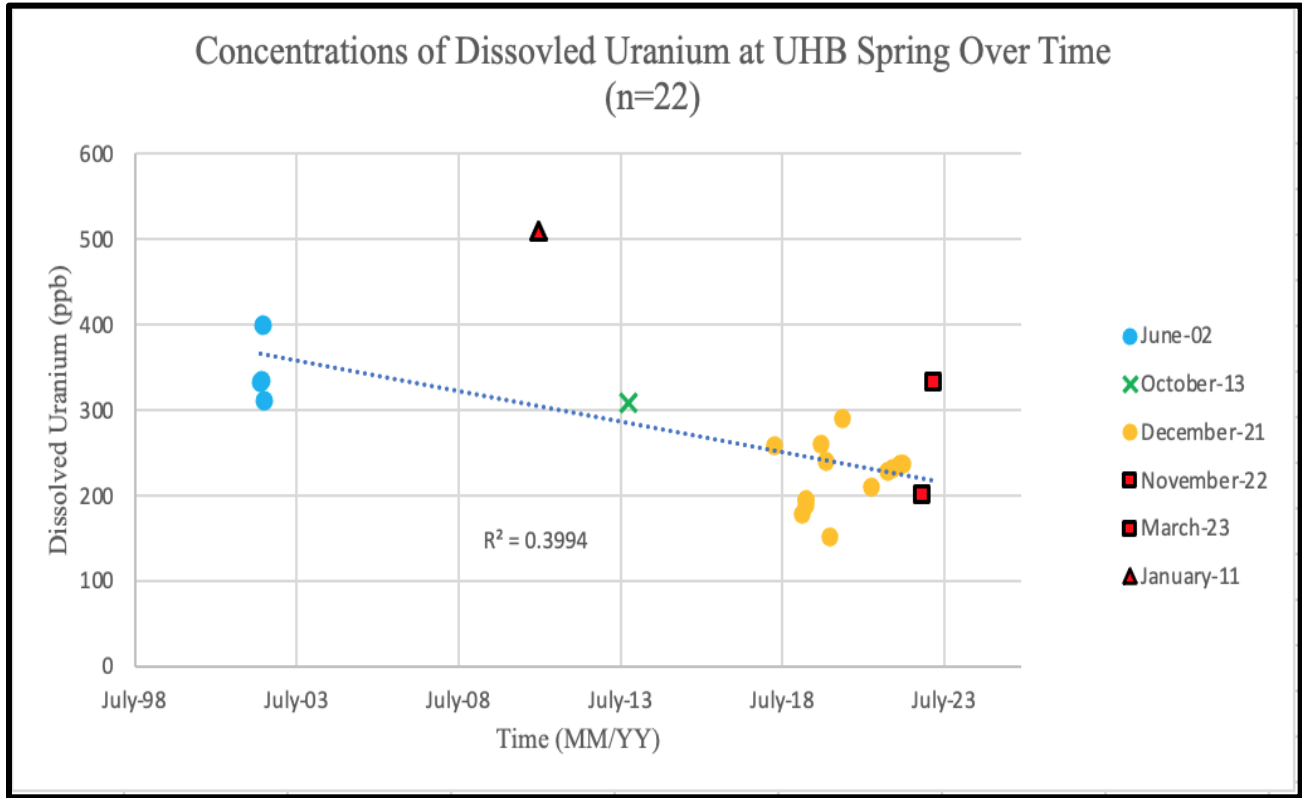


Fig. 22 Dissolved uranium in parts per billion sampled at Upper Horn Bedrock Spring from July 2002 to March 2023. Symbology corresponds to the five separate studies that measured dissolved uranium over a roughly 20-year period. Samples in 2002 were collected by Liebe (2003), the sample collected in 2011 was collected by Scharr (2011, unpublished), the sample collected in 2013 was collected by URS Inc. (2014), and the samples collected from 2018 to 2022 were collected by the USGS (NWIS). November 2022 and March 2023 were samples collected in this study.

Fig. 23 Precipitation vs. Total Dissolved Uranium at UHB Spring from 2002 to 2023

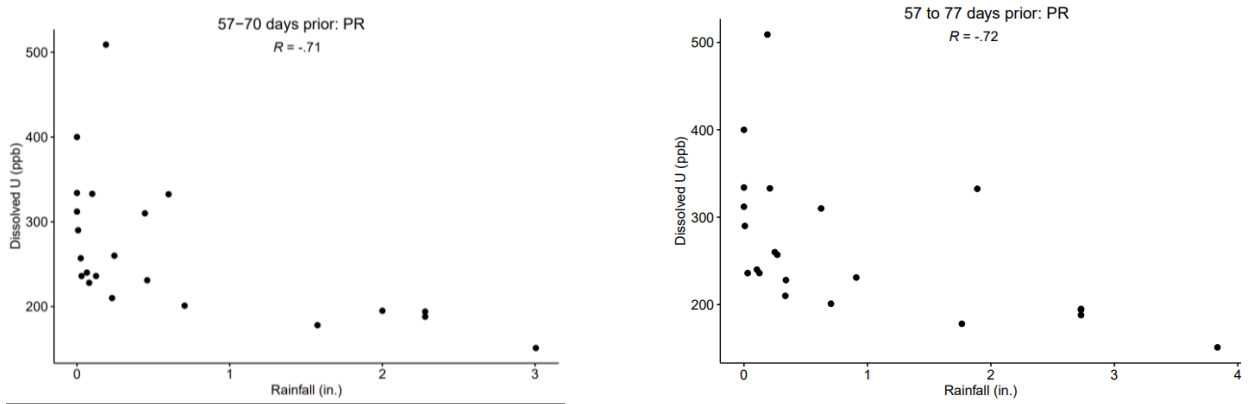


Fig. 23 Relationship between dissolved uranium sampled at Upper Horn Bedrock from 2002-2023 (n=22) and total precipitation recorded at Phantom Ranch weather station between the period of 57 to 70 days prior to the sampling of dissolved uranium and the period of 57 to 77 days prior to sampling at Upper Horn Bedrock spring.

Fig. 24 Stable Isotopes and Bedrock Lithology of Springs

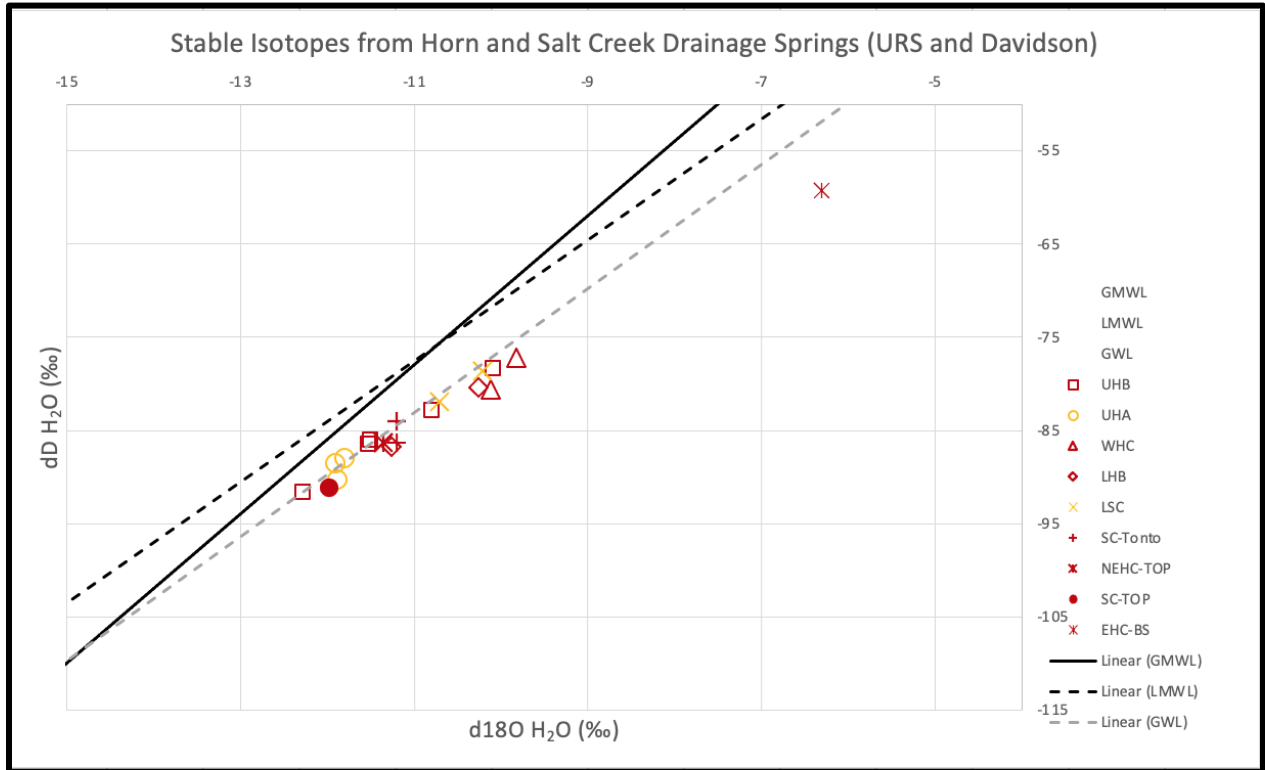


Fig. 24 Stable isotopes from Horn and Salt Creek drainages from URS Inc. (October 2013) and this study (November 2022 and April 2023). Data includes all samples collected at spring orifices, including one outlier, EHC-BS spring, which was significantly enriched relative to other springs in the drainage. Springs were assigned a color based on bedrock or alluvial aquifer (red indicates a bedrock spring, while yellow indicates an alluvial spring), while shape remained consistent with other figures in this study.

Fig. 25 Stable Isotopes vs. Dissolved Uranium Plot

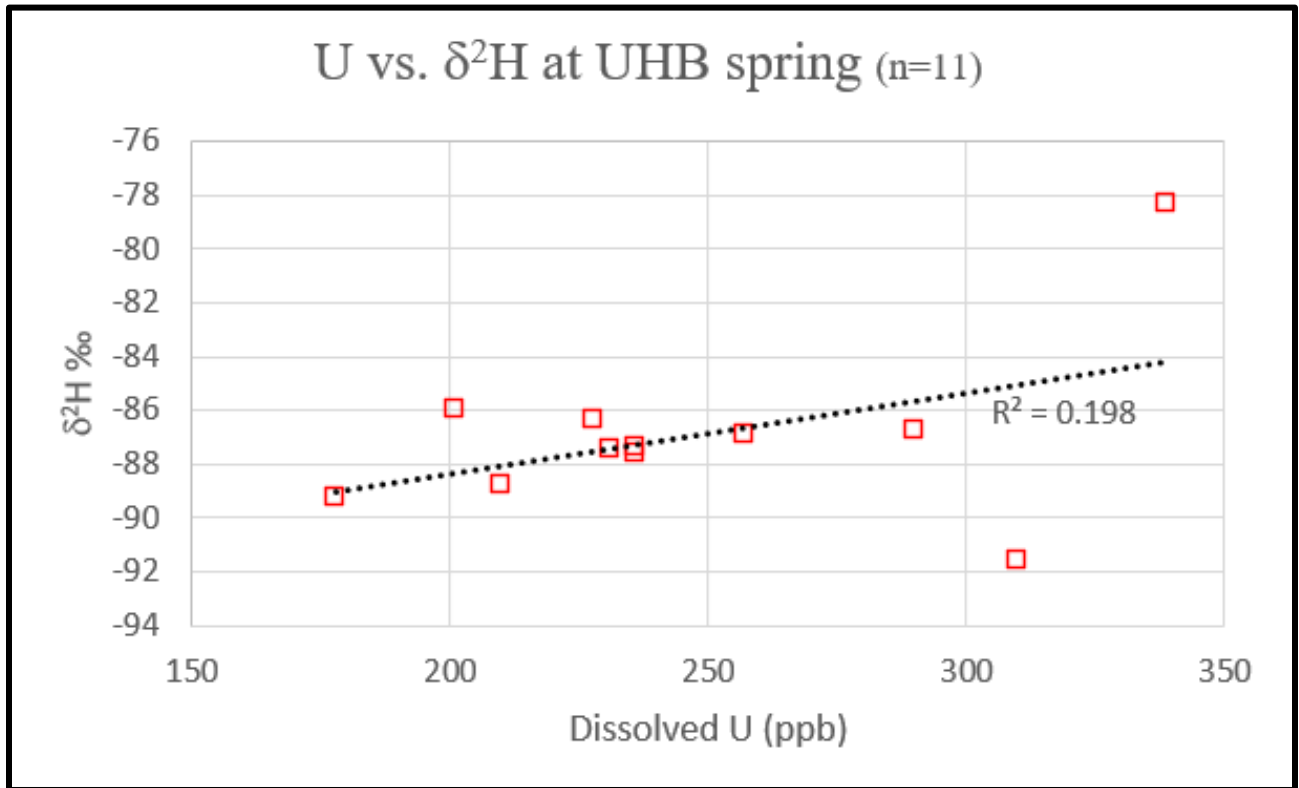


Fig. 25 Dissolved uranium versus $\delta^2\text{H}$ ‰ at Upper Horn Bedrock Spring. Data was compiled from URS, USGS, and this study, ranging from October 2013 to April 2023. Similar correlations ($R^2=0.192$) were found for $\delta^{18}\text{O}$ ‰ and dissolved U.

Appendix B: Sampling Locations and Data Tables

Table 1: Sampling Locations

| Spring Name | Abbreviation | Lithology | Latitude | Longitude | Elev. | Oct. 2013 | Nov. 2022 | Mar. 2023 |
|---------------------------------|--------------|--------------------|----------|------------|-------|-----------|-----------|-----------|
| Battle Ship Pools | BS-POOL | Alluvium | 36.07826 | -112.14261 | 1201m | | x | |
| East Horn Creek - Battle Ship | EHC-BS | Muav Limestone | 36.07641 | -112.14248 | 1275m | x | | |
| Havasupai Gardens | HG | Alluvium | 36.07658 | -112.12872 | 1169m | | x | |
| Lower Horn Alluvium | LHA | Alluvium | 36.08299 | -112.14337 | 1096m | x | x | |
| Lower Horn Alluvium - Tonto | LHA-TONTO | Alluvium | 36.08460 | -112.14388 | 1077m | x | x | |
| Lower Horn Alluvium-Tonto-Below | LHA-TONTO-B | Alluvium | 36.08460 | -112.14388 | 1070m | x | | |
| Lower Horn Bedrock | LHB | Vishnu Schist | 36.09328 | -112.13873 | 926m | x | | x |
| Lower Salt Creek - Vishnu | LSC-V | Alluvium | 36.08921 | -112.16247 | 973m | x | x | |
| North East Horn Creek - Top | NEHC-TOP | Muav Limestone | 36.08170 | -112.13902 | 1289m | x | | |
| Salt Creek - Tonto | SC-TONTO | Tapeats Sandstone | 36.08477 | -112.16211 | 1038m | x | x | |
| Salt Creek - Top | SC-TOP | Muav Limestone | 36.07756 | -112.16162 | 1157m | x | x | |
| Upper Horn Alluvium | UHA | Alluvium | 36.08064 | -112.14351 | 1130m | x | x | x |
| Upper Horn Alluvium-Below | UHA-B | Alluvium | 36.08126 | -112.14334 | 1119m | x | | |
| Upper Horn Bedrock | UHB | Muav Limestone | 36.07739 | -112.14594 | 1263m | x | x | x |
| Upper Horn Bedrock-Below | UHB-B | Overflow from Muav | 36.07768 | -112.14581 | 1253m | x | | x |
| West Horn Creek (2013) | WHC-13 | Bright Angel | 36.08226 | -112.14991 | 1131m | x | | |
| West Horn Creek (2023) | WHC-23 | Muav Limestone | 36.08111 | -112.15000 | 1390m | | | x |
| West Horn Creek-Below | WHC-B | Bright Angel Shale | 36.08273 | -112.14991 | 1120m | x | | |

Table 2: Groundwater chemistry data collected in November of 2022

| | Analyte | UHA | LHA | BS-Pools | UHB | SC-Top-E | SC-Top-W | LSC-V | HG | HG #2 | Blank |
|-----------------------------------|---------------------------------|------------------------------------|--------|----------|--------|----------|----------|--------|-------|-------|-------|
| TOC/TN (ppm) | Total Carbon | 54.37 | 93.13 | 36.94 | 29.95 | 36.74 | 37.95 | 71.46 | 55.35 | n/a | n/a |
| | Inorganic Carbon | 55.15 | 92.64 | 29.31 | 29.40 | 37.63 | 38.16 | 76.29 | 57.50 | n/a | n/a |
| | Organic Carbon | 0.00 | 0.4854 | 7.626 | 0.5485 | 0.00 | 0.00 | 0.00 | 0.00 | n/a | n/a |
| | Total Nitrogen | 1.965 | 0.9180 | 8.072 | 0.6960 | 1.39 | 1.21 | 0.14 | 0.40 | n/a | n/a |
| | pH | 7.23 | 7.50 | 7.93 | 8.20 | n/a | 8.82 | 8.03 | 7.52 | n/a | n/a |
| °C | Temp (°C) | 13.80 | 9.50 | 7.70 | 9.00 | n/a | 11.50 | 10.10 | 14.40 | n/a | n/a |
| mS/cm | Conductivity | 712 | 1050 | 371 | 862 | n/a | 684 | 1420 | 453 | n/a | n/a |
| Major Ions (ppm) | F- | BDL | BDL | BDL | BDL | BDL | BDL | BDL | BDL | n/a | n/a |
| | Cl- | 31.7 | 46.9 | 3.67 | 18.2 | 20.1 | 19.9 | 36.0 | 0.838 | n/a | n/a |
| | Br- | BDL | BDL | 34.4 | BDL | BDL | BDL | BDL | 0.368 | n/a | n/a |
| | NO3- | BDL | BDL | BDL | BDL | BDL | BDL | BDL | BDL | n/a | n/a |
| | NO2- | 4.54 | 0.590 | 32.4 | 2.53 | 4.11 | BDL | BDL | 18.1 | n/a | n/a |
| | SO4-- | n/a | n/a | n/a | n/a | n/a | n/a | n/a | n/a | n/a | n/a |
| | PO4--- | 6.47 | 6.48 | 46.3 | 6.52 | 11.0 | 215 | 215 | 11.0 | n/a | n/a |
| | Ca | 36.25 | 100.02 | 27.67 | 45.59 | 36.83 | 37.07 | 111.78 | 30.63 | 30.00 | BDL |
| | K | 9.21 | 13.53 | 6.91 | 12.48 | 5.72 | 7.01 | 24.58 | 1.94 | 1.90 | BDL |
| | Mg | 52.76 | 96.51 | 21.43 | 75.33 | 59.31 | 58.26 | 187.59 | 37.74 | 37.49 | BDL |
| | Na | 25.54 | 46.47 | 2.94 | 23.24 | 19.57 | 21.13 | 54.92 | 6.86 | 6.82 | BDL |
| | Alkalinity as CaCO ₃ | 193 | 348 | 106 | 108 | 166 | 144 | 254 | 212 | n/a | n/a |
| | TDS | 475 | 725 | 255 | 589 | n/a | 465 | 996 | 304 | n/a | n/a |
| | ‰ | d ¹⁸ O H ₂ O | -11.8 | -11.5 | -8.1 | -11.5 | n/a | n/a | -10.7 | -12.4 | -12.4 |
| d ² H H ₂ O | | -88 | -86 | -57 | -86 | n/a | n/a | -82 | -92 | -92 | n/a |
| Trace Metals (ppb) | Ag | BDL | BDL | BDL | BDL | BDL | BDL | BDL | BDL | BDL | BDL |
| | Al | 4.27 | BDL | 11.7 | BDL | BDL | 11.9 | BDL | BDL | BDL | BDL |
| | As | 2.35 | 1.72 | 8.22 | 4.26 | 1.77 | 1.87 | 0.064 | 1.44 | 1.46 | BDL |
| | B | 84.5 | 129 | 47.0 | 66.9 | 69.8 | 73.9 | 141 | 26.9 | 25.1 | BDL |
| | Ba | 55.3 | 49.8 | 86.5 | 29.1 | 26.7 | 27.4 | 22.7 | 281 | 284 | BDL |
| | Be | BDL | BDL | BDL | BDL | BDL | BDL | BDL | BDL | BDL | BDL |
| | Cd | BDL | BDL | BDL | BDL | BDL | BDL | BDL | BDL | BDL | BDL |
| | Co | 0.010 | 0.064 | 0.153 | 0.012 | BDL | 0.030 | 0.015 | 0.004 | 0.002 | BDL |
| | Cr | 0.562 | 0.075 | 0.179 | 0.304 | 0.206 | 0.263 | 0.051 | 0.445 | 0.448 | BDL |
| | Cu | 0.037 | 0.372 | 0.970 | 0.083 | BDL | 1.45 | BDL | BDL | 0.003 | BDL |
| | Fe | 5.79 | 1.13 | 24.7 | 1.05 | 0.405 | 42.2 | 3.13 | 0.730 | 1.21 | BDL |
| | Li | 10.7 | 22.4 | 1.45 | 14.7 | 13.5 | 13.8 | 46.8 | 2.16 | 1.89 | BDL |
| | Mo | 2.56 | 6.11 | 2.71 | 10.6 | 2.21 | 2.14 | 1.27 | 0.409 | 0.415 | BDL |
| | Ni | 0.082 | 0.287 | 0.744 | 0.282 | 0.050 | 0.354 | 0.178 | 0.056 | 0.064 | BDL |
| | Pb | BDL | BDL | BDL | BDL | BDL | 0.013 | BDL | BDL | BDL | BDL |
| | Sb | 0.102 | 0.039 | 0.155 | 0.029 | 0.036 | 0.041 | 0.025 | BDL | 0.027 | BDL |
| | Se | 1.92 | 1.59 | 1.31 | 4.57 | 1.65 | 1.90 | 0.115 | 0.032 | 0.145 | BDL |
| | Si | 5,993 | 6,365 | 5,298 | 4,543 | 4,436 | 4,375 | 5,465 | 4,590 | 4,632 | BDL |
| | Sr | 182 | 248 | 88.2 | 328 | 193 | 179 | 373 | 85.1 | 85.7 | BDL |
| | Tl | 0.020 | 0.049 | 0.024 | 0.034 | 0.003 | 0.005 | 0.003 | 0.009 | 0.005 | BDL |
| | U234 | 0.003 | 0.010 | 0.001 | 0.072 | 0.016 | 0.013 | 0.009 | 0.003 | 0.003 | BDL |
| | U235 | 0.157 | 0.733 | 0.032 | 5.06 | 0.845 | 0.714 | 0.382 | 0.028 | 0.020 | BDL |
| | U238 | 5.34 | 22.3 | 1.63 | 199 | 25.3 | 21.9 | 12.0 | 1.41 | 1.34 | BDL |
| | U total | 5.41 | 22.6 | 1.65 | 201 | 25.7 | 22.1 | 12.2 | 1.43 | 1.35 | BDL |
| | V | 1.59 | 0.470 | 3.00 | 1.25 | 0.759 | 0.784 | 0.225 | 0.989 | 1.01 | BDL |
| | W | 0.012 | 0.010 | 0.033 | 0.022 | 0.012 | 0.012 | 0.007 | 0.016 | 0.017 | BDL |
| | Zn | 8.86 | 3.36 | 6.12 | 3.57 | 1.85 | 27.1 | 3.57 | 20.0 | 20.4 | BDL |

n/a = data was not collected

BDL= below laboratory detection level

HG#2 is a duplicate sample of HG

Table 3: Groundwater chemistry data collected March 30th-April 1st, 2023

| | Analyte | WHC | LHB | UHA | UHB | UHB-B | Blank | UHB #2 |
|-----------------------|--|--------|---------|---------|---------|---------|-------|--------|
| (ppm) | Total Carbon | 57.7 | 64.4 | 57.2 | 46.3 | 48.1 | n/a | n/a |
| | Inorganic Carbon | 48.0 | 61.5 | 54.8 | 39.8 | 43.4 | n/a | n/a |
| | Total Organic Carbon | 9.76 | 2.90 | 2.46 | 6.52 | 4.66 | n/a | n/a |
| | Total Nitrogen | 1.77 | 0.53 | 0.69 | 1.44 | 1.43 | n/a | n/a |
| | pH | 8.58 | 8.08 | 8.18 | 8.60 | 8.66 | n/a | n/a |
| °C | Temperature | 4.0 | 14.8 | 12.2 | 6.7 | 14.7 | n/a | n/a |
| kg/L | Density (25 °C) | 0.9975 | 0.9997 | 0.9974 | 0.9975 | 0.9976 | n/a | n/a |
| µS/cm | Conductivity (25 °C) | 768.72 | 4610.05 | 849.90 | 955.96 | 957.03 | n/a | n/a |
| Ω ² cm | Resistivity (25 °C) | 1,301 | 217 | 1,177 | 1,046 | 1,045 | n/a | n/a |
| major ions (mg/L) | TDS | 492.0 | 2950.4 | 543.9 | 611.8 | 612.5 | n/a | n/a |
| | Ca | 65.24 | 235.11 | 75.70 | 86.11 | 102.72 | n/a | n/a |
| | K | 13.93 | 37.21 | 7.42 | 14.60 | 10.98 | n/a | n/a |
| | Mg | 60.37 | 133.65 | 65.92 | 70.58 | 73.51 | n/a | n/a |
| | Na | 16.68 | 677.52 | 24.76 | 28.00 | 15.71 | n/a | n/a |
| | F- | 0.49 | 0.44 | 0.32 | 0.35 | 0.33 | n/a | n/a |
| | Cl- | 16.13 | 1214.00 | 30.12 | 35.44 | 20.19 | n/a | n/a |
| | Br- | <0.08 | 2.88 | <0.08 | <0.08 | <0.08 | n/a | n/a |
| | SO ₄ ²⁻ | 221.94 | 738.35 | 242.56 | 355.56 | 387.49 | n/a | n/a |
| | NO ₃ ⁻ | 5.51 | 0.28 | 2.07 | 4.97 | 4.89 | n/a | n/a |
| | PO ₄ ³⁻ | <0.06 | <0.06 | <0.06 | <0.06 | <0.06 | n/a | n/a |
| | Alkalinity (as HCO ₃ ⁻) | 244.4 | 317.2 | 292.8 | 207.4 | 220.9 | n/a | n/a |
| | Alkalinity (as CaCO ₃) | 203 | 235 | 225 | 172 | 192 | n/a | n/a |
| | Alkalinity (as CO ₃ ²⁻) | 5.5 | 0.0 | 0.0 | 3.0 | 3.4 | n/a | n/a |
| ‰ | δ ¹⁸ O H ₂ O | -80.6 | -86.8 | -88.6 | -78.3 | -82.8 | n/a | n/a |
| | δ ² H H ₂ O | -10.11 | -11.26 | -11.90 | -10.09 | -10.79 | n/a | n/a |
| Trace elements (µg/L) | As | 8.97 | 0.305 | 2.10 | 16.8 | 7.65 | BDL | 16.1 |
| | Ba | 61.75 | <70 | 57.57 | 131.91 | 65.46 | n/a | n/a |
| | Ce | 0.005 | BDL | BDL | 0.006 | BDL | BDL | 0.011 |
| | Dy | 0.003 | 0.001 | 0.003 | 0.003 | 0.002 | BDL | 0.003 |
| | Er | 0.002 | 0.001 | 0.002 | 0.002 | 0.001 | BDL | 0.002 |
| | Eu | 0.007 | 0.003 | 0.005 | 0.010 | 0.005 | BDL | 0.010 |
| | Fe | 0.61 | 3.57 | BDL | 1.13 | 0.69 | BDL | 5.04 |
| | Gd | 0.025 | 0.009 | 0.019 | 0.039 | 0.019 | BDL | 0.038 |
| | Ho | 0.001 | BDL | 0.001 | 0.001 | BDL | BDL | 0.001 |
| | La | 0.002 | 0.002 | 0.005 | 0.004 | 0.002 | BDL | 0.007 |
| | Nd | 0.005 | 0.003 | 0.006 | 0.007 | 0.003 | BDL | 0.007 |
| | Mn | <10 | <20 | <10 | <10 | <10 | n/a | n/a |
| | Pb | BDL | BDL | BDL | BDL | BDL | BDL | 0.024 |
| | Pr | 0.001 | BDL | 0.001 | 0.001 | 0.000 | BDL | 0.001 |
| | Sb | 0.126 | 0.057 | 0.059 | 0.114 | 0.131 | BDL | 0.120 |
| | Se | 5.57 | BDL | BDL | 5.32 | BDL | BDL | 4.98 |
| | Sm | 0.022 | 0.006 | 0.015 | 0.032 | 0.015 | BDL | 0.031 |
| | Sr | 372.34 | 3396.37 | 331.21 | 462.55 | 422.98 | n/a | n/a |
| | Tb | 0.280 | 0.057 | 0.239 | 0.308 | 0.102 | BDL | 0.300 |
| | Th | 0.087 | 0.051 | 0.030 | 0.032 | 0.025 | BDL | 0.029 |
| | Tm | BDL | BDL | BDL | BDL | BDL | BDL | BDL |
| U | 186 | 36.4 | 71.0 | 339 | 183 | BDL | 326 | |
| meq/L | Yb | 0.003 | 0.002 | 0.003 | 0.002 | 0.002 | BDL | 0.002 |
| | Total Cation | 9.314 | 53.214 | 10.476 | 11.708 | 12.148 | n/a | n/a |
| | Total Anion | -9.378 | -54.827 | -10.747 | -11.997 | -12.464 | n/a | n/a |
| | Charge Difference | -0.06 | -1.61 | -0.27 | -0.29 | -0.32 | n/a | n/a |
| % | Charge Balance | -0.34% | -1.49% | -1.28% | -1.22% | -1.28% | n/a | n/a |

n/a = data was not collected

BDL= below laboratory detection level

HG#2 is a duplicate sample of HG

Table 4: Dissolved Uranium Data at UHB

| Sampling Date | Dissolved Uranium (pp) | Study |
|---|------------------------|------------|
| 3/19/1995 | 92.7* | Fitzgerald |
| 6/5/2002 | 333 | Liebe |
| 6/25/2002 | 334 | Liebe |
| 7/16/2002 | 400 | Liebe |
| 7/30/2002 | 312 | Liebe |
| 1/11/2011 | 509 | Scharr |
| 10/21/2013 | 310 | URS Inc. |
| 5/1/2018 | 257 | USGS |
| 3/14/2019 | 178 | USGS |
| 4/16/2019 | 188 | USGS |
| 4/16/2019 | 194 | USGS |
| 4/18/2019 | 195 | USGS |
| 10/8/2019 | 260 | USGS |
| 12/2/2019 | 240 | USGS |
| 1/21/2020 | 151 | USGS |
| 6/2/2020 | 290 | USGS |
| 4/27/2021 | 210 | USGS |
| 11/3/2021 | 228 | USGS |
| 12/22/2021 | 231 | USGS |
| 3/22/2022 | 236 | USGS |
| 4/20/2022 | 236 | USGS |
| 11/11/2022 | 201 | Davidson |
| 3/31/2023 | 332.5 | Davidson |
| * U ²³⁸ value, not total dissolved U | | |

Table 5: Groundwater chemistry data collected October 2013 by URS Inc.

| Analyte | EHC-BS | UHB | UHB-B | UHA | UHA-B | LHA | LHA-Tonto | LHA-Tonto-B | NEHC-TOP | WHC (2013) | WHC-B | LHB | SC-Top | SC-Tonto | LSC-V |
|------------------------------------|---------|---------|---------|---------|---------|---------|-----------|-------------|----------|------------|---------|-------------|---------|----------|---------|
| mg/L | | | | | | | | | | | | | | | |
| Total Inorganic Carbon | 39 | 32 | 45 | 62 | 51 | 72 | 75 J | 77 | 36 | 69 | 64 | 73 | 39 | 64 | 62 |
| Total Organic Carbon | NA | 0.75 J | 1.1 | 0.86 J | 0.83 J | 1.2 | 0.76 J | 0.98 J | 3.5 | 1.7 | 2.9 | 1.4 | < 1.2 | 1.2 | 0.64 J |
| Nitrogen, Nitrate-Nitrite | NA | 0.9 | 0.77 | 1.1 | 1.2 | 0.43 | 0.036 J | 0.04 J | 1.4 | 0.061 J | 0.047 J | 0.1 | 0.87 | 0.078 J | 0.062 J |
| pH | 8.9 | 8.3 | 8.6 | 8 | 8.8 | 8.2 | 8.3 | 8.2 | 8.7 | 8.9 | n/a | 8.2 | 9 | 8.3 | 8.5 |
| mL/min | | | | | | | | | | | | | | | |
| Flow Rate | 17.9 | 153 | 192 | 750 | 60 | 17.4 | 968 | 720 | 60 | 170 | 175 | 10000-15000 | 1360 | 480 | 8700 |
| mS/cm | | | | | | | | | | | | | | | |
| Conductivity | 0.582 | 0.977 | 1.050 | 0.793 | 0.736 | 0.916 | 0.942 | 0.982 | 0.621 | 1.468 | n/a | 4.730 | 0.671 | 1.131 | 1.295 |
| °C | | | | | | | | | | | | | | | |
| Temperature | 8.8 | 14.0 | 12.0 | 12.7 | 8.0 | 10.4 | 14.9 | 12.5 | 15.2 | 8.3 | n/a | 17.9 | 13.1 | 13.9 | 12.6 |
| Major Ions (mg/L) | | | | | | | | | | | | | | | |
| TDS | 280 J | 700 J | 750 J | 460 J | 410 | 520 | 560 | 580 J | 330 | 1000 | 1200 | 2700 J | 440 | 770 | 900 J |
| Ca | 35 | 79 | 100 | 71 | 59 | 78 | 91 | 86 | 39 | 99 | 130 | 190 | 58 | 91 | 93 |
| K | 5.3 | 11 | 12 | 6.7 | 7.1 | 11 | 11 | 11 | 10 | 20 | 25 | 36 | 5.5 | 17 | 17 |
| Mg | 36 | 66 | 68 | 45 | 45 | 58 | 60 | 63 | 35 | 110 | 130 | 110 | 44 | 85 | 96 |
| Na | 10 | 22 | 22 | 24 | 26 | 27 | 29 | 31 | 26 | 44 | 54 | 610 | 19 | 36 | 44 |
| F- | 0.1 J | 0.26 J | 0.3 J | 0.22 J | 0.21 J | 0.28 J | 0.28 J | 0.28 J | 0.35 J | 0.32 J | 0.32 J | 0.41 J | 0.28 J | 0.27 J | 0.24 J |
| Cl- | 12 | 19 | 20 | 31 | 33 | 35 | 35 | 37 | 32 | 37 | 42 | 940 | 20 | 28 | 35 |
| SO ₄ ²⁻ | 88 | 450 | 440 | 130 | 120 | 150 | 140 | 170 | 100 | 580 | 710 | 820 | 190 | 370 | 480 |
| Alkalinity, Bicarbonate (as CaCO3) | 160 SJ | 130 SJ | 180 SJ | 240 SJ | 220 SJ | 310 SJ | 300 SJ | 330 SJ | 150 SJ | 270 SJ | 260 SJ | 260 SJ | 160 SJ | 260 SJ | 290 SJ |
| Alkalinity, Carbonate (as CaCO3) | 9.5 SJ | 2.3 SJ | 8.7 SJ | 16 SJ | 3.6 SJ | R | R | R | R | 23 SJ | 14 SJ | R | 6.3 SJ | 11 SJ | 9.1 SJ |
| Alkalinity, Total (as CaCO3) | 170 SJ | 130 SJ | 190 SJ | 250 SJ | 220 SJ | 310 SJ | 300 SJ | 330 SJ | 150 SJ | 300 SJ | 270 SJ | 260 SJ | 170 SJ | 270 SJ | 300 SJ |
| Trace elements (µg/L) | | | | | | | | | | | | | | | |
| Ag | < 0.033 | < 0.033 | < 0.033 | < 0.033 | < 0.033 | < 0.033 | < 0.033 | < 0.033 | < 0.033 | < 0.033 | < 0.033 | < 0.033 | < 0.033 | < 0.033 | < 0.033 |
| Al | < 18 | < 18 | < 18 | < 18 | < 18 | < 18 | < 18 | < 18 | < 18 | < 18 | < 18 | < 18 | < 18 | < 18 | < 18 |
| As | 5.3 | 6.3 | 14 | 5.3 | 4.9 J | 2.3 J | 1.8 J | 3.4 J | 5.5 | 1.1 J | 3.7 J | 1.5 J | 2.3 J | 1.1 J | 0.51 J |
| B | 59 J | 130 | 130 | 110 | 120 | 140 | 160 | 170 | 190 | 230 | 240 | 1600 | 93 J | 180 | 200 |
| Ba | 89 | 29 | 59 | 81 | 71 | 71 | 56 | 55 | 53 | 27 | 98 | 22 | 29 | 120 | 57 |
| Be | < 0.08 | < 0.08 | < 0.08 | < 0.08 | < 0.08 | < 0.08 | < 0.08 | < 0.08 | < 0.08 | < 0.08 | < 0.08 | < 0.08 | < 0.08 | < 0.08 | < 0.08 |
| Cd | < 0.1 | < 0.1 | < 0.1 | < 0.1 | < 0.1 | < 0.1 | < 0.1 | < 0.1 | < 0.1 | < 0.1 | < 0.1 | < 0.1 | < 0.1 | < 0.1 | < 0.1 |
| Co | 6.2 | < 0.054 | < 0.054 | < 0.054 | < 0.054 | 1.7 | < 0.054 | 0.054 J | < 0.054 | 0.26 J | 2.1 | 0.79 J | < 0.054 | < 0.054 | < 0.054 |
| Cr | < 0.5 | < 0.5 | < 0.5 | < 0.5 | < 0.5 | < 0.5 | < 0.5 | < 0.5 | < 0.5 | < 0.5 | < 0.5 | < 0.5 | < 0.5 | < 0.5 | < 0.5 |
| Cu | 2.9 | 0.88 J | 1.4 J | 0.9 J | 0.75 J | 0.84 J | 0.67 J | 1.2 J | 0.73 J | 0.96 J | 0.86 J | 0.84 J | 1.2 J | 1.1 J | 0.68 J |
| Fe | < 22 | < 22 | < 22 | < 22 | < 22 | < 22 | < 22 | < 22 | < 22 | < 22 | < 22 | < 22 | < 22 | < 22 | < 22 |
| Li | 8.4 J | 34 | 35 | 25 | 24 | 35 | 35 | 37 | 25 | 72 | 85 | 1100 | 24 | 59 | 80 |
| Mn | 11 | 0.38 J | 0.67 J | 1.5 | 1.4 | 4.4 | 0.61 J | 2.9 | 0.41 J | 0.77 J | 5.1 | 2.2 | 1 | 0.68 J | 0.41 J |
| Mo | 3.2 | 12 | 16 | 6 | 4 | 5.1 | 5.5 | 6.5 | 3 | 5.9 | 3.8 | 9 | 2.2 | 2.2 | 1.7 J |
| Ni | 1.2 J | 0.89 J | 2.1 | 0.95 J | 0.62 J | 0.8 J | 1.1 J | 0.61 J | < 0.3 | < 0.81 | 1.1 J | 0.62 J | 0.66 J | 0.72 J | 0.36 J |
| Pb | < 0.18 | < 0.18 | < 0.18 | < 0.18 | < 0.18 | < 0.18 | < 0.18 | < 0.18 | < 0.18 | < 0.18 | < 0.18 | < 0.18 | < 0.18 | < 0.18 | < 0.18 |
| Re | < 1.7 | < 1.7 | < 1.7 | < 1.7 | < 1.7 | < 1.7 | < 1.7 | < 1.7 | < 1.7 | < 1.7 | < 1.7 | < 1.7 | < 1.7 | < 1.7 | < 1.7 |
| Sb | < 0.4 | < 0.4 | < 0.4 | < 0.4 | < 0.4 | < 0.4 | < 0.4 | < 0.4 | < 0.4 | < 0.4 | < 0.4 | < 0.4 | < 0.4 | < 0.4 | < 0.4 |
| Se | 2.9 J | 15 | 15 | 6.2 | 6.4 | 5.3 | 5.3 | 3.6 J | 13 | 9.5 | 6.2 | 6.1 | 11 | 3.9 J | 9 |
| Silica (as SiO2) | 12000 | 9100 | 10000 | 11000 | 11000 | 11000 | 14000 | 13000 | 11000 | 12000 | 11000 | 16000 | 8900 | 12000 | 11000 |
| Sr | 170 | 540 | 560 | 280 | 280 | 320 | 370 | 370 | 410 | 580 | 620 | 2800 | 270 | 430 | 510 |
| Tl | < 0.05 | < 0.05 | 0.11 J | 0.14 J | 0.072 J | < 0.05 | 0.05 J | 0.072 J | < 0.05 | < 0.05 | 0.13 J | 0.077 J | < 0.05 | 0.07 J | < 0.05 |
| U | 5.4 | 310 | 280 | 28 | 11 | 21 | 21 | 25 | 9.3 | 97 | 66 | 46 | 27 | 15 | 13 |
| V | 3J | 1.3 J | 1.5 J | 1.2 J | 1.3 J | 0.5 J | < 0.5 | 0.59 J | 1.2 J | 0.57 J | 0.92 J | 0.56 J | 0.67 J | 1.4 J | 0.8 J |
| W | < 20 | < 20 | < 20 | < 20 | < 20 | < 20 | < 20 | < 20 | < 20 | < 20 | < 20 | < 20 | < 20 | 30 J | < 20 |
| Zn | 6.8 J | 3.3 J | 5.1 J | 4.3 J | 2.8 J | 4.9 J | 3.2 J | 3J | 2.1 J | 2.9 J | 4.4 J | 6.7 J | 5.1 J | 6.3 J | 2.9 J |
| ‰ | | | | | | | | | | | | | | | |
| Delta oxygen-18 isotope (δ18O H2O) | -6.31 | -12.28 | -11.52 | -11.88 | -11.63 | -11 | -11.62 | -10.74 | -11.35 | -9.82 | -8.57 | -10.25 | -11.97 | -11.2 | -10.21 |
| Delta deuterium (δD H2O) | -59.3 | -91.6 | -86.5 | -90.3 | -90.6 | -85.3 | -85.9 | -82 | -86.3 | -77.3 | -68.4 | -80.4 | -91.2 | -86.4 | -78.7 |
| pCi/L | | | | | | | | | | | | | | | |
| Alpha, Gross | NA | 202 J | 238 J | 16.7 J | 9.16 J | 13.3 J | 8.36 J | 14.8 J | 21.5 J | 68.2 J | NA | 48.3 J | 20.1 J | 12.4 J | <0J |
| Beta, Gross | NA | 99.1 | 80 | 15.9 | 24.7 | 13.5 | 18.7 | 22.7 | 27.2 | 49.2 | NA | 43.5 | 12.4 J | 20.2 | 26.8 |
| Uranium-234 | 2.27 J | 125 J | 114 J | 9.59 J | 4.05 J | 6.24 J | 6.68 | 9.47 J | 7.83 J | 34.9 J | 32.5 J | 22.1 J | 12.8 J | 9.85 J | 8.43 J |
| Uranium-235 | <0 | 3.68 | 3.76 | 0.435 | <0 | <0 | 0.312 | 0.368 | 0.543 | 1.35 | 1.18 | 0.344 | 0.301 | <0 | <0 |
| Uranium-238 | 2.5 J | 106 J | 99.7 J | 10.4 J | 3.41 J | 6.03 J | 7.84 | 8.6 J | 5.9 J | 32.7 J | 26.1 J | 15.2 J | 9.8 J | 6.59 J | 5.67 J |

NA = not analyzed R = data rejected during validation
 J Flag denotes an estimated value, as it was detected between the reporting limit and method detection limit
 SJ Flag denotes a screening value, as it was performed out of holding times

Table 5: Groundwater chemistry data collected October 2013 by URS Inc.

| Analyte | Volatile Organic Compounds (VOCs) by Method SW8260B (µg/L) | | | | | | | | | | | | | | |
|---------------------------------------|--|----------|----------|----------|----------|----------|-----------|-------------|----------|------------|-------|----------|----------|----------|----------|
| | EHC-BS | UHB | UHB-B | UHA | UHA-B | LHA | LHA-Tonto | LHA-Tonto-B | NEHC-TOP | WHC (2013) | WHC-B | LHB | SC-Top | SC-Tonto | LSC-V |
| 1,1,1-Trichloroethane | NA | < 0.16 | < 0.16 | < 0.16 | < 0.16 | < 0.16 | < 0.16 | < 0.16 | < 0.16 | < 0.16 | NA | < 0.16 | < 0.16 | < 0.16 | < 0.16 |
| 1,1,2,2-Tetrachloroethane | NA | < 0.21 | < 0.21 | < 0.21 | < 0.21 | < 0.21 | < 0.21 | < 0.21 | < 0.21 | < 0.21 | NA | < 0.21 | < 0.21 | < 0.21 | < 0.21 |
| 1,1,2-Trichloro-1,2,2-Trifluoroethane | NA | < 0.42 | < 0.42 | < 0.42 | < 0.42 | < 0.42 | < 0.42 | < 0.42 | < 0.42 | < 0.42 | NA | < 0.42 | < 0.42 | < 0.42 | < 0.42 |
| 1,1,2-Trichloroethane | NA | < 0.27 | < 0.27 | < 0.27 | < 0.27 | < 0.27 | < 0.27 | < 0.27 | < 0.27 | < 0.27 | NA | < 0.27 | < 0.27 | < 0.27 | < 0.27 |
| 1,1-Dichloroethane | NA | < 0.22 | < 0.22 | < 0.22 | < 0.22 | < 0.22 | < 0.22 | < 0.22 | < 0.22 | < 0.22 | NA | < 0.22 | < 0.22 | < 0.22 | < 0.22 |
| 1,1-Dichloroethene | NA | < 0.23 | < 0.23 | < 0.23 | < 0.23 | < 0.23 | < 0.23 | < 0.23 | < 0.23 | < 0.23 | NA | < 0.23 | < 0.23 | < 0.23 | < 0.23 |
| 1,2,3-Trichlorobenzene | NA | < 0.21 | < 0.21 | < 0.21 | < 0.21 | < 0.21 | < 0.21 | < 0.21 | < 0.21 | < 0.21 | NA | < 0.21 | < 0.21 | < 0.21 | < 0.21 |
| 1,2,4-Trichlorobenzene | NA | < 0.21 | < 0.21 | < 0.21 | < 0.21 | < 0.21 | < 0.21 | < 0.21 | < 0.21 | < 0.21 | NA | < 0.21 | < 0.21 | < 0.21 | < 0.21 |
| 1,2-Dibromo-3-Chloropropane | NA | < 0.47 J | < 0.47 J | < 0.47 J | < 0.47 J | < 0.47 J | < 0.47 J | < 0.47 J | < 0.47 J | < 0.47 J | NA | < 0.47 J | < 0.47 J | < 0.47 J | < 0.47 J |
| 1,2-Dibromoethane | NA | < 0.18 | < 0.18 | < 0.18 | < 0.18 | < 0.18 | < 0.18 | < 0.18 | < 0.18 | < 0.18 | NA | < 0.18 | < 0.18 | < 0.18 | < 0.18 |
| 1,2-Dichlorobenzene | NA | < 0.15 | < 0.15 | < 0.15 | < 0.15 | < 0.15 | < 0.15 | < 0.15 | < 0.15 | < 0.15 | NA | < 0.15 | < 0.15 | < 0.15 | < 0.15 |
| 1,2-Dichloroethane | NA | < 0.13 | < 0.13 | < 0.13 | < 0.13 | < 0.13 | < 0.13 | < 0.13 | < 0.13 | < 0.13 | NA | < 0.13 | < 0.13 | < 0.13 | < 0.13 |
| 1,2-Dichloropropane | NA | < 0.18 | < 0.18 | < 0.18 | < 0.18 | < 0.18 | < 0.18 | < 0.18 | < 0.18 | < 0.18 | NA | < 0.18 | < 0.18 | < 0.18 | < 0.18 |
| 1,3-Dichlorobenzene | NA | < 0.13 | < 0.13 | < 0.13 | < 0.13 | < 0.13 | < 0.13 | < 0.13 | < 0.13 | < 0.13 | NA | < 0.13 | < 0.13 | < 0.13 | < 0.13 |
| 1,4-Dichlorobenzene | NA | < 0.16 | < 0.16 | < 0.16 | < 0.16 | < 0.16 | < 0.16 | < 0.16 | < 0.16 | < 0.16 | NA | < 0.16 | < 0.16 | < 0.16 | < 0.16 |
| 1,4-Dioxane (P-Dioxane) | NA | < 57 | < 57 | < 57 | < 57 | < 57 | < 57 | < 57 | < 57 | < 57 | NA | < 57 | < 57 | < 57 | < 57 |
| 2-Hexanone | NA | < 1.7 J | < 1.7 J | < 1.7 J | < 1.7 J | < 1.7 J | < 1.7 J | < 1.7 J | < 1.7 J | < 1.7 J | NA | < 1.7 J | < 1.7 J | < 1.7 J | < 1.7 J |
| Acetone | NA | < 1.9 | < 1.9 | < 1.9 | < 1.9 J | < 1.9 | < 1.9 | < 1.9 | < 1.9 | < 1.9 | NA | < 1.9 | < 1.9 | < 1.9 | < 1.9 |
| Benzene | NA | < 0.16 | < 0.16 | < 0.16 | < 0.16 | < 0.16 | < 0.16 | < 0.16 | < 0.16 | < 0.16 | NA | < 0.16 | < 0.16 | < 0.16 | < 0.16 |
| Bromochloromethane | NA | < 0.1 | < 0.1 | < 0.1 | < 0.1 | < 0.1 | < 0.1 | < 0.1 | < 0.1 | < 0.1 | NA | < 0.1 | < 0.1 | < 0.1 | < 0.1 |
| Bromodichloromethane | NA | < 0.17 | < 0.17 | < 0.17 | < 0.17 | < 0.17 | < 0.17 | < 0.17 | < 0.17 | < 0.17 | NA | < 0.17 | < 0.17 | < 0.17 | < 0.17 |
| Bromoform | NA | < 0.19 | < 0.19 | < 0.19 | < 0.19 | < 0.19 | < 0.19 | < 0.19 | < 0.19 | < 0.19 | NA | < 0.19 | < 0.19 | < 0.19 | < 0.19 |
| Bromomethane | NA | < 0.21 J | < 0.21 J | < 0.21 J | < 0.21 J | < 0.21 J | < 0.21 J | < 0.21 J | < 0.21 J | < 0.21 J | NA | < 0.21 J | < 0.21 J | < 0.21 J | < 0.21 J |
| Carbon Disulfide | NA | < 0.45 | < 0.45 | < 0.45 | < 0.45 | < 0.45 | < 0.45 | < 0.45 | < 0.45 | < 0.45 | NA | < 0.45 | < 0.45 | < 0.45 | < 0.45 |
| Carbon Tetrachloride | NA | < 0.19 | < 0.19 | < 0.19 | < 0.19 | < 0.19 | < 0.19 | < 0.19 | < 0.19 | < 0.19 | NA | < 0.19 | < 0.19 | < 0.19 | < 0.19 |
| Chlorobenzene | NA | < 0.17 | < 0.17 | < 0.17 | < 0.17 | < 0.17 | < 0.17 | < 0.17 | < 0.17 | < 0.17 | NA | < 0.17 | < 0.17 | < 0.17 | < 0.17 |
| Chloroethane | NA | < 0.41 | < 0.41 | < 0.41 | < 0.41 | < 0.41 | < 0.41 | < 0.41 | < 0.41 | < 0.41 | NA | < 0.41 | < 0.41 | < 0.41 | < 0.41 |
| Chloroform | NA | < 0.16 | < 0.16 | < 0.16 | < 0.16 | < 0.16 | < 0.16 | < 0.16 | < 0.16 | < 0.16 | NA | < 0.16 | < 0.16 | < 0.16 | < 0.16 |

NA = not analyzed R = data rejected during validation

J Flag denotes an estimated value, as it was detected between the reporting limit and method detection limit

SJ Flag denotes a screening value, as it was performed out of holding times

Table 5: Groundwater chemistry data collected October 2013 by URS Inc.

| Analyte | EHC-BS | UHB | UHB-B | UHA | UHA-B | LHA | LHA-Tonto | LHA-Tonto-B | NEHC-TOP | WHC (2013) | WHC-B | LHB | SC-Top | SC-Tonto | LSC-V |
|--|---------------|-----------|-----------|-----------|-----------|----------|-----------|-------------|----------|------------|-------|----------|-----------|----------|----------|
| | Chloromethane | NA | < 0.3 | < 0.3 | < 0.3 | < 0.3 | < 0.3 | < 0.3 | < 0.3 | < 0.3 | < 0.3 | NA | < 0.3 | < 0.3 | < 0.3 |
| cis-1,2-Dichloroethylene | NA | < 0.15 | < 0.15 | < 0.15 | < 0.15 | < 0.15 | < 0.15 | < 0.15 | < 0.15 | < 0.15 | NA | < 0.15 | < 0.15 | < 0.15 | < 0.15 |
| cis-1,3-Dichloropropene | NA | < 0.16 | < 0.16 | < 0.16 | < 0.16 | < 0.16 | < 0.16 | < 0.16 | < 0.16 | < 0.16 | NA | < 0.16 | < 0.16 | < 0.16 | < 0.16 |
| Cyclohexane | NA | < 0.28 | < 0.28 | < 0.28 | < 0.28 | < 0.28 | < 0.28 | < 0.28 | 0.48 J | < 0.28 | NA | < 0.28 | < 0.28 | < 0.28 | < 0.28 |
| Dibromochloromethane | NA | < 0.17 | < 0.17 | < 0.17 | < 0.17 | < 0.17 | < 0.17 | < 0.17 | < 0.17 | < 0.17 | NA | < 0.17 | < 0.17 | < 0.17 | < 0.17 |
| Dichlorodifluoromethane | NA | < 0.31 | < 0.31 | < 0.31 | < 0.31 | < 0.31 | < 0.31 | < 0.31 | < 0.31 | < 0.31 | NA | < 0.31 | < 0.31 | < 0.31 | < 0.31 |
| Ethylbenzene | NA | < 0.16 | < 0.16 | < 0.16 | < 0.16 | < 0.16 | < 0.16 | < 0.16 | < 0.16 | < 0.16 | NA | < 0.16 | < 0.16 | < 0.16 | < 0.16 |
| Isopropylbenzene (Cumene) | NA | < 0.19 | < 0.19 | < 0.19 | < 0.19 | < 0.19 | < 0.19 | < 0.19 | < 0.19 | < 0.19 | NA | < 0.19 | < 0.19 | < 0.19 | < 0.19 |
| m,p-Xylene (Sum Of Isomers) | NA | < 0.34 | < 0.34 | < 0.34 | < 0.34 | < 0.34 | < 0.34 | < 0.34 | < 0.34 | < 0.34 | NA | < 0.34 | < 0.34 | < 0.34 | < 0.34 |
| Methyl Acetate | NA | < 1.6 | < 1.6 | < 1.6 | < 1.6 | < 1.6 | < 1.6 | < 1.6 | < 1.6 | < 1.6 | NA | < 1.6 | < 1.6 | < 1.6 | < 1.6 |
| Methyl Ethyl Ketone | NA | < 2 | < 2 | < 2 | < 2 | < 2 | < 2 | < 2 | < 2 | < 2 | NA | < 2 | < 2 | < 2 | < 2 |
| Methyl Isobutyl Ketone | NA | < 0.98 J | < 0.98 J | < 0.98 J | < 0.98 J | < 0.98 J | < 0.98 J | < 0.98 J | < 0.98 J | < 0.98 J | NA | < 0.98 J | < 0.98 J | < 0.98 J | < 0.98 J |
| Methylcyclohexane | NA | < 0.36 | < 0.36 | < 0.36 | < 0.36 | < 0.36 | < 0.36 | < 0.36 | < 0.36 | < 0.36 | NA | < 0.36 | < 0.36 | < 0.36 | < 0.36 |
| Methylene Chloride | NA | < 0.32 J | < 0.32 J | < 0.32 J | < 0.32 J | < 0.32 J | < 0.32 J | < 0.32 J | < 0.32 J | < 0.32 J | NA | < 0.32 J | < 0.32 J | < 0.32 J | < 0.32 J |
| o-Xylene | NA | < 0.19 | < 0.19 | < 0.19 | < 0.19 | < 0.19 | < 0.19 | < 0.19 | < 0.19 | < 0.19 | NA | < 0.19 | < 0.19 | < 0.19 | < 0.19 |
| Styrene | NA | < 0.17 | < 0.17 | < 0.17 | < 0.17 | < 0.17 | < 0.17 | < 0.17 | < 0.17 | < 0.17 | NA | < 0.17 | < 0.17 | < 0.17 | < 0.17 |
| Tert-Butyl Methyl Ether | NA | < 0.25 J | < 0.25 J | < 0.25 J | < 0.25 J | < 0.25 J | < 0.25 J | < 0.25 J | < 0.25 J | < 0.25 J | NA | < 0.25 J | < 0.25 J | < 0.25 J | < 0.25 J |
| Tetrachloroethylene (PCE) | NA | < 0.2 | < 0.2 | < 0.2 | < 0.2 | < 0.2 | < 0.2 | < 0.2 | < 0.2 | < 0.2 | NA | < 0.2 | < 0.2 | < 0.2 | < 0.2 |
| Toluene | NA | < 0.17 | < 0.17 | < 0.17 | < 0.17 | < 0.17 | < 0.17 | < 0.17 | < 0.17 | < 0.17 | NA | < 0.17 | < 0.17 | < 0.17 | < 0.17 |
| trans-1,2-Dichloroethene | NA | < 0.15 | < 0.15 | < 0.15 | < 0.15 | < 0.15 | < 0.15 | < 0.15 | < 0.15 | < 0.15 | NA | < 0.15 | < 0.15 | < 0.15 | < 0.15 |
| trans-1,3-Dichloropropene | NA | < 0.19 | < 0.19 | < 0.19 | < 0.19 | < 0.19 | < 0.19 | < 0.19 | < 0.19 | < 0.19 | NA | < 0.19 | < 0.19 | < 0.19 | < 0.19 |
| Trichloroethylene (TCE) | NA | < 0.16 | < 0.16 | < 0.16 | < 0.16 | < 0.16 | < 0.16 | < 0.16 | < 0.16 | < 0.16 | NA | < 0.16 | < 0.16 | < 0.16 | < 0.16 |
| Trichlorofluoromethane | NA | < 0.29 J | < 0.29 J | < 0.29 J | < 0.29 J | < 0.29 J | < 0.29 J | < 0.29 J | < 0.29 J | < 0.29 J | NA | < 0.29 J | < 0.29 J | < 0.29 J | < 0.29 J |
| Vinyl Chloride | NA | < 0.1 | < 0.1 | < 0.1 | < 0.1 | < 0.1 | < 0.1 | < 0.1 | < 0.1 | < 0.1 | NA | < 0.1 | < 0.1 | < 0.1 | < 0.1 |
| 1,3,5-Trinitrobenzene | < 0.017 J | < 0.016 | < 0.019 | < 0.017 | < 0.018 J | NA | NA | NA | NA | < 0.016 J | NA | NA | < 0.016 | NA | NA |
| 1,3-Dinitrobenzene | < 0.014 J | < 0.013 | < 0.016 | < 0.014 | < 0.015 J | NA | NA | NA | NA | < 0.013 J | NA | NA | < 0.013 | NA | NA |
| 2,4,6-Trinitrotoluene | < 0.022 J | < 0.021 J | < 0.025 J | < 0.023 J | < 0.024 J | NA | NA | NA | NA | < 0.021 J | NA | NA | < 0.021 J | NA | NA |
| 2,4-Dinitrotoluene | < 0.019 J | < 0.018 | < 0.022 | < 0.02 | < 0.02 J | NA | NA | NA | NA | < 0.018 J | NA | NA | < 0.018 | NA | NA |
| 2,6-Dinitrotoluene | < 0.022 J | < 0.021 | < 0.025 | < 0.023 | < 0.024 J | NA | NA | NA | NA | < 0.021 J | NA | NA | < 0.021 | NA | NA |
| 2-Amino-4,6-Dinitrotoluene | < 0.021 J | < 0.02 | < 0.024 | < 0.022 | < 0.023 J | NA | NA | NA | NA | < 0.02 J | NA | NA | < 0.02 | NA | NA |
| 2-Nitrotoluene | < 0.022 J | < 0.021 | < 0.025 | < 0.023 | < 0.024 J | NA | NA | NA | NA | < 0.021 J | NA | NA | < 0.021 J | NA | NA |
| 3-Nitrotoluene | < 0.024 J | < 0.024 | < 0.029 | < 0.026 | < 0.027 J | NA | NA | NA | NA | < 0.024 J | NA | NA | < 0.024 | NA | NA |
| 4-Amino-2,6-Dinitrotoluene | < 0.019 J | < 0.018 | < 0.022 | < 0.02 | < 0.02 J | NA | NA | NA | NA | < 0.018 J | NA | NA | < 0.018 | NA | NA |
| 4-Nitrotoluene | < 0.025 J | < 0.025 | < 0.03 | < 0.027 | < 0.028 J | NA | NA | NA | NA | < 0.025 J | NA | NA | < 0.025 J | NA | NA |
| Hexahydro-1,3,5-Trinitro-1,3,5-Triazine | < 0.021 J | < 0.02 | < 0.024 | < 0.022 | < 0.023 J | NA | NA | NA | NA | < 0.02 J | NA | NA | < 0.02 | NA | NA |
| Nitrobenzene | < 0.032 J | < 0.032 | < 0.038 | < 0.034 | < 0.035 J | NA | NA | NA | NA | < 0.031 J | NA | NA | < 0.031 | NA | NA |
| Nitroglycerin | < 0.044 J | < 0.043 | < 0.052 | < 0.046 | < 0.048 J | NA | NA | NA | NA | < 0.043 J | NA | NA | < 0.043 | NA | NA |
| Octahydro-1,3,5,7-Tetranitro-1,3,5,7-Tetrazocine | < 0.093 J | < 0.018 | < 0.022 | < 0.02 | < 0.02 J | NA | NA | NA | NA | < 0.018 J | NA | NA | < 0.018 | NA | NA |
| Pentaerythritol Tetranitrate | < 0.018 J | < 0.017 | < 0.021 | < 0.019 | < 0.019 J | NA | NA | NA | NA | < 0.017 J | NA | NA | < 0.017 | NA | NA |
| Tetryl | < 0.021 J | < 0.02 | < 0.024 | < 0.022 | < 0.023 J | NA | NA | NA | NA | < 0.02 J | NA | NA | < 0.02 | NA | NA |

NA = not analyzed R = data rejected during validation
 J Flag denotes an estimated value, as it was detected between the reporting limit and method detection limit
 SJ Flag denotes a screening value, as it was performed out of holding times

Appendix C: PHREEQC Modeling Summaries

Table 6: S1.R1 Summary

S1.R1

| Mineral | Model # | | | | | | | | | | |
|---------|---------|------------|-----------|-----------|-----------|-----------|-----------|----------|-----------|-----------|------------------|
| | | K-feldspar | CO2(g) | Calcite | Quartz | Dolomite | Kaolinite | Hematite | Illite | Gypsum | Sum of residuals |
| | 1 | 4.76E+01 | -1.98E+01 | -1.98E+01 | -3.80E-04 | 1.98E+01 | 6.74E+01 | | -7.93E+01 | 2.41E-03 | 1.82E+00 |
| | 2 | 1.48E+01 | -6.16E+00 | -6.16E+00 | 1.35E-04 | 6.16E+00 | 2.10E+01 | | -2.47E+01 | | 2.88E+00 |
| | 3 | -1.84E-04 | 7.01E-04 | 9.57E-04 | 3.68E-04 | -1.29E-04 | 9.19E-05 | | | -1.09E-03 | 3.36E+00 |
| | 4 | -1.84E-04 | 6.91E-04 | 7.10E-04 | 3.68E-04 | | 9.19E-05 | | | -1.09E-03 | 4.19E+00 |
| | 5 | -2.49E-04 | 7.28E-04 | 9.84E-04 | 3.77E-04 | -1.56E-04 | | | 1.08E-04 | -1.09E-03 | 3.36E+00 |
| | 6 | -2.49E-04 | 6.91E-04 | 7.10E-04 | 3.68E-04 | | | | 1.08E-04 | -1.09E-03 | 4.63E+00 |
| | 7 | 1.25E-04 | 5.73E-04 | 8.28E-04 | 3.68E-04 | | 5.29E-04 | | -5.15E-04 | -1.09E-03 | 3.36E+00 |
| | 8 | 2.34E+01 | -9.75E+00 | -9.75E+00 | | 9.75E+00 | 3.32E+01 | | -3.90E+01 | 6.33E-04 | 2.60E+00 |
| | 9 | 2.11E-03 | -2.56E-04 | | 3.68E-04 | 8.28E-04 | 3.35E-03 | | -3.83E-03 | -1.09E-03 | 3.36E+00 |
| | 10 | 1.77E-03 | | | 3.68E-04 | 7.00E-04 | 2.87E-03 | | -3.26E-03 | -9.74E-04 | 3.42E+00 |
| | 11 | 1.50E-03 | | 2.56E-04 | 3.68E-04 | 5.73E-04 | 2.48E-03 | | -2.81E-03 | -1.09E-03 | 3.36E+00 |
| | 12 | | 6.25E-04 | 8.80E-04 | 3.68E-04 | -5.21E-05 | 3.52E-04 | | -3.06E-04 | -1.09E-03 | 3.36E+00 |
| | 13 | | | 9.49E-04 | 3.68E-04 | | 3.52E-04 | | -3.06E-04 | -1.16E-03 | 6.98E+00 |
| | 14 | 6.12E-04 | | 1.13E-03 | 3.68E-04 | | 1.22E-03 | | -1.33E-03 | -1.29E-03 | 5.31E+00 |
| | 15 | | 6.25E-04 | 7.76E-04 | 3.68E-04 | | 3.52E-04 | | -3.06E-04 | -1.09E-03 | 3.47E+00 |
| | 16 | | 8.82E-04 | | 3.68E-04 | 3.37E-05 | 3.52E-04 | | -3.06E-04 | -1.13E-03 | 6.93E+00 |


Model did not meet 1:1 parent:daughter ratio

Scenario 1-Run 1 (S1.R1) included minerals documented in the literature from the known lithology and excluded dissolved uranium in the chemistries of UHB and UHA springs. S1.R1 models the change in major ion chemistry from UHB to UHA via water-rock interactions. This table lists the phase mole transfers from the 16 models produced. Negative values indicate precipitation out of solution, while positive values indicate dissolution.

Table 7: S1.R2 Summary

S1.R2

| Mineral | Model # | K-feldspar | CO2(g) | Calcite | Quartz | Dolomite | Kaolinite | Hematite | Illite | Gypsum | Sum of residuals |
|---------|---------|------------|-----------|-----------|----------|----------|-----------|----------|-----------|-----------|------------------|
| | 1 | 1.21E-02 | -7.54E-03 | -8.09E-03 | 3.67E-04 | 6.96E+03 | 1.75E-02 | | -2.05E-02 | 8.70E-04 | 4.93E+00 |
| | 2 | 2.08E-02 | | -1.02E-02 | | 8.48E-03 | 2.95E-02 | | -3.47E-02 | 1.50E-03 | 7.95E+00 |
| | 3 | 1.87E+01 | -7.80E+00 | -7.80E+00 | 7.36E-05 | 7.80E+00 | 2.65E+01 | | -3.12E+01 | | 8.77E-01 |
| | 4 | 1.24E-02 | -7.48E-03 | -8.13E-03 | | 6.95E-03 | 1.75E-02 | | -2.06E-02 | 9.21E-04 | 5.69E+00 |
| | 5 | 1.61E-02 | -9.08E-03 | | 3.67E-04 | 3.73E-03 | 2.31E-02 | | -2.71E-02 | -1.38E-03 | 6.60E+00 |
| | 6 | 2.06E-02 | | -1.02E-02 | 3.67E-04 | 8.45E-03 | 2.95E-02 | | -3.46E-02 | 1.48E-03 | 7.24E+00 |
| | 7 | 1.87E+01 | -7.80E+00 | -7.80E+00 | | 7.80E+00 | 2.65E+01 | | -3.12E+01 | | 1.04E+00 |
| | 8 | 1.30E-02 | -8.63E-03 | | 3.67E-04 | 2.36E-03 | 1.88E-02 | | -2.20E-02 | | 9.18E+00 |

 Model did not meet 1:1 parent:daughter ratio

Scenario1-Run2 (S1.R2) includes the same minerals as in S1.R1 plus uraninite and the measured dissolved U at UHB and UHA. S1.R2 models the change in major ion chemistry and dissolved uranium concentrations via water-rock interactions with the known lithology. This table lists the phase mole transfers from the 8 models produced. Negative values indicate precipitation out of solution, while positive values indicate dissolution.

Table 8: S1.R3 Summary


| S1.R3 | | | | | | | | | | | | | | | | |
|--------------|---------|------------|-----------|-----------|----------|-----------|-----------|-----------|-----------|-----------|-----------|----------|-----------|----------|-----------|------------------|
| Mineral | Model # | K-feldspar | CO2(g) | Calcite | Quartz | Dolomite | Kaolinite | Hematite | Illite | Gypsum | Uraninite | Pyrite | Fe(3) | S(-2) | U(4) | Sum of Residuals |
| | 1 | -6.97E-02 | 2.97E-02 | 2.99E-02 | 3.69E-04 | -2.91E-02 | -9.84E-02 | -7.34E-08 | 1.16E-01 | -1.08E-03 | -1.10E-06 | 1.47E-07 | -1.47E-07 | 2.57E-07 | -1.10E-06 | 3.24E+00 |
| | 2 | 9.33E-04 | | | 3.68E-04 | | 3.52E-04 | -7.33E-04 | -3.06E-04 | -1.18E-03 | -1.10E-06 | 1.47E-07 | -1.47E-07 | 2.57E-07 | -1.10E-06 | 6.47E+00 |
| | 3 | 1.47E+01 | -6.10E+00 | 6.11E+00 | 1.38E-04 | 6.11E+00 | 2.08E+01 | -4.46E-08 | -2.44E+01 | | -6.69E-07 | 8.92E-08 | -8.92E-08 | 1.56E-07 | -6.69E-07 | 2.78E+00 |
| | 4 | -1.84E-04 | 7.01E-04 | 9.32E-04 | 3.68E-04 | -1.16E-04 | 9.19E-05 | -7.33E-08 | | -1.08E-03 | -1.10E-06 | 1.47E-07 | -1.47E-07 | 2.57E-07 | -1.10E+06 | 3.23E+00 |
| | 5 | -1.84E-04 | | 9.33E-04 | 3.68E-04 | | 9.19E-05 | -7.33E-08 | | -1.11E-03 | -1.10E-06 | 1.47E-07 | -1.47E-07 | 2.57E-07 | -1.10E-06 | 8.13E+00 |
| | 6 | -2.49E-04 | 7.28E-04 | 9.59E-04 | 3.68E-04 | -1.43E-04 | | -7.33E-08 | 1.08E-04 | -1.08E-03 | -1.10E-06 | 1.47E-07 | -1.47E-07 | 2.57E-07 | -1.10E-06 | 3.23E+00 |
| | 7 | -2.49E-04 | 7.07E-04 | 6.93E-04 | 3.68E-04 | | | -7.33E-08 | 1.08E-04 | -1.08E-03 | -1.10E-06 | 1.47E-07 | -1.47E-07 | 2.57E-07 | -1.10E-06 | 4.35E+00 |
| | 8 | 9.53E-05 | 5.85E-04 | 8.16E-04 | 3.68E-04 | | 4.87E-04 | -7.33E-08 | -4.65E-04 | -1.08E-03 | -1.10E-06 | 1.47E-07 | -1.47E-07 | 2.57E-07 | -1.10E-06 | 3.23E+00 |
| | 9 | 2.34E+01 | -9.75E+00 | -9.75E+00 | | 9.75E+00 | 3.32E+01 | -2.75E-08 | 3.90E+01 | 6.43E-04 | -4.12E-07 | 5.49E-08 | -5.49E-08 | 9.61E-08 | -4.12E-07 | 2.51E+00 |
| | 10 | 2.05E-03 | -2.31E-04 | | 3.68E-04 | 8.16E-04 | 3.26E-03 | -7.33E-08 | -3.73E-03 | -1.08E-03 | -1.10E-06 | 1.47E-07 | -1.47E-07 | 2.57E-07 | -1.10E-06 | 3.23E+00 |
| | 11 | 1.76E-03 | | | 3.68E-04 | 7.00E-04 | 2.85E-03 | -7.33E-08 | -3.42E-03 | -9.67E-04 | -1.10E-06 | 1.47E-07 | -1.47E-07 | 2.57E-07 | -1.10E-06 | 3.27E+00 |
| | 12 | 1.50E-03 | | 2.31E-04 | 3.68E-04 | 5.85E-04 | 2.48E-03 | -7.33E-08 | -2.81E-03 | -1.08E-03 | -1.10E-06 | 1.47E-07 | -1.47E-07 | 2.57E-07 | -1.10E-06 | 3.23E+00 |
| | 13 | | 6.25E-04 | 8.56E-04 | 3.68E-04 | -3.97E-05 | 3.52E-04 | -7.33E-08 | -3.06E-04 | -1.08E-03 | -1.10E-06 | 1.47E-07 | -1.47E-07 | 2.57E-07 | -1.10E-06 | 3.23E+00 |
| | 14 | -1.84E-04 | 7.01E-04 | 6.99E-04 | 3.68E-04 | | 9.19E-05 | -7.33E-08 | | -1.08E-03 | -1.10E-06 | 1.47E-07 | -1.47E-07 | 2.57E-07 | -1.10E-06 | 3.93E+00 |
| | 15 | -1.84E-04 | | 1.01E-03 | 3.68E-04 | -3.75E-05 | 9.19E-05 | -7.33E-08 | | -1.14E-03 | -1.10E-06 | 1.47E-07 | -1.47E-07 | 2.57E-07 | -1.10E-06 | 7.68E+00 |
| | 16 | 6.46E-04 | | 1.13E-03 | 3.68E-04 | | 1.27E-03 | -7.33E-08 | -1.38E-03 | -1.28E-03 | -1.10E-06 | 1.47E-07 | -1.47E-07 | 2.57E-07 | -1.10E-06 | 5.06E+00 |
| | 17 | | 6.25E-04 | 7.76E-04 | 3.68E-04 | | 3.52E-04 | -7.33E-08 | -3.06E-04 | -1.08E-03 | -1.10E-06 | 1.47E-07 | -1.47E-07 | 2.57E-07 | -1.10E-06 | 3.32E+00 |
| | 18 | | | 8.55E-04 | 3.68E-04 | 3.91E-05 | 3.52E-04 | -7.33E-08 | -3.06E-04 | -1.14E-03 | -1.10E-06 | 1.47E-07 | -1.47E-07 | 2.57E-07 | -1.10E-06 | 6.42E+00 |

Model did not meet 1:1 parent:daughter ratio

Scenario1-Run3 (S1.R3) includes the same minerals as in S1.R2 plus Pyrite, a mineral found in the breccia pipe, but not documented in the literature in the typical lithology of the region. S1.R3 models the change in major ion chemistry and dissolved uranium chemistry from UHB to UHA via water-rock interactions if pyrite were present in the inner basin alluvial material. This table lists the phase mole transfers from the 18 models produced. Negative values indicate precipitation out of solution, while positive values indicate

Table 9: S1.R4 Summary

| S1.R4 | | | | | | | | | | | | |
|--------------|---------|------------|-----------|-----------|----------|-----------|-----------|----------|-----------|-----------|-----------|------------------|
| Mineral | Model # | K-feldspar | CO2(g) | Calcite | Quartz | Dolomite | Kaolinite | Hematite | Illite | Gypsum | Halite | Sum of Residuals |
| | 1 | -1.99E+00 | 8.28E-01 | 8.28E-01 | 3.99E-04 | -8.27E-01 | -2.81E+00 | | 3.31E+00 | -1.15E-03 | -1.92E-04 | 1.93E+00 |
| | 2 | | | 9.49E-04 | 3.68E-04 | | 3.52E-04 | | -3.06E-04 | -1.21E-03 | -1.50E-04 | 5.59E+00 |
| | 3 | 7.15E+00 | -2.98E+00 | -2.98E+00 | 2.55E-04 | 2.98E+00 | 1.01E+01 | | -1.19E+01 | -4.90E-04 | | 2.28E+00 |
| | 4 | -1.84E-04 | 7.01E-04 | 7.85E-04 | 3.68E-04 | -4.29E-05 | 9.19E-05 | | | -1.00E-03 | -1.50E-04 | 2.00E+00 |
| | 5 | -2.14E-04 | | 9.49E-04 | 4.29E-04 | | 1.07E-04 | | | -1.21E-03 | -1.50E-04 | 8.90E+00 |
| | 6 | -2.49E-04 | 7.28E-04 | 8.12E-04 | 3.68E-04 | -6.99E-05 | | | 1.08E-04 | -1.00E-03 | -1.50E-04 | 2.00E+00 |
| | 7 | -2.49E-04 | 7.28E-04 | 6.73E-04 | 3.68E-04 | | | | 1.08E-04 | -9.75E-04 | -1.50E-04 | 2.93E+00 |
| | 8 | -8.09E-05 | 6.58E-04 | 7.42E-04 | 3.68E-04 | | 2.38E-04 | | -1.18E-04 | -1.00E-03 | -1.50E-04 | 2.00E+00 |
| | 9 | 1.70E-03 | -8.40E-05 | | 3.68E-04 | 7.42E-04 | 2.76E-03 | | -3.14E-03 | -1.00E-03 | -1.50E-04 | 2.00E+00 |
| | 10 | 1.70E-03 | | | 3.68E-04 | 7.42E-04 | 2.76E-03 | | -3.14E-03 | -1.00E-03 | -1.50E-04 | 2.32E+00 |
| | 11 | 1.50E-03 | | 8.40E-05 | 3.68E-04 | 6.58E-04 | 2.48E-03 | | -2.81E-03 | -1.00E-03 | -1.50E-04 | 2.00E+00 |
| | 12 | | 6.25E-04 | 7.09E-04 | 3.68E-04 | 3.37E-05 | 3.52E-04 | | -3.06E-04 | -1.00E-03 | -1.50E-04 | 2.00E+00 |
| | 13 | -1.84E-04 | 7.01E-04 | 7.00E-04 | 3.68E-04 | | 9.19E-05 | | | -9.75E-04 | -1.50E-04 | 2.54E+00 |
| | 14 | -2.14E-04 | | 1.04E-03 | 4.29E-04 | -4.29E-05 | 1.07E-04 | | | -1.25E-03 | -1.50E-04 | 8.42E+00 |
| | 15 | 6.61E-04 | | 1.07E-03 | 3.68E-04 | | 1.29E-03 | | -1.41E-03 | -1.32E-03 | -1.50E-04 | 3.77E+00 |
| | 16 | | 6.25E-04 | 7.67E-04 | 3.68E-04 | | 3.52E-04 | | -3.06E-04 | -1.04E-03 | -1.50E-04 | 2.02E+00 |
| | 17 | | | 8.82E-04 | 3.68E-04 | 3.37E-05 | 3.52E-04 | | -3.06E-04 | -1.18E-03 | -1.50E-04 | 5.57E+00 |

 Model did not meet 1:1 parent:daughter ratio

Scenario 1-Run 4 (S1.R4) included minerals documented in the literature from the known lithology, added halite, and excluded dissolved uranium in the chemistries of UHB and UHA springs. S1.R4 models the change in major ion chemistry from UHB to UHA via water-rock interactions if halite were present. This table lists the phase mole transfers from the 17 models produced. Negative values indicate precipitation out of solution, while positive values indicate dissolution.

Table 10: S1.R5 Summary

S1.R5

| Mineral | Model # | K-feldspar | CO2(g) | Calcite | Quartz | Dolomite | Kaolinite | Hematite | Illite | Gypsum | Halite | Uraninite | % of Solution | Sum of Residuals |
|---------|---------|------------|-----------|-----------|----------|----------|-----------|----------|-----------|-----------|-----------|-----------|---------------|------------------|
| | 1 | 1.87E+01 | -7.80E+00 | -7.80E+00 | 7.36E-05 | 7.80E+00 | 2.65E+01 | | -3.12E+01 | 2.80E-04 | | | 6.07E-01 | 1.49E+00 |
| | 2 | 2.08E-02 | | -1.02E-02 | | 8.48E-03 | 2.95E-02 | | -3.47E-02 | 1.50E-03 | | | 9.997E-01 | 8.38E+00 |
| | 3 | 4.23E-02 | -1.70E-02 | -1.89E-02 | 3.67E-04 | 1.86E-02 | 6.02E-02 | | -7.08E-02 | | -1.49E-04 | | 9.991E-01 | 3.11E+00 |
| | 4 | 1.33E-02 | -8.63E-03 | | | 2.36E-03 | 1.88E-02 | | -2.22E-02 | | | | 9.997E-01 | 1.04E+01 |
| | 5 | 1.66E-02 | -8.90E-03 | | 3.67E-04 | 3.85E-03 | 2.39E-02 | | -2.80E-02 | -1.49E-03 | -1.50E-04 | | 9.997E-01 | 6.59E+00 |
| | 6 | 2.06E-02 | | -1.02E-02 | 3.67E-04 | 8.45E-03 | 2.95E-02 | | -3.46E-02 | 1.48E-03 | -1.50E-04 | | 9.997E-01 | 7.28E+00 |
| | 7 | 2.45E-02 | -9.58E-03 | -1.15E-02 | 3.67E-04 | 1.12E-02 | 3.51E-02 | | -4.11E-02 | | | | 9.995E-01 | 3.51E+00 |
| | 8 | 1.66E-02 | -8.90E-03 | | 3.67E-04 | 3.85E-03 | 2.39E-02 | | -2.80E-02 | -1.49E-03 | | | 9.997E-01 | 6.99E+00 |
| | 9 | 1.30E-02 | -8.63E-03 | | 3.67E-04 | 2.36E-03 | 1.88E-02 | | -2.20E-02 | | -1.50E-04 | | 9.997E-01 | 9.21E+00 |
| | 10 | 2.06E-02 | | -1.02E-02 | 3.67E-04 | 8.45E-03 | 2.95E-02 | | -3.46E-02 | 1.48E-03 | | | 9.997E-01 | 7.67E+00 |
| | 11 | 1.30E-02 | -8.63E-03 | | 3.67E-04 | 2.36E-03 | 1.88E-02 | | -2.20E-02 | | | | 9.997E-01 | 9.61E+00 |

Model did not meet 1:1 parent:daughter ratio

Scenario1-Run5 (S1.R5) includes the same minerals as in S1.R1 plus uraninite, the measured dissolved U at UHB and UHA, and the mineral halite. S1.R5 models the change in major ion chemistry and dissolved uranium concentrations via water-rock interactions with the known lithology plus halite. This table lists the phase mole transfers from the 16 models produced. Negative values indicate precipitation out of solution, while positive values indicate dissolution.

Table 11: S1.R6 Summary

S1.R6

| Mineral | Model # | K-feldspar | CO2(g) | Calcite | Quartz | Dolomite | Kaolinite | Hematite | Illite | Gypsum | Uraninite | Pyrite | Halite | Fe(3) | S(-2) | U(4) | Sum of Residuals |
|---------|---------|------------|-----------|-----------|----------|-----------|-----------|-----------|-----------|-----------|-----------|----------|-----------|-----------|----------|-----------|------------------|
| | 1 | -1.99E+00 | 8.28E-01 | 8.28E-01 | 3.99E-04 | -8.27E-01 | -2.81E+00 | -7.72E-08 | 3.31E+00 | -1.14E-03 | -1.16E-06 | 1.54E-07 | -1.92E-04 | -1.54E-07 | 2.70E-07 | -1.16E-06 | 1.86E+00 |
| | 2 | | | 9.33E-04 | 3.68E-04 | | 3.52E-04 | -7.33E-08 | -3.06E-04 | -1.19E-03 | -1.10E-06 | 1.47E-07 | -1.50E-04 | -1.47E-07 | 2.57E-07 | -1.10E-06 | 5.20E+00 |
| | 3 | 7.15E+00 | -2.98E+00 | -2.98E+00 | 2.55E-04 | 2.98E+00 | 1.01E+01 | -5.93E-08 | -1.19E+01 | -4.89E-04 | -8.90E-07 | 1.19E-07 | | -1.19E-07 | 2.08E-07 | -8.90E-07 | 2.20E+00 |
| | 4 | -1.84E-04 | 7.01E-04 | 7.84E-04 | 3.68E-04 | -4.23E-05 | 9.19E-05 | -7.33E-08 | | -1.00E-03 | -1.10E-06 | 1.47E-07 | -1.50E-04 | -1.47E-07 | 2.57E-07 | -1.10E-06 | 1.94E+00 |
| | 5 | -1.84E-04 | | 9.33E-04 | 3.68E-04 | | 9.19E-05 | -7.33E-08 | | -1.19E-03 | -1.10E-06 | 1.47E-07 | -1.50E-04 | -1.47E-07 | 2.57E-07 | -1.10E-06 | 6.67E+00 |
| | 6 | -2.49E-04 | 7.28E-04 | 8.11E-04 | 3.68E-04 | -6.93E-05 | | -7.33E-08 | 1.08E-04 | -1.00E-03 | -1.10E-06 | 1.47E-07 | 1.50E-04 | -1.47E-07 | 2.57E-07 | -1.10E-06 | 1.94E+00 |
| | 7 | -2.49E-04 | 7.28E-04 | 6.72E-04 | 3.68E-04 | | | -7.33E-08 | 1.08E-04 | -9.62E-04 | -1.10E-06 | 1.47E-07 | -1.50E-04 | -1.47E-07 | 2.57E-07 | -1.10E-06 | 2.80E+00 |
| | 8 | -8.24E-05 | 6.59E-04 | 7.42E-04 | 3.68E-04 | | 2.36E-04 | -7.33E-08 | -1.69E-04 | -1.00E-03 | -1.10E-06 | 1.47E-07 | -1.50E-04 | -1.47E-07 | 2.57E-07 | -1.10E-06 | 1.94E+00 |
| | 9 | 1.70E-03 | -8.26E-05 | | 3.68E-04 | 7.42E-04 | 2.76E-03 | -7.33E-08 | -3.14E-03 | -1.00E-03 | -1.10E-06 | 1.47E-07 | -1.50E-04 | -1.47E-07 | 2.57E-07 | -1.10E-06 | 1.94E+00 |
| | 10 | 1.70E-03 | | | 3.68E-04 | 7.42E-04 | 2.76E-03 | -7.33E-08 | -3.14E-03 | -1.00E-03 | -1.10E-06 | 1.47E-07 | -1.50E-04 | -1.47E-07 | 2.57E-07 | -1.10E-06 | 2.24E+00 |
| | 11 | 1.50E-03 | | 8.26E-05 | 3.68E-04 | 6.59E-04 | 2.48E-03 | -7.33E-08 | -2.81E-03 | -1.00E-03 | -1.10E-06 | 1.47E-07 | -1.50E-04 | -1.47E-07 | 2.57E-07 | -1.10E-06 | 1.94E+00 |
| | 12 | | 6.25E-04 | 7.07E-04 | 3.68E-04 | 3.43E-05 | 3.52E-04 | -7.33E-08 | -3.06E-04 | -1.00E-03 | -1.10E-06 | 1.47E-07 | -1.50E-04 | -1.47E-07 | 2.57E-07 | -1.10E-06 | 1.94E+00 |
| | 13 | -1.84E-04 | 7.01E-04 | 6.99E-04 | 3.68E-04 | | 9.19E-05 | -7.33E-08 | | -9.62E-04 | -1.10E-06 | 1.47E-07 | -1.50E-04 | -1.47E-07 | 2.57E-07 | -1.10E-06 | 2.41E+00 |
| | 14 | -1.84E-04 | | 1.01E-03 | 3.68E-04 | -3.75E-05 | 9.19E-05 | -7.33E-08 | | -1.23E-03 | -1.10E-06 | 1.47E-07 | -1.50E-04 | -1.47E-07 | 2.57E-07 | -1.10E-06 | 6.27E+00 |
| | 15 | 6.75E-04 | | 1.07E-03 | 3.68E-04 | | 1.31E-03 | -7.33E-08 | -1.43E-03 | -1.32E-03 | -1.10E-06 | 1.47E-07 | -1.50E-04 | -1.47E-07 | 2.57E-07 | -1.10E-06 | 3.59E+00 |
| | 16 | | 6.25E-04 | 7.76E-04 | 3.68E-04 | | 3.52E-04 | -7.33E-08 | -3.06E-04 | -1.04E-03 | -1.10E-06 | 1.47E-07 | -1.50E-04 | -1.47E-07 | 2.57E-07 | -1.10E-06 | 1.95E+00 |
| | 17 | | | 8.55E-04 | 3.68E-04 | 3.91E-05 | 3.52E-04 | -7.33E-08 | -3.06E-04 | -1.15E-03 | -1.10E-06 | 1.47E-07 | -1.50E-04 | -1.47E-07 | 2.57E-07 | -1.10E-06 | 5.18E+00 |

Model did not meet 1:1 parent:daughter ratio

Scenario1-Run6 (S1.R6) includes the same minerals as in S1.R2 plus pyrite and halite. S1.R6 models the change in major ion chemistry and dissolved uranium chemistry from UHB to UHA via water-rock interactions if pyrite were present in the inner basin alluvial material. This table lists the phase mole transfers from the 17 models produced. Negative values indicate precipitation out of solution, while positive values indicate dissolution.

Table 12: S2.R1 Summary

| S2.R1 | | | | | | | | | | | | Mixing Ratios | | UHA Diss. U using Mixing Ratio |
|---------|---------|------------|----------|-----------|----------|----------|-----------|-----------|-----------|-----------|------------------|---------------|----------|--------------------------------|
| Mineral | Model # | K-feldspar | CO2(g) | Calcite | Quartz | Dolomite | Kaolinite | Hematite | Illite | Gypsum | Sum of Residuals | UHB % | EHC-BS % | U (ppb) |
| | 1 | | | | | | | | | | | 2.55E-11 | 0 | |
| | 2 | | | | | | | | | | | 1.00E+00 | 0 | 332.5 |
| | 3 | | | | | | | | | | | 1 | 0 | |
| | 4 | | | | | | | | | | | 6.83E-01 | 0 | |
| | 5 | | | | | | | | | | | 1.00E+00 | 0 | 332.5 |
| | 6 | | | | | | | | | | | 1.00E+00 | 0 | 332.5 |
| | 7 | | | | | | | | | | | 1.00E+00 | 0 | 332.5 |
| | 8 | | | | | | | | | | | 1.00E+00 | 0 | 332.5 |
| | 9 | | | | | | | | | | | 1.00E+00 | 0 | 332.5 |
| | 10 | | | | | | | | | | | 1.00E+00 | 0 | 332.5 |
| | 11 | | | | | | | | | | | 1.00E+00 | 0 | 332.5 |
| | 12 | | | | | | | | | | | 1.00E+00 | 0 | 332.5 |
| | 13 | | | | | | | | | | | 1.00E+00 | 0 | 332.5 |
| | 14 | -9.48E-05 | 8.87E-04 | -1.87E-04 | 1.90E-04 | 3.88E-04 | 4.74E-05 | | | | 4.55E+00 | 6.26E-01 | 3.74E-01 | 210.16 |
| | 15 | -8.73E-05 | 8.92E-04 | | 1.75E-04 | 2.95E-04 | 4.36E-05 | | | | 4.84E+00 | 5.95E-01 | 4.06E-01 | 199.89 |
| | 16 | | 8.28E-04 | -1.20E-03 | | 9.65E-04 | | | | 9.29E-04 | 5.43E+00 | 2.28E-01 | 7.72E-01 | 80.01 |
| | 17 | -1.28E-04 | 9.01E-04 | -1.73E-04 | 1.90E-04 | 3.74E-04 | | 5.57E-05 | | | 4.55E+00 | 6.26E-01 | 3.74E-01 | 210.16 |
| | 18 | -1.17E-04 | 9.06E-04 | | 1.72E-04 | 2.89E-04 | | 5.07E-05 | | | 4.82E+00 | 5.90E-01 | 4.10E-01 | 198.42 |
| | 19 | -1.58E-04 | 7.19E-04 | 7.03E-04 | 3.17E-04 | | 7.92E-05 | | | -8.32E-04 | 3.90E+00 | 8.94E-01 | 1.07E-01 | 297.66 |
| | 20 | -1.03E-03 | 1.28E-03 | 2.01E-04 | 1.90E-04 | | -1.27E-03 | 1.55E-03 | | | 4.55E+00 | 6.26E-01 | 3.74E-01 | 210.16 |
| | 21 | -2.09E-04 | 7.44E-04 | 6.81E-04 | 3.09E-04 | | | 9.10E-05 | | -7.91E-04 | 3.93E+00 | 8.78E-01 | 1.22E-01 | 292.53 |
| | 22 | -1.10E-04 | 8.76E-04 | | 2.21E-04 | 2.93E-04 | 5.51E-05 | | | -1.73E-04 | 4.40E+00 | 6.91E-01 | 3.09E-01 | 231.52 |
| | 23 | -5.43E-04 | 1.07E-03 | | 1.90E-04 | 2.01E-04 | -5.88E-04 | 7.47E-04 | | | 4.55E+00 | 6.26E-01 | 3.74E-01 | 210.16 |
| | 24 | -1.47E-04 | 8.93E-04 | | 2.18E-04 | 2.85E-04 | | 6.41E-05 | | -1.58E-04 | 4.41E+00 | 6.87E-01 | 3.14E-01 | 230.13 |
| | 25 | -1.49E-03 | 1.50E-03 | | 1.22E-04 | | -1.99E-03 | 2.38E-03 | 3.76E-04 | | 4.88E+00 | 4.84E-01 | 5.16E-01 | 163.65 |
| | 26 | 2.03E-03 | | -1.07E-03 | 1.90E-04 | 1.28E-03 | 3.06E-03 | -3.55E-03 | | | 4.55E+00 | 6.26E-01 | 3.74E-01 | 210.16 |
| | 27 | | | | | | | | | | | 1.00E+00 | 0.00E+00 | 332.50 |
| | 28 | 1.81E+00 | | | 3.58E-04 | 7.02E-04 | 2.91E-03 | -3.32E-03 | -9.39E-04 | | 3.73E+00 | 9.81E-01 | 1.93E-02 | 326.19 |
| | 29 | | 8.48E-04 | -2.26E-04 | 1.90E-04 | 4.27E-04 | 1.82E-04 | -1.58E-04 | | | 4.55E+00 | 6.26E-01 | 3.74E-01 | 210.16 |
| | 30 | | 8.52E-04 | | 1.81E-04 | 3.13E-04 | 1.73E-04 | -1.51E-04 | | | 4.90E+00 | 6.08E-01 | 3.92E-01 | 204.18 |
| | 31 | | 6.40E-04 | 7.72E-04 | 3.40E-04 | | 3.26E-04 | -2.84E-04 | -9.61E-04 | | 3.78E+00 | 9.42E-01 | 5.77E-01 | 316.46 |
| | 32 | | 8.26E-04 | | 2.29E-04 | 3.17E-04 | 2.19E-04 | -1.90E-04 | -2.17E-04 | | 4.36E+00 | 7.08E-01 | 2.92E-01 | 236.95 |
| | 33 | | | | | | | | | | | 1.00E+00 | 0.00E+00 | 332.5 |
| | 34 | | | | | | | | | | | 1.00E+00 | 0.00E+00 | 332.5 |

- Model did not have significant mixing between "parent" groundwaters
- Model had closest mixing ratio to predicted theoretical mixing ratio

Scenario2-Run1 (S2.R1) includes the known minerals in the lithology along the flow path and excludes the sampled dissolved uranium at UHB, EHC-BS, and UHA springs. S2.R1 models the change in major ion chemistry from UHB and EHC-BS to UHA via water-rock interactions and mixing. This table lists the phase mole transfers from the 16 models produced. Negative values indicate precipitation out of solution, while positive values indicate dissolution.

Table 13: S2.R2 Summary

S2.R2 (S2.R3 is identical)

| Mineral | Model # | | | | | | | | | | | Mixing Ratios | | UHA Diss. U using Mixing Ratio | |
|---------|---------|------------|----------|----------|----------|----------|-----------|----------|-----------|-----------|-----------------|------------------|----------|--------------------------------|---------|
| | | K-feldspar | CO2(g) | Calcite | Quartz | Dolomite | Kaolinite | Hematite | Illite | Gypsum | Halite | Sum of Residuals | UHB % | EHC-BS % | U (ppb) |
| | 1 | | | | | | | | | | | 1.00E+00 | 0 | 332.50 | |
| | 2 | | | | | | | | | | | 1.00E+00 | 0 | 332.50 | |
| | 3 | | | | | | | | | | | 1.00E+00 | 4.52E-14 | 332.50 | |
| | 4 | | | | | | | | | | | 1.00E+00 | 0 | 332.50 | |
| | 5 | | | | | | | | | | | 1.00E+00 | 0 | 332.50 | |
| | 6 | | | | | | | | | | | 1.00E+00 | 0 | 332.50 | |
| | 7 | | | | | | | | | | | 1.00E+00 | 0 | 332.50 | |
| | 8 | | | | | | | | | | | 1.00E+00 | 0 | 332.50 | |
| | 9 | | | | | | | | | | | 1.00E+00 | 0 | 332.50 | |
| | 10 | | | | | | | | | | | 1.00E+00 | 0 | 332.50 | |
| | 11 | -1.69E-04 | 7.13E-04 | 7.00E-04 | 3.37E-04 | | 8.43E-05 | | -9.09E-04 | -1.06E-04 | 3.55E+00 | 9.35E-01 | 6.51E-02 | 311.24 | |
| | 12 | -2.22E-04 | 7.41E-04 | 6.77E-04 | 3.29E-04 | | | 9.67E-05 | -8.62E-04 | -9.45E-05 | 3.66E+00 | 9.17E-01 | 8.27E-02 | 305.45 | |
| | 13 | -1.20E-04 | 7.98E-04 | | 2.41E-04 | 3.28E-04 | 6.02E-05 | | -3.12E-04 | | 7.72E+00 | 7.30E-01 | 2.70E-01 | 244.12 | |
| | 14 | -1.61E-04 | 8.20E-04 | | 2.37E-04 | 3.18E-04 | | 6.98E-05 | -2.92E-04 | | 8.03E+00 | 7.22E-01 | 2.78E-01 | 241.66 | |
| | 15 | | | | | | | | | | | 1.00E+00 | 4.97E-14 | 332.50 | |
| | 16 | 1.63E-03 | | | 3.54E-04 | 7.03E-04 | 2.65E-03 | | -3.01E-03 | -9.61E-04 | -1.31E-04 | 3.32E+00 | 9.72E-01 | 2.84E-02 | 323.21 |
| | 17 | | 6.27E-04 | 7.75E-04 | 3.63E-04 | | 3.48E-04 | | -3.03E-04 | -1.06E-03 | -1.44E-04 | 3.18E+00 | 9.90E-01 | 9.80E-03 | 329.33 |
| | 18 | | 7.41E-04 | | 2.50E-04 | 3.55E-04 | 2.40E-04 | | -2.08E-04 | -3.65E-04 | | 6.85E+00 | 7.49E-01 | 2.51E-01 | 250.53 |

Model did not have significant mixing between "parent" groundwaters

Model had closest mixing ratio to predicted theoretical mixing ratio

Scenario2-Run2 (S2.R2) has the same minerals inputs as S2.R1 and includes the mineral halite, which was told to precipitate. Scenario2-Run3 (S2.R3) included the same minerals as S2.R2, except hematite was excluded from the inputs. S2.R2 and S2.R3 model the change in chemistry from UHB and EHC-BS to UHA via water-rock interactions and mixing. This table lists the phase mole transfers from the 16 models produced. Negative values indicate precipitation out of solution, while positive values indicate dissolution.

Table 14: S2.R4 Summary

| S2.R4 | | | | | | | | | | | | | | |
|---------|---------|------------|----------|-----------|----------|-----------|-----------|----------|-----------|-----------|---------------|----------|------------------|--------------------------------|
| Mineral | Model # | | | | | | | | | | Mixing Ratios | | Sum of Residuals | UHA Diss. U using Mixing Ratio |
| | | K-feldspar | CO2(g) | Calcite | Quartz | Dolomite | Kaolinite | Hematite | Gypsum | Illite | UHB % | EHC-BS % | | U (ppb) |
| | 1 | | | | | | | | | | 1.00E+00 | 1.48E-14 | | 332.50 |
| | 2 | | | | | | | | | | 1.00E+00 | 0.00E+00 | | 332.50 |
| | 3 | | | | | | | | | | 1.00E+00 | 5.88E-14 | | 332.50 |
| | 4 | | | | | | | | | | 1.00E+00 | 1.00E+00 | | 337.90 |
| | 5 | -9.59E-03 | 4.85E-03 | 3.77E-03 | 1.89E-04 | -3.57E-03 | -1.34E-02 | | | 1.58E-02 | 6.26E-01 | 3.74E-01 | 4.56E+00 | 210.10 |
| | 6 | | 8.53E-04 | | 1.81E-04 | 3.13E-04 | 1.73E-04 | | | -1.50E-04 | 6.07E-01 | 3.93E-01 | 4.91E+00 | 204.02 |
| | 7 | | | | | | | | | | 1.00E+00 | 0.00E+00 | | 332.50 |
| | 8 | | | | | | | | | | 1.00E+00 | 0.00E+00 | | 332.50 |
| | 9 | | | | | | | | | | 1.00E+00 | 0.00E+00 | | 332.50 |
| | 10 | -1.15E-02 | 5.60E-03 | 3.57E-03 | | -3.81E-03 | -1.62E-02 | | 9.29E-04 | 1.91E-02 | 2.28E-01 | 7.72E-01 | 5.44E+00 | 79.98 |
| | 11 | | 8.28E-04 | -1.20E-03 | | 9.64E-04 | | | 9.28E-04 | | 2.28E-01 | 7.72E-01 | 5.44E+00 | 80.01 |
| | 12 | | | | | | | | | | 1.00E+00 | 0.00E+00 | | 332.50 |
| | 13 | | | | | | | | | | 1.00E+00 | 0.00E+00 | | 332.50 |
| | 14 | | | | | | | | | | 1.00E+00 | 0.00E+00 | | 332.50 |
| | 15 | | | | | | | | | | 1.00E+00 | 0.00E+00 | | 332.50 |
| | 16 | -9.47E-05 | 8.88E-04 | -1.86E-04 | 1.89E-04 | 3.87E-04 | 4.74E-05 | | | | 6.26E+00 | 3.74E+00 | 4.56E+00 | 2101.32 |
| | 17 | -8.71E-05 | 8.93E-04 | | 1.74E-04 | 2.95E-04 | 4.36E-05 | | | | 5.94E-01 | 4.06E-01 | 4.85E+00 | 199.70 |
| | 18 | | | | | | | | | | 6.83E-01 | 1.15E-10 | 3.13E+00 | 227.13 |
| | 19 | -1.28E-04 | 9.02E-04 | -1.72E-04 | 1.89E-04 | 3.73E-04 | | | | 5.57E-05 | 6.26E-01 | 3.74E-01 | 4.56E+00 | 210.13 |
| | 20 | -1.17E-04 | 9.06E-04 | | 1.72E-04 | 2.88E-04 | | | | 5.06E-05 | 5.90E-01 | 4.10E-01 | 4.83E+00 | 198.26 |
| | 21 | -1.58E-04 | 7.20E-04 | 7.02E-04 | 3.16E-04 | | 7.91E-05 | | -1.17E-03 | | 8.92E-01 | 1.08E-01 | 3.91E+00 | 297.27 |
| | 22 | -1.02E-03 | 1.28E-03 | 2.01E-04 | 1.89E-04 | | -1.27E-03 | | | 1.55E-03 | 6.26E-01 | 3.74E-01 | 4.56E+00 | 210.10 |
| | 23 | -2.09E-04 | 7.46E-04 | 6.80E-04 | 3.09E-04 | | | | | -7.88E-04 | 8.77E-01 | 1.23E-01 | 3.95E+00 | 292.17 |
| | 24 | -2.31E-03 | 1.79E-03 | -2.37E-04 | | -3.28E-03 | | 9.28E-04 | 3.86E-03 | | 2.28E-01 | 7.72E-01 | 5.44E+00 | 80.01 |
| | 25 | -1.01E-04 | 8.77E-04 | | | 2.93E-04 | 5.51E-05 | | -1.72E-04 | | 6.91E-01 | 3.09E-01 | 4.41E+00 | 231.33 |
| | 26 | -5.40E-04 | 1.07E-03 | | 1.89E-04 | 2.01E-04 | -5.84E-04 | | | 7.43E-04 | 6.26E-01 | 3.74E-01 | 4.56E+00 | 210.13 |
| | 27 | -1.47E-04 | 8.94E-04 | | 2.18E-04 | 2.85E-04 | | | -1.57E-04 | 6.40E-05 | 6.85E-01 | 3.15E-01 | 4.43E+00 | 229.50 |
| | 28 | -1.49E-03 | 1.50E-03 | | 1.22E-04 | | -1.99E-03 | | 3.77E-04 | 2.37E-03 | 4.84E-01 | 5.17E-01 | 4.89E+00 | 163.55 |
| | 29 | -2.88E-03 | 2.03E-03 | | | -2.37E-04 | -4.08E-03 | | 9.28E-04 | 4.80E-03 | 2.28E-01 | 7.72E-01 | 5.44E+00 | 80.01 |
| | 30 | 2.04E-03 | | -1.07E-03 | 1.89E-04 | 1.28E-03 | 3.07E-03 | | | -3.55E-03 | 6.26E-01 | 3.74E-01 | 4.56E+00 | 210.13 |
| | 31 | | | | | | | | | | 1.00E+00 | 0.00E+00 | 5.91E+00 | 332.50 |
| | 32 | 1.99E-03 | | -2.03E-03 | | 1.79E-03 | 2.82E-03 | | 9.28E-04 | -3.31E-03 | 2.28E-01 | 7.72E-01 | 5.44E+00 | 80.01 |
| | 33 | 1.81E-03 | | | 3.58E-04 | 7.02E-04 | 2.91E-03 | | -9.38E-04 | -3.32E-03 | 9.80E-01 | 1.96E-02 | 3.75E+00 | 326.09 |
| | 34 | | 8.48E-04 | -2.25E-04 | 1.89E-04 | 4.26E-04 | 1.82E-04 | | | -1.58E-04 | 6.26E-01 | 3.74E-01 | 4.56E+00 | 210.13 |
| | 35 | | 6.42E-04 | 7.71E-04 | 3.40E-04 | | 3.25E-04 | | -9.58E-04 | -2.83E-04 | 9.41E-01 | 5.90E-02 | 3.80E+00 | 313.23 |
| | 36 | | 8.27E-04 | | 2.28E-04 | 3.16E-04 | 2.19E-04 | | -2.15E-04 | -1.90E-04 | 7.07E-01 | 2.93E-01 | 4.37E+00 | 236.76 |
| | 37 | | | | | | | | | | 1.00E+00 | 0.00E+00 | 8.65E+00 | 332.50 |
| | 38 | | | | | | | | | | 0.00E+00 | 1.00E+00 | 5.96E+00 | 5.40 |
| | 39 | | | | | | | | | | 0.00E+00 | 1.00E+00 | 5.96E+00 | 5.40 |
| | 40 | | | | | | | | | | 0.00E+00 | 1.00E+00 | 5.96E+00 | 5.40 |
| | 41 | | | | | | | | | | 0.00E+00 | 1.00E+00 | 1.30E+00 | 5.40 |
| | 42 | | | | | | | | | | 0.00E+00 | 1.00E+00 | 5.96E+00 | 5.40 |
| | 43 | | | | | | | | | | 0.00E+00 | 1.00E+00 | 5.96E+00 | 5.40 |
| | 44 | | | | | | | | | | 0.00E+00 | 1.00E+00 | 5.96E+00 | 5.40 |
| | 45 | | | | | | | | | | 0.00E+00 | 1.00E+00 | 5.96E+00 | 5.40 |
| | 46 | | | | | | | | | | 1.72E-10 | 0.00E+00 | 1.97E+00 | 0.00 |
| | 47 | | | | | | | | | | 5.08E-01 | 0.00E+00 | 2.83E+00 | 168.98 |
| | 48 | | | | | | | | | | 1.00E+00 | 0.00E+00 | 3.86E+00 | 332.50 |

Model did not have significant mixing between "parent" groundwaters

Model had closest mixing ratio to predicted theoretical mixing ratio

Scenario2-Run4 (S2.R4) includes the known minerals in the lithology along the flow path and includes the sampled dissolved uranium at UHB, EHC-BS, and UHA springs. S2.R5 models the change in major ion chemistry from UHB and EHC-BS to UHA via water-rock interactions and mixing. This table lists the phase mole transfers from the 16 models produced. Negative values indicate precipitation out of solution, while positive values indicate dissolution.

Table 15: S2.R5 Summary

| S2.R5 | | | | | | | | | | | | | | | | |
|---------|---------|------------|----------|-----------|----------|----------|-----------|----------|-----------|-----------|-----------|---------------|----------|------------------|--------------------------------|--|
| Mineral | Model # | K-feldspar | CO2(g) | Calcite | Quartz | Dolomite | Kaolinite | Hematite | Gypsum | Illite | Halite | Mixing Ratios | | Sum of Residuals | UHA Diss. U using Mixing Ratio | |
| | | | | | | | | | | | | UHB % | EHC-BS % | | U (ppb) | |
| | 1 | | | | | | | | | | | | | | | |
| | 2 | | | | | | | | | | | | | | | |
| | 3 | 9.32E-05 | 6.39E-04 | 3.20E-04 | 2.81E-04 | 2.39E-04 | 4.02E-04 | | -5.10E-04 | -3.90E-04 | | 8.16E-01 | 1.84E-01 | 4.42E+00 | 272.35 | |
| | 4 | | 7.43E-04 | | 2.50E-04 | 3.54E-04 | 2.39E-04 | | -3.63E-04 | -2.08E-04 | | 7.49E-01 | 2.51E-01 | 6.87E+00 | 250.33 | |
| | 5 | | | | | | | | | | | 1.00E+00 | 0.00E+00 | 3.02E+00 | 332.50 | |
| | 6 | | | | | | | | | | | 1.00E+00 | 0.00E+00 | 5.13E+00 | 332.50 | |
| | 7 | | | | | | | | | | | 1.00E+00 | 0.00E+00 | 3.02E+00 | 332.50 | |
| | 8 | | | | | | | | | | | 1.00E+00 | 5.70E-14 | 3.02E+00 | 332.50 | |
| | 9 | | | | | | | | | | | 1.00E+00 | 0.00E+00 | 3.02E+00 | 332.50 | |
| | 10 | | | | | | | | | | | 1.00E+00 | 0.00E+00 | 3.59E+00 | 332.50 | |
| | 11 | | | | | | | | | | | 1.00E+00 | 0.00E+00 | 3.02E+00 | 332.50 | |
| | 12 | | | | | | | | | | | 1.00E+00 | 0.00E+00 | 3.02E+00 | 332.50 | |
| | 13 | -1.41E-04 | 7.37E-04 | 4.17E-04 | 2.81E-04 | 1.42E-04 | 7.03E-05 | | -5.91E-04 | | | 8.16E-01 | 1.84E-01 | 4.42E+00 | 272.35 | |
| | 14 | -1.20E-04 | 8.00E-04 | | 2.41E-04 | 3.28E-04 | 6.02E-05 | | -3.11E-04 | | | 7.29E-01 | 2.71E-01 | 7.74E+00 | 243.95 | |
| | 15 | | | | | | | | | | | 8.60E+00 | 0.00E+00 | 3.38E+00 | 2858.84 | |
| | 16 | -1.90E-04 | 7.57E-04 | 4.38E-04 | 2.81E-04 | 1.21E-04 | | | -5.91E-04 | 8.28E-05 | | 8.16E-01 | 1.84E-01 | 4.42E+00 | 272.35 | |
| | 17 | -1.60E-04 | 8.22E-04 | | 2.37E-04 | 3.17E-04 | | | -2.91E-04 | 6.79E-05 | | 7.22E-01 | 2.78E-01 | 8.05E+00 | 241.50 | |
| | 18 | -4.18E-04 | 8.78E-04 | 5.59E-04 | 2.81E-04 | | -4.12E-04 | | -5.91E-04 | 5.68E-04 | | 8.16E-01 | 1.84E-01 | 4.42E+00 | 272.35 | |
| | 19 | | 7.44E-04 | 6.92E-04 | 2.85E-04 | | 2.73E-04 | | -7.33E-04 | -2.38E-04 | | 8.24E-01 | 1.76E-01 | 5.20E+00 | 274.83 | |
| | 20 | -1.69E-04 | 7.15E-04 | 6.99E-04 | 3.37E-04 | | 8.43E-05 | | -9.10E-04 | | -1.06E-04 | 9.35E-01 | 6.51E-02 | 3.57E+00 | 311.24 | |
| | 21 | -2.22E-04 | 7.42E-04 | 6.75E-04 | 3.29E-04 | | | | -8.62E-04 | 9.67E-05 | -9.45E-05 | 9.17E-01 | 8.27E-02 | 3.69E+00 | 305.45 | |
| | 22 | -1.90E-04 | 8.11E-04 | 6.26E-04 | 2.81E-04 | | | | -6.58E-04 | 8.28E-05 | | 8.16E-01 | 1.84E-01 | 4.55E+00 | 272.35 | |
| | 23 | 8.61E-04 | 3.19E-04 | | 2.81E-04 | 5.59E-04 | 1.49E-03 | | -5.91E-04 | -1.67E-03 | | 8.16E-01 | 1.84E-01 | 4.42E+00 | 272.35 | |
| | 24 | 1.63E-03 | | -3.19E-04 | 2.81E-04 | 8.79E-04 | 2.58E-03 | | -5.91E-04 | -2.95E-03 | | 8.16E-01 | 1.84E-01 | 4.42E+00 | 272.35 | |
| | 25 | 1.63E-03 | | | 2.81E-04 | 7.19E-04 | 2.58E-03 | | -7.09E-04 | -2.95E-03 | | 8.16E-01 | 1.84E-01 | 4.76E+00 | 272.35 | |
| | 26 | | | | | | | | | | | 1.00E+00 | 8.53E-14 | 6.51E+00 | 332.50 | |
| | 27 | 1.63E-03 | | | 3.55E-04 | 7.03E-04 | 2.66E-03 | | -9.64E-04 | -3.02E-03 | -1.32E-04 | 9.73E-01 | 2.72E-02 | 3.34E+00 | 323.60 | |
| | 28 | | 6.78E-04 | 3.59E-04 | 2.81E-04 | 2.01E-04 | 2.70E-04 | | -5.91E-04 | -2.35E-04 | | 8.16E-01 | 1.84E-01 | 4.42E+00 | 272.35 | |
| | 29 | | 6.29E-04 | 7.74E-04 | 3.63E-04 | | 3.48E-04 | | -1.06E-03 | -3.03E-04 | -1.44E-04 | 9.90E-01 | 9.80E-03 | 3.21E+00 | 329.29 | |
| | 30 | -1.41E-04 | 7.91E-04 | 6.50E-04 | 2.81E-04 | | 7.03E-05 | | -6.78E-04 | | | 8.16E-01 | 1.84E-01 | 4.59E+00 | 272.35 | |

- Model did not have significant mixing between "parent" groundwaters
- Model had closest mixing ratio to predicted theoretical mixing ratio

Scenario2-Run5 (S2.R5) the known minerals in the lithology along the flow path, the sampled dissolved uranium at UHB, and includes the mineral halite, which was told to precipitate. S2.R5 models the change in chemistry from UHB and EHC-BS to UHA via water-rock interactions and mixing. This table lists the phase mole transfers from the 16 models produced. Negative values indicate precipitation out of solution, while positive values indicate dissolution.

Appendix D: Precipitation Analysis Data

Table 16: Precipitation vs. Dissolved Uranium Spearman's Rho Coefficients table

| | PR | GRCA-AP | GRCA-VC |
|-------------|--------|-----------|-----------|
| Time Series | R | R | R |
| 1-7 DPS | -0.31 | -0.22 | -0.42 |
| 8-14 DPS | 0.12 | -0.033 | 0.19 |
| 15-21 DPS | 0.006 | 0.01 | -0.11 |
| 22-28 DPS | -0.32 | -0.34 | -0.63 |
| 29-35 DPS | -0.42 | -0.62 | -0.47 |
| 36-42 DPS | -0.47 | -0.4 | -0.38 |
| 43-49 DPS | -0.19 | -0.33 | -0.39 |
| 50-56 DPS | -0.32 | -0.25 | -0.41 |
| 57-63 DPS | -0.64 | -0.63 | -0.66 |
| 64-70 DPS | -0.49 | -0.12 | -0.13 |
| 71-77 DPS | -0.52 | -1.90E-01 | -0.15 |
| 78-84 DPS | 0.31 | -0.31 | 0.3 |
| 85-91 DPS | 0.0047 | -0.24 | 0.2 |
| 92-98 DPS | 0.011 | -0.035 | 0.087 |
| 99-105 DPS | -0.28 | -0.22 | -0.16 |
| 106-112 DPS | -0.11 | -0.082 | -0.22 |
| 113-119 DPS | 0.12 | -0.051 | -0.42 |
| 60 DPS | -0.43 | -0.51 | -0.48 |
| 90 DPS | -0.46 | -0.43 | -0.27 |
| 120 DPS | -0.44 | -0.43 | -0.34 |
| 0-2 WPS | -0.16 | -0.028 | -0.12 |
| 3-4 WPS | -0.26 | -0.21 | -0.58 |
| 5-6 WPS | -0.59 | -0.52 | -0.52 |
| 7-8 WPS | -0.29 | -0.38 | -0.48 |
| 9-10 WPS | -0.71 | -0.61 | -0.61 |
| 11-12 WPS | -0.16 | 0.02 | -0.25 |
| 13-14 WPS | -0.12 | -0.18 | 1.50E-02 |
| 15-16 WPS | -0.22 | -0.22 | -0.25 |
| 2-3 WPS | 0.058 | -0.087 | 0.078 |
| 4-5 WPS | -0.37 | -0.47 | -0.49 |
| 6-7 WPS | -0.47 | -0.51 | -0.36 |
| 8-9 WPS | -0.57 | -0.51 | -0.57 |
| 10-11 WPS | -0.51 | -0.14 | -1.00E-01 |
| 12-13 WPS | 0.1 | -0.042 | 0.1 |
| 14-15 WPS | -0.15 | -0.11 | 0.099 |
| 16-17 WPS | -0.15 | 0.038 | -0.4 |
| 0-4 WPS | -0.2 | -0.12 | -0.37 |
| 5-8 WPS | -0.54 | -0.56 | -0.48 |
| 9-12 WPS | -0.59 | -0.38 | -0.41 |
| 13-16 WPS | -0.2 | -0.17 | -0.19 |
| 8-11 WPS | -0.64 | -0.49 | -0.54 |
| 9-11 WPS | -0.72 | -0.53 | -0.5 |
| 58-78 DPS | -0.61 | -0.51 | -0.47 |
| 57-77 DPS | -0.72 | -0.53 | -0.5 |
| 59-79 DPS | -0.58 | -0.44 | -0.43 |
| 60-80 DPS | -0.58 | -0.41 | -0.4 |

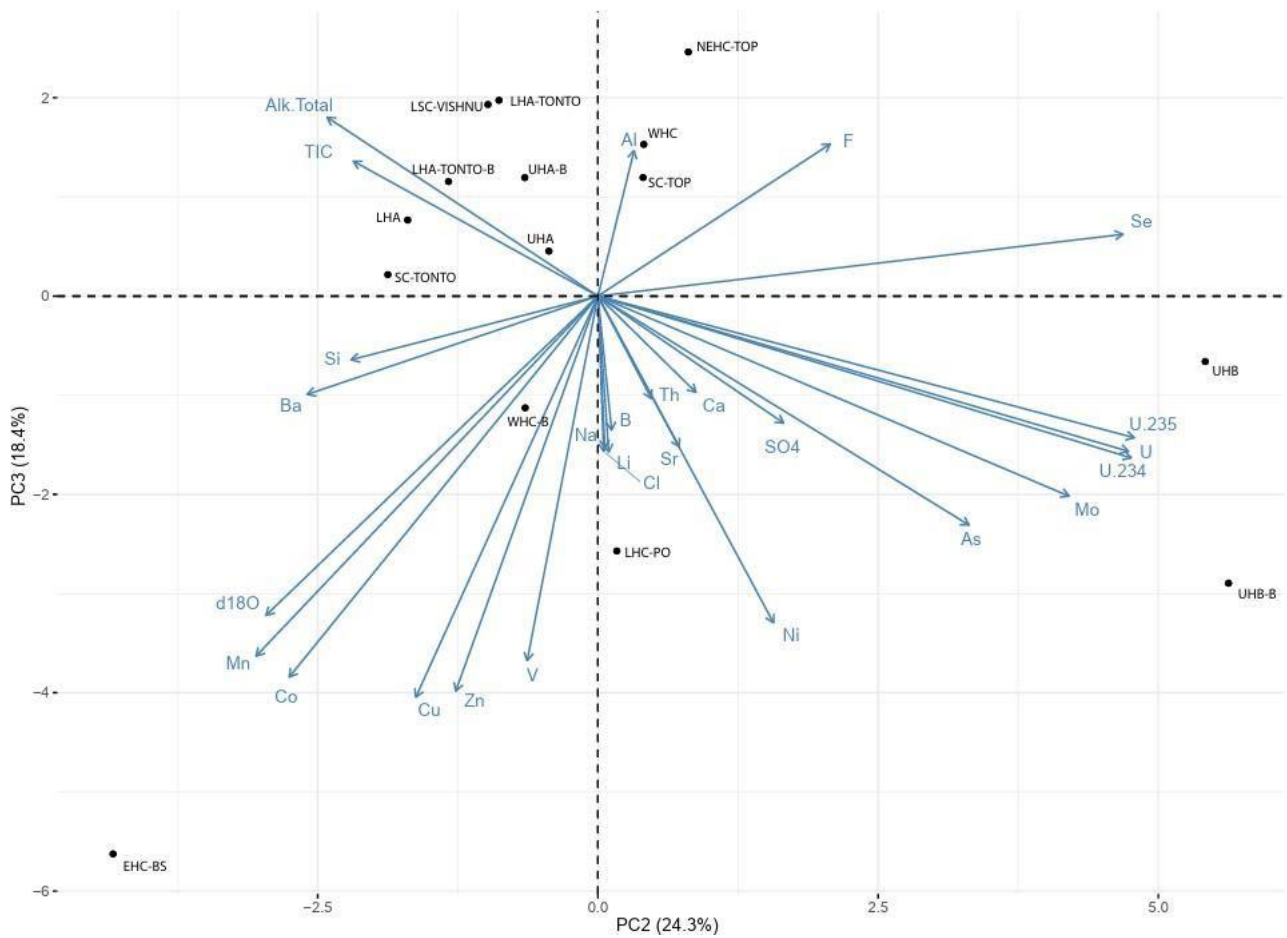
| | PR | GRCA-AP | GRCA-VC |
|-------------|-------|---------|---------|
| Time Series | R | R | R |
| 61-81 DPS | -0.57 | -0.35 | -0.37 |
| 45-58 DPS | -0.59 | -0.6 | -0.62 |
| 46-59 DPS | -0.53 | -0.59 | -0.55 |
| 47-60 DPS | -0.51 | -0.52 | -0.46 |
| 48-61 DPS | -0.53 | -0.46 | -0.51 |
| 49-62 DPS | -0.52 | -0.45 | -0.55 |
| 50-63 DPS | -0.57 | -0.51 | -0.55 |
| 51-64 DPS | -0.62 | -0.51 | -0.54 |
| 52-65 DPS | -0.63 | -0.56 | -0.55 |
| 53-66 DPS | -0.63 | -0.57 | -0.58 |
| 54-67 DPS | -0.65 | -0.57 | -0.6 |
| 55-68 DPS | -0.61 | -0.55 | -0.59 |
| 56-69 DPS | -0.62 | -0.56 | -0.59 |
| 57-70 DPS | -0.71 | -0.61 | -0.61 |
| 58-71 DPS | -0.54 | -0.6 | -0.61 |
| 59-72 DPS | -0.52 | -0.56 | -0.6 |
| 60-73 DPS | -0.56 | -0.57 | -0.45 |
| 61-74 DPS | -0.55 | -0.56 | -0.39 |
| 62-75 DPS | -0.55 | -0.51 | -0.17 |
| 63-76 DPS | -0.53 | -0.35 | -0.11 |
| 64-77 DPS | -0.51 | -0.14 | -0.10 |
| 65-78 DPS | -0.49 | -0.086 | -0.2 |
| 66-79 DPS | -0.42 | -0.13 | -0.15 |
| 67-80 DPS | -0.41 | -0.13 | -0.19 |
| 68-81 DPS | -0.36 | -0.11 | -0.075 |
| 58-70 DPS | -0.52 | -0.61 | -0.6 |
| 59-70 DPS | -0.53 | -0.52 | -0.59 |
| 60-70 DPS | -0.62 | -0.52 | -0.56 |
| 61-70 DPS | -0.63 | -0.55 | -0.52 |
| 62-70 DPS | -0.62 | -0.48 | -0.33 |
| 63-70 DPS | -0.59 | -0.37 | -0.26 |
| 64-70 DPS | -0.49 | -0.12 | -0.13 |
| 57-69 DPS | -0.63 | -0.57 | -0.58 |
| 57-68 DPS | -0.62 | -0.55 | -0.59 |
| 57-67 DPS | -0.67 | -0.55 | -0.59 |
| 57-66 DPS | -0.66 | -0.55 | -0.59 |
| 57-65 DPS | -0.66 | -0.55 | -0.59 |
| 57-64 DPS | -0.66 | -0.6 | -0.6 |
| 57-63 DPS | -0.64 | -0.63 | -0.66 |
| 57-62 DPS | -0.59 | -0.52 | -0.65 |
| 57-61 DPS | -0.59 | -0.53 | -0.61 |
| 58-67 DPS | -0.5 | -0.54 | -0.54 |
| 59-67 DPS | -0.5 | -0.48 | -0.55 |
| 60-67 DPS | -0.59 | -0.49 | -0.54 |
| 61-67 DPS | -0.6 | -0.52 | -0.54 |
| 62-67 DPS | -0.6 | -0.46 | -0.27 |

| | |
|------|---|
| 0.57 | R-coefficient greater than -0.7 closest R-coefficient to 1 or -1 |
|------|---|

PR = Phantom Ranch Weather Station
 GRCA-AP = Grand Canyon Airport weather station
 GRCA-VC = Grand Canyon Visitor Center weather station

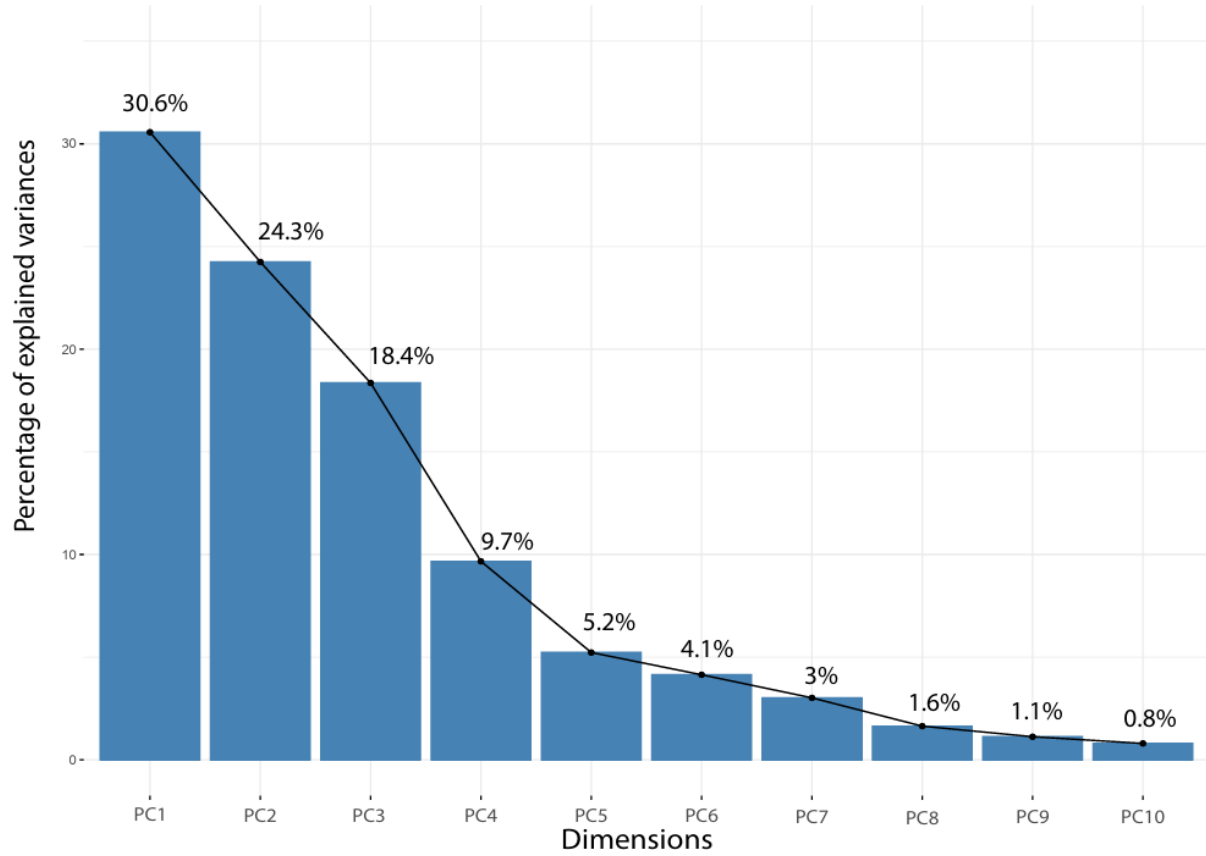
Appendix E: Additional Multivariate Analyses Plots

Fig. 26 All analytes PCA: PC2-PC3 Biplot



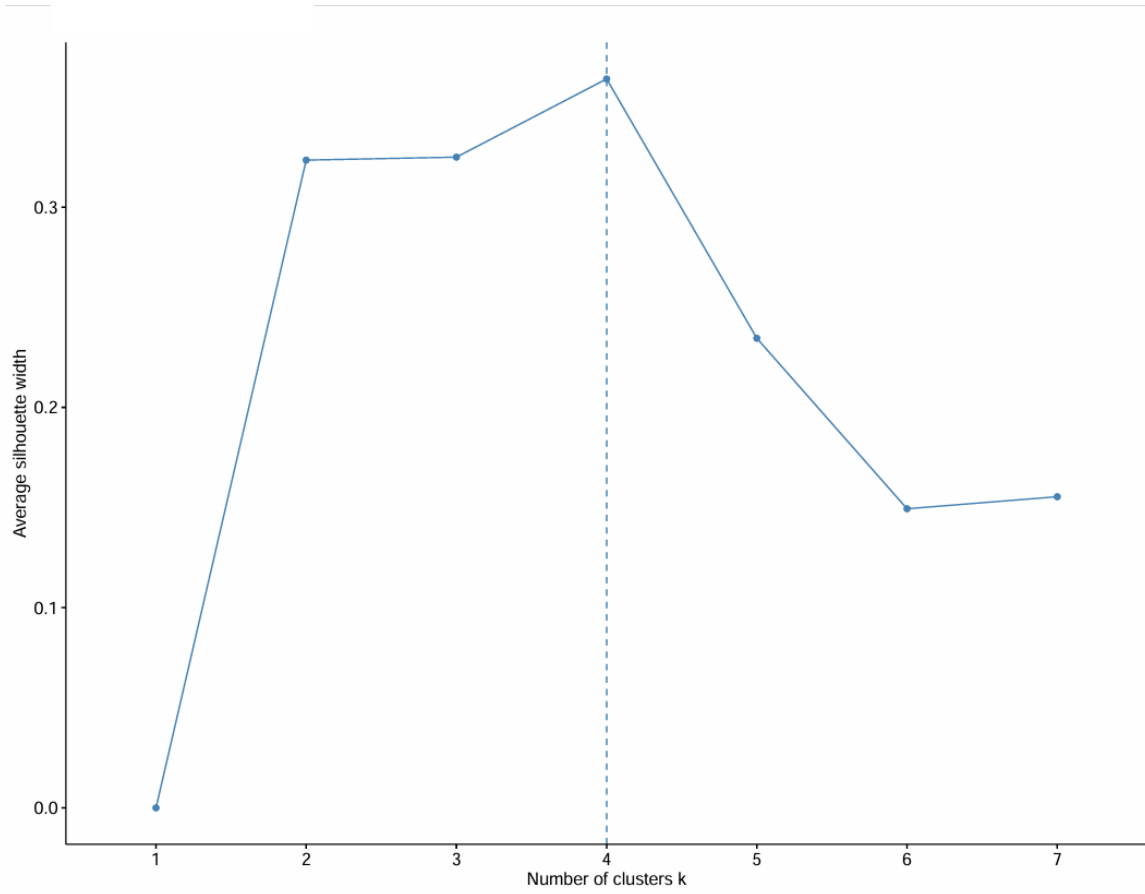
Bi-plot of the PC2 and PC3 from the Principal Component Analysis including all analytes collected in October 2013

Fig. 27 All analytes PCA: Eigenvalues of Principal Components 1-10



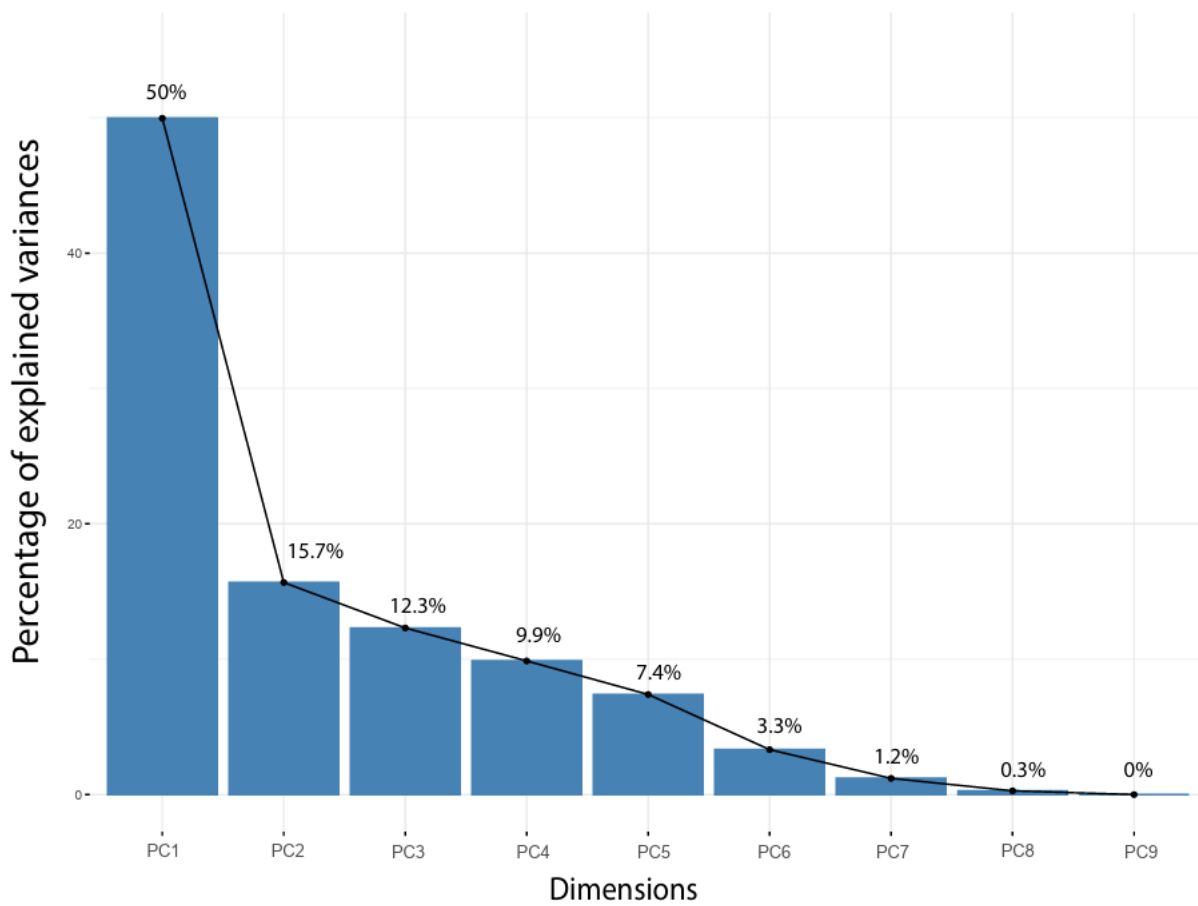
Eigenvalues of Principal Components 1-10 from the Principal Component Analysis including all analytes collected in October 2013

Fig. 28 All analytes Kmeans: Optimal number of clusters



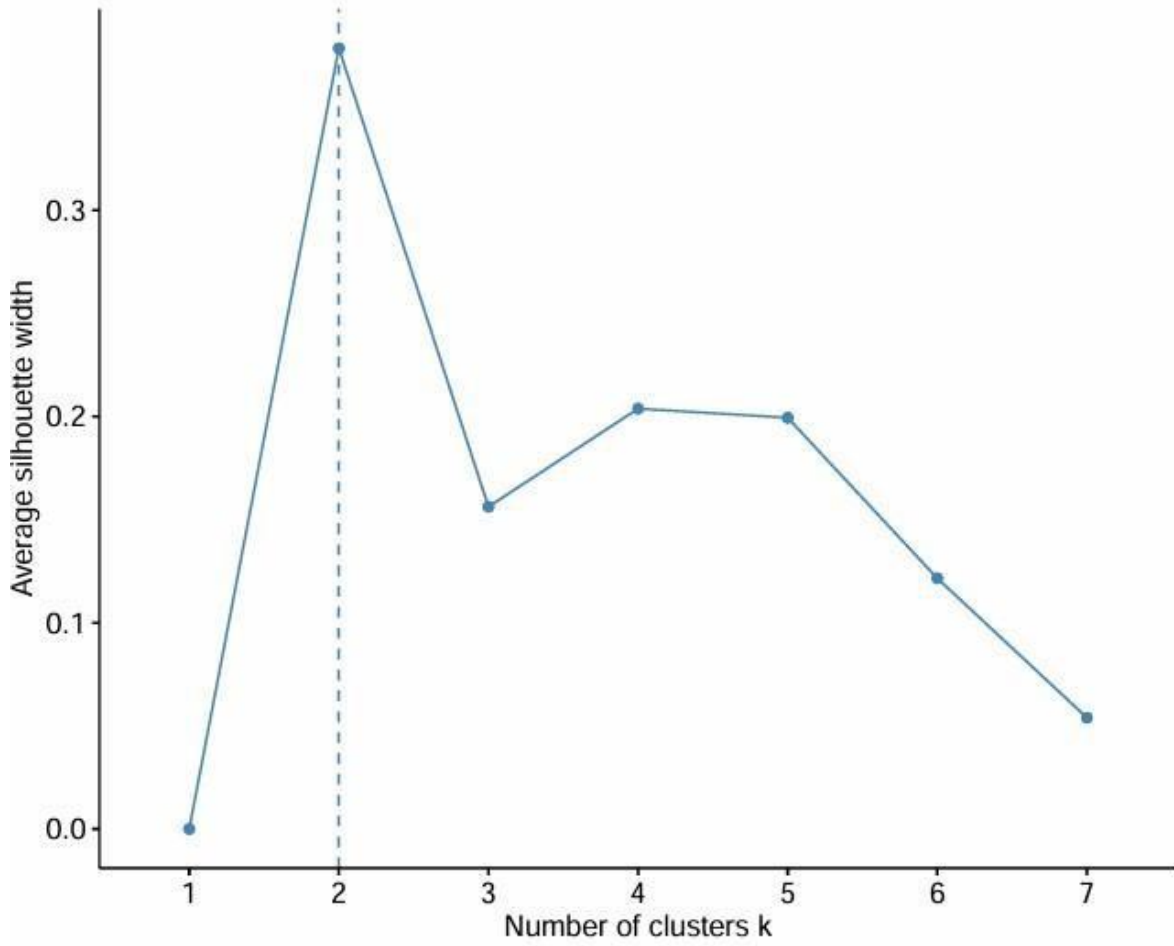
Optimal number of clusters for the K- means clustering from the multivariate analysis including all analytes collected in October 2013

Fig. 29 Time PCA: Eigenvalues of Principal Components 1-9



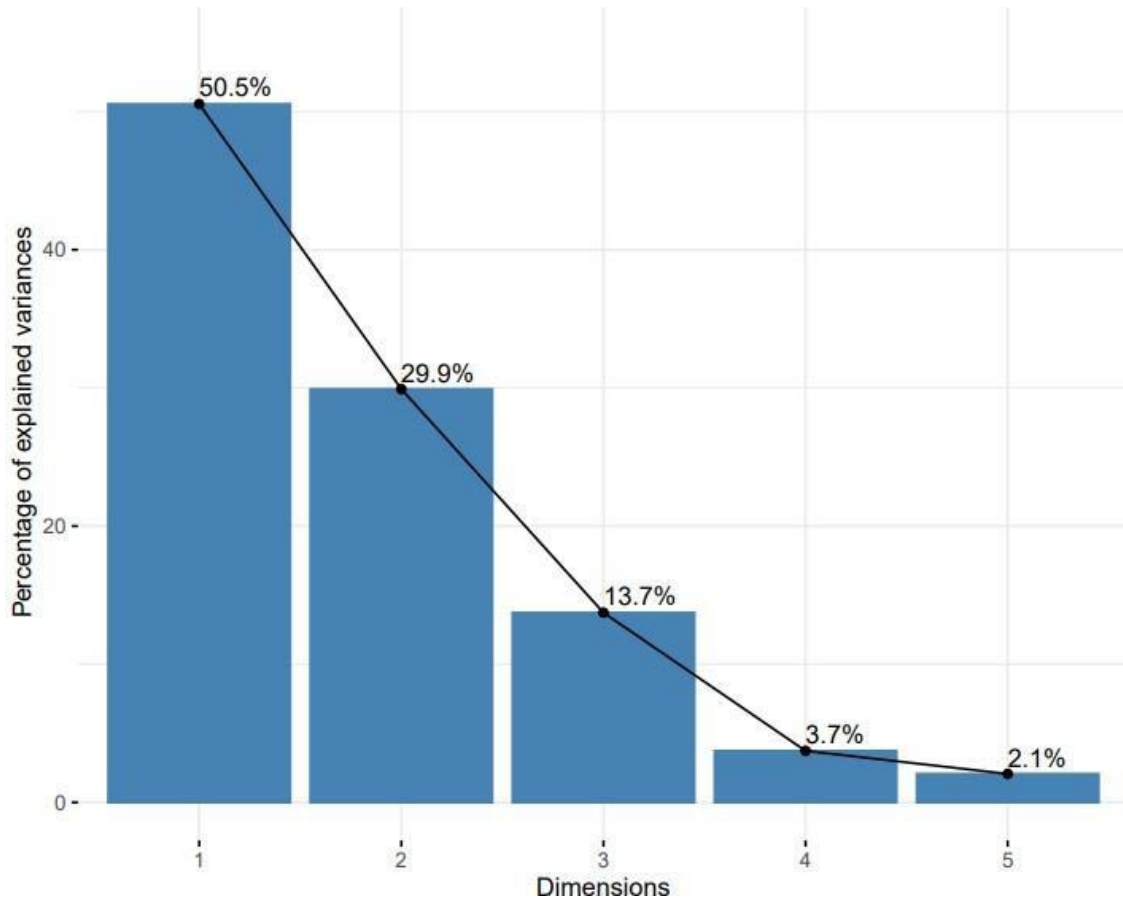
Eigenvalues of Principal Components 1
-10 from the Principal Component Analysis
comparing analytes collected in October
2013 and March 2023

Fig 30 Time Kmeans: Optimal number of clusters



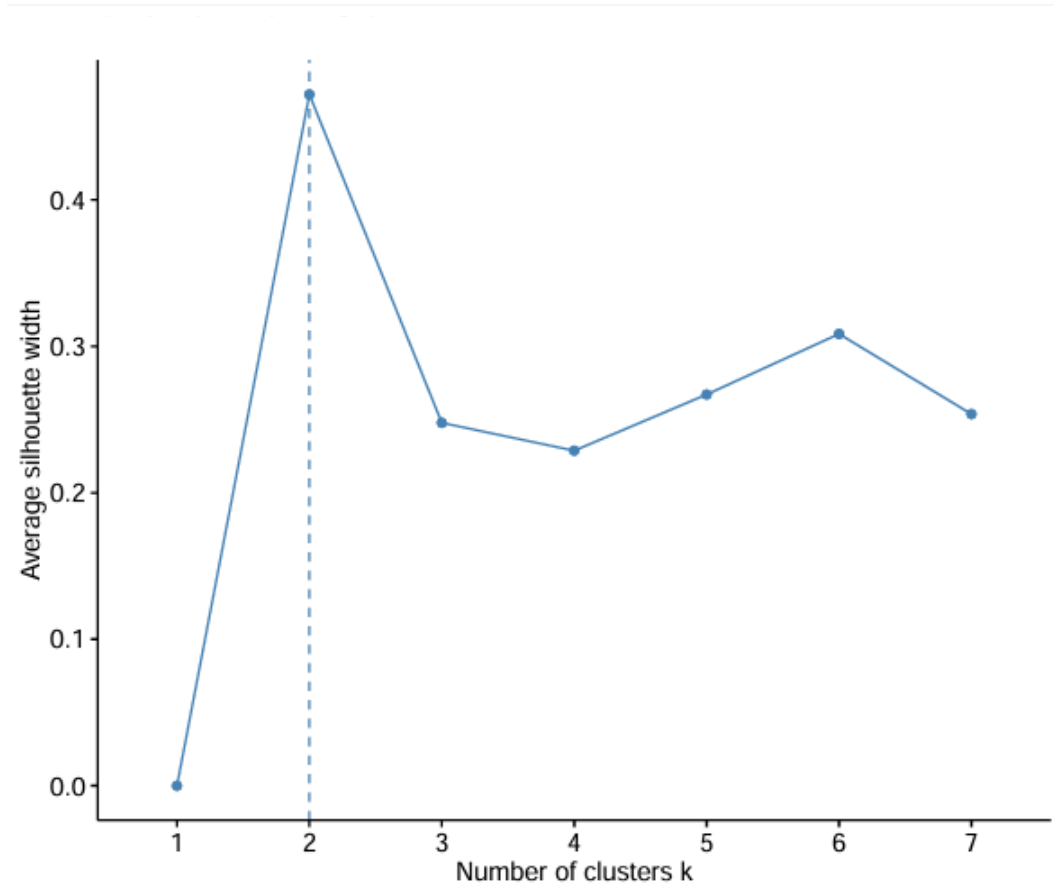
Optimal number of clusters for the K- means clustering from the multivariate analysis that compared analytes collected in October 2013 and March 2023

Fig 31 Uranium PCA: Eigenvalues of Principal Components 1-9



Eigenvalues of Principal Components 1
-5 from the Principal Component Analysis
comparing analytes correlated with dissolved
uranium from data collected in October 2013

Fig. 32 Uranium H-Kmeans: Optimal number of clusters



Optimal number of clusters for the K- means clustering from the multivariate analysis including analytes correlated with dissolved uranium from data collected in October 2013

References Cited

- Abdi, H., and Williams, L.J., 2010, Principal component analysis: WIREs Computational Statistics, v. 2, Iss. 4, p. 433-459, doi:10.1002/wics.101
- Alpine, A. E. & Brown, K. M., 2010, Introduction, in *Hydrological, geological, and biological sites characterization of breccia pipe uranium deposits in northern Arizona* (ed. Alpine, A. E.): *US Geol. Surv. Sci. Investig. Rep.* 2010–5025, <http://pubs.usgs.gov/sir/2010/5025/>.
- Amundson, M. A., 2001, Mining the Grand Canyon to save it—The Orphan Lode uranium mine and national security: *West. Hist. Q.*, v. 32, p. 320–345, <https://doi.org/10.2307/3650738>.
- Appelo, C.J., and Postma, D., 2005, *Geochemistry, groundwater and pollution*: Leiden, the Netherlands, A.A. Balkema Publishers, 649 p.
- Beisner, K.R., Tillman, F.D., Anderson, J.R., Antweiler, R.C., Bills, D.J., 2017, Geochemical Characterization of Groundwater Discharging from Springs North of the Grand Canyon, Arizona, 2009-2016: *US Geol. Surv. Sci. Investig. Rep.* 2017 – 5068, 58 p., <https://doi.org/10.3133/sir20175068>
- Beisner, K. R., Solder, J. E., Tillman, F. D., Anderson, J. R. & Antweiler, R. C., 2020, Geochemical characterization of groundwater evolution south of Grand Canyon, Arizona (USA): *Hydrogeol. J.* v. 28, p. 1615–1633, <https://doi.org/10.1007/s10040-020-02192-0>.
- Beisner, K. R. & Tillman, F. D., 2020, Spatial and temporal changes in geochemistry at spring sites near breccia pipe uranium deposits of Grand Canyon Region, AZ: *Goldschmidt Abstracts*, p. 157, <https://doi.org/10.46427/gold2020.157>.
- Beisner, K.R., Davidson, C.T., Tillman, F.D, 2023, Anthropogenic influence on groundwater geochemistry in Horn Creek Watershed near the Orphan Mine in Grand Canyon National Park, Arizona, USA: *Geochemistry: Exploration, Environment, Analysis*, v.23, doi:10.1144/geochem2023-007
- Bethke, C. M., Farrell, B., Sharifi, M., 2022, *Geochemist’s Workbench: Aqueous Solutions LLC*, <https://www.gwb.com/index.php>
- Beus, S.S., and Billingsley, G.H., 1989, Paleozoic strata of the Grand Canyon, Arizona, in Elston, D.P., Billingsley, G.H., and Young, R.A., eds., *Geology of Grand Canyon, northern Arizona (with Colorado River guides)*: American Geophysical Union, International Geological Congress, 28th, Field Trip Guidebook T115/315, p. 122-127.
- Beus, S.S. and Morales, M., 1990, *Grand Canyon Geology*: New York, Oxford University Press, 518 p.

- Billingsley, G.H., 2000, Geologic Map of the Grand Canyon 30' x 60' Quadrangle, Coconino and Mohave Counties, Northwestern Arizona: U.S. Geological Survey, Pamphlet to accompany Geologic Investigations Series I-2688, 15 p.
- Bills, D. J., Tillman, F. D., Anning, D. W., Antweiler, R. C. & Kraemer, T. F., 2010, Historical and 2009 water chemistry of wells, perennial and intermittent streams, and springs in northern Arizona, in *Hydrological, geological, and biological sites characterization of breccia pipe uranium deposits in northern Arizona* (ed. Alpine, A. E.): US Geol. Surv. Sci. Investig. Rep. 2010-5025, <http://pubs.usgs.gov/sir/2010/5025/>.
- Brathovde, J. E., 1986, Stratigraphy of the Grand Wash Dolomite (Upper? Cambrian), western Grand Canyon, Mohave County, Arizona [M.S. Thesis]: Northern Arizona University, 140 p.
- Canadian Council of Ministers of the Environment, 2011, Canadian water quality guidelines for the protection of aquatic life: Uranium, in Canadian environmental quality guidelines: Canadian Council of Ministers of the Environment, Winnipeg: <http://ceqg-rcqe.ccme.ca/download/en/328>. (Accessed 21 Nov 2021).
- Chenoweth, W. L., 1986, The Orphan Lode Mine, Grand Canyon, Arizona—A case history of a mineralized, collapse-breccia pipe: *US Geol. Surv. Open-File Rep.*, p. 86-510, <https://doi.org/10.3133/ofr86510>.
- Craig, H., 1961, Isotopic Variations in Meteoric Waters: *Science*, vol. 133, p. 1702-1703, DOI: 10.1126/science.133.3465.1702
- Crossey, L.J., Fischer, T.P., Patchett, P.J., Karlstrom, K.E., Hilton, D.R., Newell, D.L., Huntoon, P., Reynolds, A.C., de Leeuw, G.A.M., 2006, Dissected hydrologic system at the Grand Canyon: Interaction between deeply derived fluids and plateau aquifer waters in modern springs and travertine: *Geology*, v. 34, no. 1, p. 25-28, doi:10.1130/G22057.1
- Everret, B.S., Dunn, G., 2001, *Applied Multivariate Data Analysis, Second Edition*: West Sussex, UK, John Wiley & Sons Ltd, 335p.
- Fetter, C., Boving, T., Kreamer, D., 2018, *Contaminant Hydrogeology*: Long Grove, IL, Waveland Press, Inc., p. 360-364
- Fitzgerald, J. 1996, Residence time of groundwater issuing from the South Rim aquifer in the eastern Grand Canyon, [MSc Thesis]: University of Nevada, Las Vegas, NV, 103 p.
- Gat, J.R., 1996, Oxygen and Hydrogen Isotopes in the Hydrologic Cycle: *Anny. Rev. Earth Planet. Sci.*, v. 24, p. 225-262, <https://doi.org/10.1146/annurev.earth.24.1.225>
- Goings, D.B., 1985, Spring flow in a portion of Grand Canyon National Park, Arizona [M.S. thesis]: University of Nevada, Las Vegas, 65 p.

- Gornitz, V., Kerr, P.F., 1970, Uranium Mineralization and Alteration, Orphan Mine, Grand Canyon, Arizona: *Economic Geology*, v. 65, no. 7, p 751-768, <https://doi.org/10.2113/gsecongeo.65.7.751>
- Guler, C., Thyne, G.D., McCray, J.E., Turner, A.K., 2002, Evaluation of graphical and multivariate statistical methods for classification of water chemistry data: *Hydrogeology Journal*, v. 10, p 455-474, DOI 10.1007/s10040-002-0196-6
- Hach Company, 2014, Alkalinity, Phenolphthalein and Total Alkalinity Method 10244 Digital Titrator., <https://my.hach.com/asset-get.download.jsa?id=10803910351>
- Harrell Jr., F.E., 2023, R package ‘Hmisc’, Harrell Miscellaneous, Version 5.1-1, <https://cran.r-project.org/web/packages/Hmisc/Hmisc.pdf>
- Hartigan, J.A., and Wong, M.A., 1979, Algorithm AS 136: A K-Means Clustering Algorithm: *Journal of the Royal Statistical Society. Series C (Applied Statistics)*, v. 28, Iss.1, p. 100-108, <https://doi.org/10.2307/2346830>
- Huntoon, PW, 1974, The karstic groundwater basins of the Kaibab Plateau, Arizona: *Water Resources Research*, v. 10, Iss. 3, p. 570-590
- Huntoon, PW, 2000, Variability of karstic permeability between unconfined and confined aquifers, Grand Canyon region Arizona: *Environ Eng Sci*, v. 6, p. 155–170, <https://doi.org/10.2113/gseegeosci.6.2.155>.
- Ingraham, N.L., and Taylor, B.E., 1991, Light Stable Isotope Systematics of Large-Scale Hydrologic Regimes in California and Nevada: *Water Resources Research*, v. 27, Iss. 1, p. 77-90, <https://doi.org/10.1029/90WR01708>
- Ingraham, N.L., Zukosky, K., Kreamer, D.K., 2001, Application of Stable Isotopes to Identify Problems in Large-Scale Water Transfer in Grand Canyon National Park: *Environmental Science & Technology*, v. 35, Iss. 7, p. 1299-1302, DOI: 10.1021/es0015186
- Jia Z, Zang H, Hobbs P et al. 2017, Application of inverse modeling in a study of the hydrogeochemical evolution of karst groundwater in the Jinci Spring region, northern China: *Environmental Earth Sciences*, v. 76, Iss. 1, p. 1-11, <https://doi.org/10.1007/s12665-017-6631-8>
- Jones, C.J.R., Springer, A.E., Tobin, B.W., Zappitello, S.J., Jones, N.A., 2017, Characterization and hydraulic behaviour of the complex karst of the Kaibab Plateau and Grand Canyon National Park, USA: *Geological Society, London, Special Publications*, v. 466, p. 237-260, <https://doi.org/10.1144/SP466.5>
- Judd, A.G., 1980, The Use of Cluster Analysis in the Derivation of Geotechnical Classifications: *Bulletin of the Association of Engineering Geologists*, v. 17, Iss. 4

- Karlstrom, K.E., Mohr, M.T., Schmitz, M.D., Sundberg, F.A., Rowland, S.M., Blakey, R., Foster, J.R., Crosse, L.J., Dehler, C.M., Hagadorn, J.W., 2020, Redefining the Tonto Group of Grand Canyon and recalibrating the Cambrian time scale: *Geology*, v. 48. Iss. 5, <https://doi.org/10.1130/G46755.1>
- Kanno-Youngs, Z., and Friedman, L., 2023, Biden to Designate Monument Near Grand Canyon, Preventing Uranium Mining: <https://www.nytimes.com/2023/08/07/us/politics/biden-grand-canyon-arizona-national-monument.html> (accessed December 2023)
- Kassambra, A., 2017, Practical Guide to Cluster Analysis in R, Unsupervised Machine Learning, Edition 1: STHDA, 187 p.
- Kassambra, A., and Mundt, F., 2020, R package ‘factoextra’, version 1.0.7, <https://cran.r-project.org/web/packages/factoextra/factoextra.pdf>
- Kreamer, D.K., Hodge, V.F., Rabinowitz, I., Johannesson, K.H., Stetzenbach, K.J., 1996, Trace Element Geochemistry in Water from Selected Springs in Death Valley National Park, California: *Groundwater*, v. 34, Iss. 1, p. 95-103, <https://doi.org/10.1111/j.1745-6584.1996.tb01869.x>
- Kurtio, P. *et al.*, 2002, Renal effects of uranium in drinking water: *Environ. Health Perspect.*, v. 110, p. 337–342, <https://doi.org/10.1289/ehp.02110337>.
- Liebe, D., 2003, The use of the $^{234}\text{U}/^{238}\text{U}$ activity ratio at the characterization of springs and surface streams in Grand Canyon National Park, Arizona, [MSc Thesis]: Hochschule für Technik und Wirtschaft Dresden. 105 p.
- Ligges, U., and Mächler, M., 2003, Scatterplot3d - an R Package for Visualizing Multivariate Data, *Journal of Statistical Software*, v. 8, Iss. 11, p. 1–20, doi:10.18637/jss.v008.i11.
- McKee, E.D., and Gutschick, R.C., 1969, History of the Redwall Limestone of Northern Arizona: *Geologic Society of America, Inc. Memoir 114*, 8 p., doi:10.1130/MEM114
- McKee, E.D., and Resser, C.E., 1945, *Cambrian History of the Grand Canyon Region*: Baltimore, The Lord Baltimore Press, 232 p.
- Metzger, D.G., 1961, Geology in Relation to Availability of Water Along the South Rim Grand Canyon National Park: U.S. Geological Survey Water-Supply Paper 1475-C, 33p., <https://pubs.usgs.gov/wsp/1475c/report.pdf>
- Middleton, L.T., and Elliot, D.K., 1990, Tonto Group in Beus, S.S., and Morales, M., eds., *Grand Canyon Geology*: New York, Oxford University Press, 518 p.
- Monroe S.A., Antweiler R.C., Hart R.J., Taylor H.E., Margot T., Rihs J.R., Felger T.J., 2005, Chemical characteristics of groundwater discharge along the South Rim of Grand Canyon

- in Grand Canyon National Park, Arizona, 2000–2001. US Geol Surv Sci Invest Rep 2004-5146, 59 p.
- National Park Service, 2021a, *National Park Service Visitor Use Statistics*: <https://irma.nps.gov/STATS/Reports/Park/GRCA> (Accessed Nov 19, 2021).
- National Park Service, 2021b, *Plants*: <https://www.nps.gov/grca/learn/nature/plants.htm>, (Accessed 23 Nov 2021)
- Noble, L.F., 1914, The Shinumo Quadrangle, Grand Canyon District, Arizona: U.S. Geological Survey Bulletin 549, 100 p.
- U.S. Geological Survey, 2022, USGS Water Data for the Nation. U.S. Geological Survey National Water Information System database, <https://doi.org/10.5066/F7P55KJN> [last accessed April 2022].
- Otton, J. K. & Van Gosen, B. S., 2010, Uranium resource availability in breccia pipes in northern Arizona, in *Hydrological, geological, and biological sites characterization of breccia pipe uranium deposits in northern Arizona* (ed. Alpine, A. E.): *US Geol. Surv. Sci. Investig. Rep.* 2010–5025, <https://doi.org/10.3133/sir20105025>.
- Parkhurst, David L., 1996, User’s Guide to PHREEQC—a Computer Program for Speciation, Reaction-Path, Advective-Transport, and Inverse Geochemical Calculations: U.S. Geol. Surv. Water-Resources Investigations Report 95-4227, p.1-151.
- Parkhurst, D.L., and Appelo, C.A.J., 2013, Description of Input and Examples for PHREEQC Version 3 – A Computer Program for Speciation, Batch-Reaction, One-Dimensional Transport, and Inverse Geochemical Calculations: U.S. Geological Survey Techniques and Methods, book 6, chap. A43, 497 p., <https://pubs.usgs.gov/tm/06/a43/>
- Putman, A.L., Fiorella, R.P., Bowen, G.J., Cai, Z., 2019, A global perspective on local meteoric water lines: Meta-analytic insight into fundamental controls and practical constraints: *Water Resources Research*, v. 55, p. 6896-6910, doi:10.1029/2019WR025181
- Rapantova, N., Licbinska, M., Babka, O., Grmela, A., Pospisil, P., 2012, Impact of uranium mines closure and abandonment on groundwater quality: *Environ. Sci. Pollut. Res.*, v. 20, p. 7590-7602, DOI 10.1007/s11356-012-1340-z
- Rowland, S.M., Korolev, S., Hagadorn, J.W., Ghosh, K., 2023, Frenchman Mountain Dolostone: A new formation of the Cambrian Tonto Group, Grand Canyon and Basin and Range, USA: *Geosphere*, v. 19, Iss. 3, p. 719-747, <https://doi.org/10.1130/GES02514.1>.
- Royal Geographic Society, A guide to Spearman’s Rank: <https://www.rgs.org/media/tywc5gni/a-guide-to-spearman-s-rank.pdf> (rgs.org) (accessed January 2024)
- Scharr Unpublished, 2011, University of Nevada, Las Vegas. Field notebook.

- Schindel, G.M., 2015, Determining groundwater residence times of the Kaibab Plateau, R-aquifer using temperature, Grand Canyon National Park, Arizona [M.S. Thesis]: Northern Arizona University, 112 p.
- Solder, J. E., and Beisner, K.R., 2020, Critical evaluation of stable isotope mixing end-members for estimating groundwater recharge sources: case study from the South Rim of the Grand Canyon, Arizona, USA
- Solder, J. E., Beisner, K. R., Anderson, J. & Bills, D. J., 2020, Rethinking groundwater flow on the South Rim of the Grand Canyon, USA: Characterizing recharge sources and flow paths with environmental tracers: *Hydrogeol. J.*, v. 28, p. 1593–1613, <https://doi.org/10.1007/s10040-020-02193-z>.
- Spamer, E.E., 1984, Paleontology in the Grand Canyon of Arizona: 125 years of lessons and enigmas from the late Precambrian to the present: *The Mosasaur*, v. 2, p. 45-128
- Springer, A.E., Boldt, E.M., Junghans, K.M., 2017, Local vs. Regional Groundwater Flow Delineation from Stable Isotopes at Western North America Springs: *Groundwater*, v. 55, Iss. 1, p. 100-109, doi:10.1111/gwat.12442
- Stevens LE, Meretsky VJ (eds), 2008, *Arid land Springs in North America: ecology and conservation*, University of Arizona, Tucson, AZ, p. 432.
- Swift Bird, K., Navarre-Sitchler, A., Singha, K., 2020, Hydrogeological controls of arsenic and uranium dissolution into groundwater of the Pine Ridge Reservation, South Dakota: *Applied Geochemistry*, v. 114, <https://doi.org/10.1016/j.apgeochem.2020.104522>
- Snelling, A.A., 2021, The Petrology of the Bright Angel Formation, Tonto Group, Grand Canyon, Arizona: *Answers Research Journal*, v. 14, p. 303-415
- The White House, 2023, FACT SHEET: President Biden Designates Baaj Nwaavjo I'tah Kukveni – Ancestral Footprints of the Grand Canyon National Monument : <https://www.whitehouse.gov/briefing-room/statements-releases/2023/08/08/fact-sheet-president-biden-designates-baaj-nwaavjo-itah-kukveni-ancestral-footprints-of-the-grand-canyon-national-monument/> (accessed January 2024).
- Tillman, F. D., Anderson, J.R., Unema, J.A., Chapin, T.P., 2020, Assessing uranium and select trace elements associated with breccia pipe uranium deposits in the Colorado River and main tributaries in Grand Canyon, USA: *PLoS ONE* v. 15, <https://doi.org/10.1371/journal.pone.0241502>
- Tillman, F.D., Beisner, K.R., Anderson, J.R. *et al.*, 2021, An assessment of uranium in groundwater in the Grand Canyon region: *Sci Rep* v. 11, <https://doi.org/10.1038/s41598-021-01621-8>.

- Tobin, B. W., Springer, A. E., Kreamer, D. K. & Schenk, E., 2018, Review: The distribution, flow, and quality of Grand Canyon Springs, Arizona (USA): *Hydrogeol. J.* v. 26, p. 721–732, <https://doi.org/10.1007/s10040-017-1688-8>.
- Trujillo, E., and Molotch, N.P., 2014, Snowpack regimes of the Western United States: *Water Resources Research*, v. 50, p. 5611-5623, doi:10.1002/2013WR014753
- URS Group Inc. 2014, Pilot Hydrologic Study Report: Investigation Operable Unit 2, Orphan Mine Site, Grand Canyon National Park, Arizona: National Park Service, 200 p.
- United States Department of the Interior, 2012, Secretary Salazar Announces Decision to Withdraw Public Lands near Grand Canyon from New Mining Claims: <https://www.doi.gov/news/pressreleases/Secretary-Salazar-Announces-Decision-to-Withdraw-Public-Lands-near-Grand-Canyon-from-New-Mining-Claims> (accessed January 2024)
- U.S. Environmental Protection Agency, 2021, Drinking water contaminants, *US Environ. Protect. Agency database*: <https://www.epa.gov/ground-water-and-drinking-water/national-primary-drinking-water-regulations>, (Accessed 21 Nov 2021).
- U.S. Environmental Protection Agency, 1994, Method 200.7 Determination of Metals and Trace Elements in Water and Wastes by Inductively Coupled Plasma-Atomic Emission Spectrometry, Revision 4.4, Cincinnati, OH
- U.S. Environmental Protection Agency, 1994, Method 200.8: Determination of Trace Elements in Waters and Wastes by Inductively Coupled Plasma-Mass Spectrometry, Revision 5.4., Cincinnati, OH
- U.S. Environmental Protection Agency, 1997, Method 300.1: Determination of Inorganic Anions in Drinking Water by Ion Chromatography, Revision 1.0., Cincinnati, OH
- U.S. Environmental Protection Agency, 2004, Method 9060A: Total Inorganic Carbon, Revision 1.0
- U.S. Environmental Protection Agency, 2018, Method SW-846, Ch. 3, Inorganic Analytes, Revision 6.0
- Ward Jr., J.H., 1963, Hierarchical Grouping to Optimize an Objective Function: *Journal of the America Statistical Association*, v. 58, p 236-244, <https://doi.org/10.1080/01621459.1963.10500845> /<https://doi.org/10.1080/01621459.1963.10500845>
- Wei, T., and Simko, V., 2021, R package ‘corrplot’: Visualization of a Correlation Matrix, Version 0.92, <https://github.com/taiyun/corrplot>.
- Wenrich, KJ, 1985, Mineralization of breccia pipes in northern Arizona: *Econ. Geol.*, v. 80, p. 1722-1735. <https://doi.org/10.2113/gsecongeo.80.6.1722>.

Wickham, H., 2016, *ggplot2: Elegant Graphics for Data Analysis*, Springer-Verlag New York. ISBN 978-3-319-24277-4, <https://ggplot2.tidyverse.org>.

Wright, Abigail, personal communication, November 1st, 2023, Senior Project Manager at ISOTECH, Inc.

Zamora, M. L., Tracy, B. L., Zielinski, J. M., Meyerhof, D. P. & Moss, M. A., 1998, Chronic ingestion of uranium in drinking water: A study of kidney bioeffects in humans: *Toxicol. Sci.*, v. 43, p. 68–77, <https://doi.org/10.1006/toxs.1998.2426>.

Zhang, Z., and Castello, A., 2017, Principal components analysis in clinical studies: *Annals of Translational Medicine*, v. 5, Iss. 17, p. 1-7, doi: 10.21037/atm.2017.07.12

Zukosky, K., 1995, An assessment of the potential to use water chemistry parameters to define groundwater flow pathways at Grand Canyon National Park, Arizona [M.S. Thesis]: University of Nevada, Las Vegas, 105 p.

Curriculum Vitae

Collin T. Davidson

Email: collin.davidson461@gmail.com

EDUCATION

Master of Science, Geoscience Aug 2021—May 2024 (Expected Graduation Date)

University of Nevada, Las Vegas | GPA: 4.0

Thesis: Investigating controls on spatial and temporal variation of dissolved uranium at springs in Horn Creek drainage, Grand Canyon National Park, AZ, USA

- **Relevant Coursework:** Hydrogeochemistry, Contaminant Hydrogeology, Geographic Information Systems (GIS): Theory and Applications, Soil Plant Water Relations, Research Methods, Advanced Field Geology, Poster Presentation and Time Management
- **Grants & Awards:** 2022 UNLV Geosymposium Best Graduate Poster (\$1,500), UNLV Graduate and Professional Student Association Research Grant (\$1,600), Paul M. Yaniga Scholarship Award (\$1,500), UNLV Graduate Assistantship (full tuition scholarship & living stipend)
- **Talks and Poster Presentations:** 2022 GSA Annual Meeting (poster), 2022 Water Smart Innovations annual conference (poster), 2021 UNLV Geosymposium (two posters)

Bachelor of Arts, Environmental Geoscience Aug 2017—May 2021

DePauw University, Greencastle, IN | GPA: 3.74 (Magna Cum Laude)

- **Honors:** Environmental Fellow, Presidential Scholarship (\$31,000/year), Peternell Scholarship (\$10,000), Ernest E. Rock Memorial Scholarship (\$1,900)
- **Off-Campus Study:** Coastal Ecology and Natural Resource Management, Zanzibar, Tanzania; DePauw Orchestra International Tour: Tokyo, Japan; Wilderness Writing: Everglades National Park

Critical Language Scholarship, Swahili

May—July 2021

United States Department of State

EXPERIENCE

Staff Hydrogeologist

Feb 2024 – Present

GSI Water Solution Inc., Portland, OR

Hydrologist

July 2023 – Feb 2024

NRCS Snow Survey, Portland, OR

Graduate Teaching Assistant

Aug 2021—June 2023

University of Nevada, Las Vegas. Las Vegas, NV

Hydrology Assistant

May—Aug 2022

Bryce Canyon National Park, UT

Student Director

Aug 2020—May 2021

Sustainability Leadership Program, DePauw University, Greencastle, IN

Project Manager Intern

Feb 2019—Dec 2019

Sustainability Leadership Program, DePauw University, Greencastle, IN

Governor's Public Service Intern

May 2019—Aug 2019

Indiana Department of Environmental Management (IDEM), Indianapolis, IN

PUBLICATIONS

Beisner, K.R, Davidson, C.T., Tillman, F.D, 2023, Anthropogenic influence on groundwater geochemistry in Horn

Creek Watershed near the Orphan Mine in Grand Canyon National Park, Arizona, USA:

Geochemistry: Exploration,

Environment, Analysis, v.23, doi:10.1144/geochem2023-007